Report SAM-TR-80-51

LEVEL II

12

ATMOSPHERIC EFFECTS ON LOW-POWER LASER BEAM PROPAGATION

T. W. Tuer, Ph.D.
J. Mudar, M.S.
J. R. Freeling, Ph.D.
G. H. Lindquist, M.S.
Nichols Research Corporation
4040 South Memorial Parkway
Huntsville, Alabama 35802

December 1980

Final Report for Period 15 August 1978 - 15 August 1979

Approved for public release; distribution unlimited.

Prepared for
USAF SCHOOL OF AEROSPACE MEDICINE
Aerospace Medical Division (AFSC)
Brooks Air Force Base, Texas 78235

NOTICES

This final report was submitted by Nichols Research Corporation, 4040 S. Memorial Parkway, Huntsville, Alabama 35802, under contract F33615-78-C-0627, job order 7757-02-62, with the USAF School of Aerospace Medicine, Aerospace Medical Division, AFSC, Brooks Air Force Base, Texas. Major Williford (USAFSAM/RZL) was the Laboratory Project Scientist-in-Charge.

When U.S. Government drawings, specifications, or other data are used for any purpose other than a definitely related Government procurement operation, the U.S. Government thereby incurs no responsibility nor any obligation whatsoever; and the fact that the U.S. Government may have formulated, furnished, or in any way supplied the said drawings, specifications, or other data is not to be regarded by implication or otherwise, as in any manner licensing the holder or any other person or corporation, or conveying any rights or permission to manufacture, use, or sell any patented invention that may in any way be related thereto.

This report has been reviewed by the Office of Public Affairs (PA) and is releasable to the National Technical Information Service (NTIS). At NTIS, it will be available to the general public, including foreign nations.

This technical report has been reviewed and is approved for publication.

Graham G. Williford

GRAHAM G. WILLIFORD, Major, USAF
Project Scientist

Ralph G. Allen

RALPH G. ALLEN, Ph.D.
Supervisor

Roy L. DeHart

ROY L. DEHART
Colonel, USAF, MC
Commander

UNCLASSIFIED

SECURITY CLASSIFICATION OF THIS PAGE (When Data Entered)

19

REPORT DOCUMENTATION PAGE

READ INSTRUCTIONS BEFORE COMPLETING FORM

18

1. REPORT NUMBER: SAM-TR-80-51

2. GOVT ACCESSION NO.: AD-A095497

3. RECIPIENT'S CATALOG NUMBER:

6

4. TITLE (and Subtitle): ATMOSPHERIC EFFECTS ON LOW-POWER LASER BEAM PROPAGATION

4

5. TYPE OF REPORT & PERIOD COVERED: Final Report, 15 Aug 78 - 15 Aug 79

14

6. PERFORMING ORG. REPORT NUMBER: NRCAA-79-LASBR-002

10

7. AUTHOR(s): T. W. Tuer, J. Mudar, J. R. Freeling, G. H. Lindquist

15

8. CONTRACT OR GRANT NUMBER(s): F33615-78-C-0627

9. PERFORMING ORGANIZATION NAME AND ADDRESS:
Nichols Research Corporation
4040 S. Memorial Parkway
~~Huntsville, Alabama 35802~~ Ann Arbor MI 76

10. PROGRAM ELEMENT, PROJECT, TASK AREA & WORK UNIT NUMBERS:
62202F
7757-02-62

17 02

11

11. CONTROLLING OFFICE NAME AND ADDRESS:
USAF School of Aerospace Medicine (RZL)
Aerospace Medical Division (AFSC)
Brooks Air Force Base, Texas 78235

12. REPORT DATE: December 1980

13. NUMBER OF PAGES: 130

14. MONITORING AGENCY NAME & ADDRESS (if different from Controlling Office):

15. SECURITY CLASS. (of this report): Unclassified

12 133

15a. DECLASSIFICATION/DOWNGRADING SCHEDULE:

16. DISTRIBUTION STATEMENT (of this Report)

Approved for public release; distribution unlimited.

17. DISTRIBUTION STATEMENT (of the abstract entered in Block 20, if different from Report)

18. SUPPLEMENTARY NOTES

19. KEY WORDS (Continue on reverse side if necessary and identify by block number)

Atmospheric transmission
Aerosol scattering
Aerosol absorption
Atmospheric conditions
Aerosol attenuation
Low-power laser propagation
Molecule extinction
Turbulence

20. ABSTRACT (Continue on reverse side if necessary and identify by block number)

A detailed discussion is presented of various theories, experiments, and models pertinent to atmospheric effects on the transmission of low-power laser radiation. The effects of molecules, aerosols, and turbulence and their levels in the atmosphere are considered. Specific conclusions and recommendations are given with regard to the state of knowledge in this field, and to models that can be used to predict atmospheric effects that are relevant to comprehensive personnel safety standards.

DD FORM 1 JAN 73 1473 EDITION OF 1 NOV 65 IS OBSOLETE

UNCLASSIFIED

SECURITY CLASSIFICATION OF THIS PAGE (When Data Entered)

411799

SUMMARY

The state-of-information is quite different for the various effects that the atmosphere has on the propagation of laser radiation. Molecular line absorption is quite well understood, and several sophisticated line-by-line computer codes and comprehensive line parameter compilations are available. On the other hand, the mechanism for the continuum molecular absorptions is still the subject of controversy, and there is considerable disagreement between various measurements and models. Molecular scattering theory is well established and supported by measurements and models.

Theories and models for aerosol absorption and scattering are also well established, but aerosol characteristics of the atmosphere (particularly the size distribution) are highly variable and difficult to characterize. As a result, the accuracy of most predictions of aerosol effects is uncertain, unless detailed measurements of aerosol size distributions are available for the situation of interest. No better than order-of-magnitude predictions should be expected from correlations of aerosol extinction in different spectral bands (e.g., the correlation of infrared transmission with the visibility).

The effects of weak to moderate levels of atmospheric turbulence on laser radiation transmission is well understood. In this "linear region" of turbulence effects, theories and models are available for parameters such as irradiance variances and others of less interest here (e.g., beam spread and wander, and polarization and coherence effects). A generally accepted theory is not available for nonlinear effects associated with higher levels of turbulence in the "saturated" or "supersaturated" region. However, there are a number of satisfactory empirical models for this situation. Once again, there is considerable uncertainty in the accuracy of available models for predicting the state of the atmosphere, this time with regard to the expected turbulence levels; also, measuring the level of atmospheric turbulence in the field

is difficult. The situation in this area, however, is not so serious since the effects of interest are not so sensitive to the level of turbulence, and the maximum turbulence effects are somewhat more predictable than the aerosol effects.

Briefly, for molecular effects, we are recommending the use of the Air Force Geophysics Laboratory's (AFGL) computer code LASER to generate simpler, user-oriented algorithms for rapid prediction of molecular extinction for various path conditions. Such algorithms have been developed for a limited number of laser lines. Besides treating molecular absorption (line and continuum) and scattering, the code LASER also treats aerosol extinction. However, to be conservative in safety considerations, we recommend that the minimum aerosol effects be considered (i.e., the Clear Model in LASER). This recommendation is made because aerosol attenuation is so poorly predicted, from the easily obtainable atmospheric parameters such as visibility, humidity, and wind speed, using currently available models. For predicting the turbulence condition of the atmosphere, we recommend using Hufnagel's 1978 analytical model with a small adjustment of parameters to bring it into better agreement with measured data. For predicting the effects of atmospheric turbulence on irradiance statistics, we recommend using the classical Rytov expression in the linear region and an empirical formula developed by Johnson, et al., for the saturated and supersaturated regions. It appears that the most turbulence can do, 99 percent of the time, is to increase the local value of irradiance over its average value by a factor of five.

TABLE OF CONTENTS

LIST OF ILLUSTRATIONS

LIST OF TABLES

ATMOSPHERIC EFFECTS UPON LOW-POWER LASER BEAM PROPAGATION

INTRODUCTION

The main objectives of this study were (1) to establish the state-of-information regarding the transmission characteristics of the atmosphere for low-power laser* radiation, and (2) to recommend models for predicting those characteristics. The models are to be employed for predicting safe ranges for personnel in the vicinity of low-power lasers and for operational planning that addresses the associated safety considerations. The study was to consider the absorption and scattering effects of natural atmospheric molecules and aerosols, as well as the effects of atmospheric turbulence over arbitrary slant paths in the atmosphere. Of primary concern for safety considerations are the prediction of the total average molecular and aerosol extinction and the irradiance statistics associated with turbulence. Models were also required to treat various meteorological conditions, including rain, snow, haze, fog, various types of clouds, and atmospheric turbulence at various altitudes. Spectral regions of interest include the ultraviolet, visible, and infrared (i.e., approximately from 0.2 to 10 μm), with the emphasis on those regions at the frequencies of commonly used lasers.

The first six months of this study were devoted to preparing a bibliography that was intended to be as comprehensive and user oriented as possible. In this report the major features of this bibliography will be reviewed, our overall conclusions and recommendations will be summarized, and available information will be evaluated. The details of our conclusions and recommendations regarding the best models for the present purposes will also be given.

*Lasers for which nonlinear effects, such as thermal blooming and aerosol modification, can be neglected.

AVAILABLE INFORMATION

A comprehensive bibliography of information relating to atmospheric effects on the transmission of low-power laser radiation was compiled during the first six months of this study [1]. This bibliography considered information on theories, measurements, and models for the effects of atmospheric molecules, aerosols, and turbulence on the propagation of laser radiation in the ultraviolet, visible, and infrared spectral regions. In peripheral areas such as the condition and composition of the atmosphere and the optical properties of aerosol materials, only the principal papers were included.

A number of sources were utilized to compile the information presented in the bibliography, including two different computerized searches, several earlier technical reviews, and discussions with experts in the field. The most useful source, in terms of the number of reports located, was the Lockheed computerized bibliographic search service called DIALOG. This system indexes papers from approximately 4400 technical journals, 1000 conference or symposium proceedings, and selected books and U.S. Government reports. Based on user-supplied key words and phrases, the system locates pertinent papers and prints the reference material (e.g., title, author, report or journal number), as well as an abstract when one is available. This search and one by the National Technical Information Service (NTIS) included many papers that were not pertinent to the present problem (e.g., papers primarily on laser fusion, flow diagnostics, nonlinear effects). Thus, considerable manual review of the titles and abstracts was required; less than 20 percent of the references listed in the two computer searches were deemed pertinent.

Over 1100 citations to pertinent reports and papers are presented in this bibliography, along with approximately 50 additional references to texts. Over 80 percent of these citations are annotated with a few sentences describing the main points of the paper. This bibliography is arranged in ten categories as shown in Table 1. This table also indicates the breakdown as to where the information appears and how many in each category are annotated.

TABLE 1. BIBLIOGRAPHY SUMMARY - ATMOSPHERIC EFFECTS ON LASER BEAM PROPAGATION

Category	Total number of citations	Journals	Reports	Symposia	Other	Number annotated
Molecule effects	146	60	69	11	6	120
Molecule conditions	35	28	6	0	1	28
Aerosol effects	142	78	45	18	1	98
Aerosol conditions	190	158	25	5	2	122
Turbulence effects	344	235	73	30	6	309
Turbulence conditions	46	32	6	6	2	35
Field measurements (molecule and aerosol effects)	206	162	35	7	2	191
General	28	5	17	5	1	25
Biological effects	19	12	5	2	0	12
Texts	47	-	-	-	47	19
Total	1203	770	281	84	68	959

A thorough cross-reference to 59 subcategories is also included in this bibliography. This cross-reference specifies (by citation number) each citation that pertains to each subcategory, with any single citation possibly appearing in several different categories. These subcategories include items such as report type (measurement report, theoretical report, etc.); various types of molecular absorption (line, continuum, and those due to various species such as H_2O and CO_2); various kinds of aerosols (dust, fog, rain, etc.) and their characteristics (optical properties and size distributions); various turbulence effects and conditions; and specifically addressed lasers. Another feature of this bibliography is the inclusion of synopses of telephone conversations with several key researchers in this field regarding their latest work and future plans.

EVALUATION OF AVAILABLE INFORMATION

In order to establish the state-of-knowledge in the field of atmospheric effects on the transmission of laser radiation and to recommend models for predicting these effects, it was necessary to evaluate the available information discussed in the previous section. In this evaluation, we concentrated on areas of primary importance (i.e., atmospheric effects that would have the most potential impact on eye-safety considerations) and on the more controversial areas where the theories, experiments, and/or models are uncertain. Thus, we examined in detail the more important papers in the bibliography (and some others), and compared and evaluated their results and conclusions.

Information on the three main atmospheric effects of interest--those due to molecules, aerosols, and turbulence--are evaluated separately in the following three sections. Due to the importance of and controversy about these effects, the evaluation in each section concentrates on the molecular continuum absorption, the comparison of aerosol extinction models with measurement, and the expected state of turbulence in the atmosphere. Each section also discusses the generally accepted theory underlying each main atmospheric effect and the more pertinent experiments and models pertaining to that effect.

Molecular Absorption and Scattering

Molecules produce the most ubiquitous effect that the atmosphere has on the transmission of laser radiation since molecules are by definition always present in the atmospheric path, whereas aerosols and turbulence need not be present in significant amounts. The number density of these molecules decreases rapidly with altitude above sea level (generally exponentially), so attenuation at high altitudes is much less than at low altitudes. Several molecules in the atmosphere (naturally occurring and others) strongly attenuate radiation in the ultraviolet, visible, and infrared spectral regions. The relative proportion of many

of these molecules (e.g., CO_2, CO, CH_4) is quite uniform both spatially and temporally throughout the atmosphere. The relative concentration of others, notably H_2O and O_3, varies strongly with locale and time and does not follow a general exponential distribution like the other species. Thus, to determine the eye-safe range to a laser operating in the atmosphere, knowing the concentration of several pertinent molecules, and their statistical variability, is also important.

Molecules affect the transmission by two different mechanisms: absorption and scattering. The absorption effects are commonly further separated into those due to individual absorption lines causing fine spectral structure and those due to "continuum absorption" varying smoothly with wavelength. The mechanism producing continuum absorption is not well understood, but is thought to be caused by either the far wings of a large number of individual lines or by the existence of dimers or polymers of certain molecules, particularly water vapor. The mechanisms of both resonant line absorption and scattering are well understood and explained by classical wave mechanics. This section evaluates the various theories, measurements, and models relating to atmospheric molecular concentration, molecular line absorption, molecular continuum absorption, and molecular scattering.

Atmospheric Molecular Concentration--The attenuation of laser radiation by a particular molecular species in the atmosphere is generally proportional to the number density of that species in the path of the beam, although self-broadening effects in continuum absorption involve a quadratic dependency. As mentioned above, the concentration of some of the more attenuating molecules can be highly variable with time and/or locale; thus, it is very important to have information on the concentration of certain pertinent molecules and their statistical variability. The molecules of primary concern are: H_2O, O_3, CO_2, CH_4, O_2, CO, and N_2O; all except the first two are generally considered uniformly mixed throughout the atmosphere (i.e., uniform relative concentration).

The measurement of these and other molecular constituents of the atmosphere has been the subject of numerous studies attempting to characterize their variation with altitude, locale, time, etc. Although the

literature survey [1] performed in the first phase of this study did not emphasize this topic, 35 references on it were given. Of particular interest in recent years have been measurements of O_3 concentration. Water vapor and carbon dioxide have historically been the subject of many measurement programs.

Most previous calculations and analyses of atmospheric attenuation of radiation have been based on standard models for molecular concentrations that were derived by the Air Force Geophysics Laboratory (AFGL) [2,3] from measurements such as these. Values from these models are reproduced in Table 2. A more recent model of atmospheric concentrations [4] considers more molecules and gives a range for their expected variation with altitude, latitude, and time of year (see Table 3). It is noted that there are large variabilities associated with the concentration of several of these molecules. Water vapor concentration is of particular concern because it is so highly variable (particularly with altitude and latitude) and because this molecule is so strongly absorbing in several spectral regions. Figure 1 shows that the measured variation in water vapor concentration with altitude for several seasons does not correlate well with the AFGL models. These models generally indicate a much slower reduction in concentration with altitude, which is not conservative with regard to eye safety. For this reason, it is advisable to base attenuation predictions on the locally (and currently) measured water vapor concentations whenever possible, rather than on values from a standard model. This is also advisable for other species, but is not as critical.

Molecular Line Absorption--Frequently the dominant attenuation of laser radiation in the atmosphere is due to absorption by individual vibration-rotation lines of atmospheric molecules. This mechanism is particularly important for radiation produced by gas lasers using a molecule present in the atmosphere, such as CO_2. In these cases, the emission and absorption are caused by the same transition (i.e., resonant absorption), so the laser frequency is right at the center of the absorption line where the absorption is greatest.

TABLE 2. CONCENTRATIONS OF IMPORTANT ABSORBING ATMOSPHERIC MOLECULES [2,3]

Uniformly mixed		Nonuniformly mixed		
			Sea level density (g/m^3)	
Molecules	Concentration (parts per million[a])	Model atmosphere	H_2O	O_3
CO_2	330	Tropical	19	5.6×10^{-5}
N_2O	0.28	Midlatitude summer	14	6.0×10^{-5}
CO	0.075	Midlatitude winter	3.5	6.0×10^{-5}
CH_4	1.6	Subarctic summer	9.1	4.9×10^{-5}
O_2	2.10×10^{5}	Subarctic winter	1.2	4.1×10^{-5}

[a]By volume in dry air.

TABLE 3. CONCENTRATION OF ABSORBING ATMOSPHERIC MOLECULES AND THEIR VARIABILITY [4]

Molecule	Average concentration (volume basis)	Molecule	Average concentration (volume basis)
N_2	0.78084	NO	10^{-8}-10^{-6}
O_2	0.20946	NO_2	10^{-9}-10^{-6}
H_2O	1.3×10^{-7} to 4.5×10^{-2}	HNO_3	2.8×10^{-9}
CO_2	3.10×10^{-4}	NH_3	$\leq10^{-6}$
CH_4	$(1\text{-}1.4)\times10^{-6}$	SO_2	$(0.5\text{-}7.2)\times10^{-9}$
H_2	5×10^{-7}	H_2S	$(1.6\text{-}16)\times10^{-9}$
CO	$(0.5\text{-}2.5)\times10^{-7}$	HCHO	$\leq10^{-7}$
O_3	$(2\text{-}7)\times10^{-8}$	HCl	$(1\text{-}2.6)\times10^{-9}$
N_2O	$(2.7\text{-}3.5)\times10^{-7}$	NO_3,OH,HO_2,CH_3O	5×10^{-11}

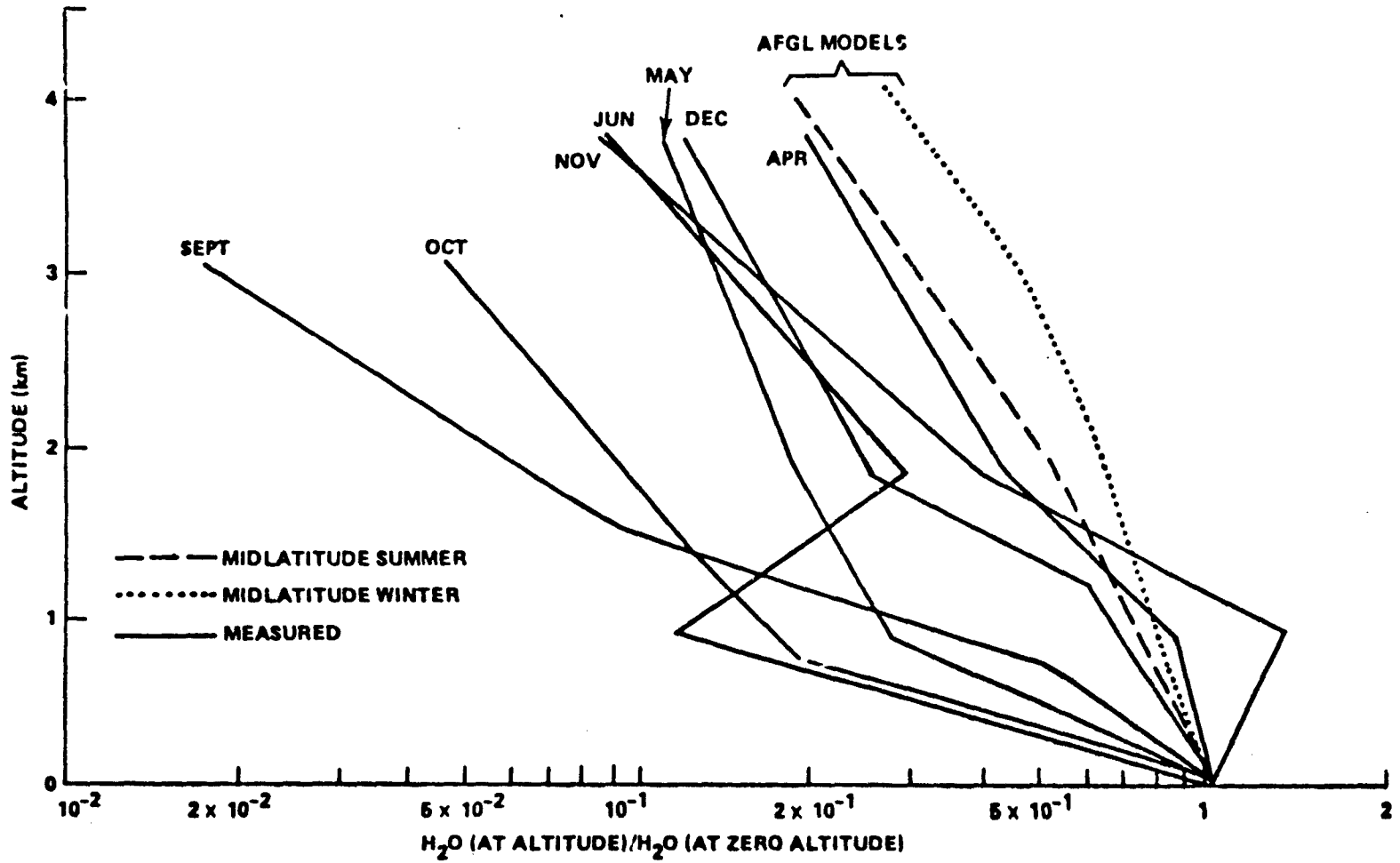

Figure 1. Atmospheric water content as a function of altitude [5].

For atmospheric conditions at low altitudes (i.e., near standard pressure), the laser absorption by an individual absorption line is generally well expressed by the simple Lorentz expression:

$$k = \frac{nS\gamma/\pi}{\left(\nu_L - \nu_0\right)^2 + \gamma^2} \tag{1}$$

where

k = Absorption coefficient per unit length; i.e. transmission $\tau = \exp(-kL)$, where L is the path length

ν_L = Laser frequency

n = Molecular concentration of the species being considered

S = Absorption line parameter of strength

γ = Absorption line parameter of halfwidth

ν_0 = Absorption line parameter of frequency.

The strength depends on temperature (T) through the vibration and rotation partition functions (Q_v and Q_r) and the Boltzmann factor [3]:

$$S(T) = S\left(T_s\right)\left[\frac{Q_v\left(T_s\right)}{Q_v(T)}\,\frac{Q_r\left(T_s\right)}{Q_r(T)}\right]\exp\left[\frac{1.439\left(T-T_s\right)E''}{TT_s}\right] \tag{2}$$

where T_s is some standard temperature when S is known, and E" is the energy of the lower state of the transition. The halfwidth is proportional to the local atmospheric pressure (p), and generally inversely proportional to temperature to some power:

$$\gamma(T,p) = \gamma\left(T_s,p_s\right)\left(p/p_s\right)\left(T_s/T\right)^n \tag{3}$$

where p_s is a standard pressure at a condition where γ is known. The power n is usually taken to be 1/2 -- corresponding to temperature-independent collision diameters, although there is some uncertainty in its actual value.

The broadening of any particular transition results from interactions with all of the molecules of the gas mixture. The separation of the contributions from the different molecules is a tedious task, though fortunately the halfwidths included in the line tabulation make this separation largely unnecessary. The halfwidths in the tabulation are diluted air halfwidths, characteristic of the line as it appears in air of normal composition. However, because the halfwidth is made up of so many contributions, and because the temperature exponents of these contributions vary widely, the use of a single pressure exponent of one-half is very much an oversimplification; so large temperature corrections should be avoided.

The AFGL Line Parameter Compilation [3] provides all of these parameters for the most important atmospheric absorption lines. To evaluate the total absorption due to all lines that significantly affect the laser radiation, it is necessary to sum the individual absorption coefficients from all of these lines. Generally, this is done by considering all of the important absorption lines within a certain cutoff frequency of the laser frequency (usually 20-50 cm^{-1}). The importance of each absorption line is determined by the absorption it would produce at its center for an extreme atmospheric path tangent to the Earth's surface and extending from space to space; lines producing less than 10 percent absorption for this path are neglected in the AFGL compilation. However, this cutoff was not employed in two situations: (1) in regions of very strong absorption where relatively weak lines above this limit are ignored; and (2) for Q-branch lines below this limit which are included when it is felt that their cumulative effect might be significant.

At higher altitudes, where the pressure is too low for collisions to have significant broadening effects, the Doppler broadening becomes dominant and the absorption coefficient is better approximated by:

$$k = \left(\frac{\ln 2}{\pi}\right)^{\frac{1}{2}} \frac{S}{\gamma_D} e^{-y^2} \qquad (4)$$

where the Doppler halfwidth is expressed as:

$$\gamma_D = \frac{\nu_0}{c} [(2 \ln 2) 2kT/m]^{\frac{1}{2}} \tag{5}$$

and

$$y = (\ln 2)^{\frac{1}{2}} (\nu_L - \nu_0)/\gamma_D \tag{6}$$

where c, k, and m are the speed of light, Boltzmann's constant, and molecular mass, respectively.

For intermediate altitudes (i.e., pressures), where the Doppler and pressure broadening are of the same order, a good approximation is obtained by convolving the two profiles to get what is referred to as the Voigt profile:

$$k = (yk_0/\pi) \int_{-\infty}^{\infty} \frac{\exp(-t^2)}{y^2 + (x - t)^2} \, dt \tag{7}$$

where

$$k_0 \equiv S/\gamma_D \pi^{\frac{1}{2}}$$

$$y \equiv \gamma/\gamma_D$$

$$x \equiv \frac{(\nu - \nu_0)}{\gamma_D} .$$

Other more complicated line shape models have been developed; for example [6], the full Lorentz:

$$k = \frac{S}{\pi} (\nu_L/\nu_0) \left[\frac{\gamma}{(\nu_L - \nu_0)^2 + \gamma^2} - \frac{\gamma}{(\nu_L + \nu_0)^2 + \gamma^2} \right] ; \tag{8}$$

and Van Vleck-Weisskopf:

$$k = \frac{S}{\pi} (\nu_L/\nu_0)^2 \left[\frac{\gamma}{(\nu_L - \nu_0)^2 + \gamma^2} + \frac{\gamma}{(\nu_L + \nu_0)^2 + \gamma^2} \right] ; \quad (9)$$

and the kinetic model*:

$$k = \frac{4S\nu_L\nu_0}{\pi} \left[\left(\gamma_L^2 - \gamma_0^2 \right)^2 + 4\nu^2\nu^2 \right] ; \quad (10)$$

but generally the simple Lorentz and Voigt models give satisfactory agreement with measurements.

Mainly two different kinds of measurements have been made to determine the molecular line absorption of laser radiation.** The first, direct measurement of the attenuation of a laser beam through a path of known composition, is easiest, but does not give enough information to extrapolate to other conditions with confidence. The second determines the basic line parameters (i.e., strength, width, and position), thus allowing accurate prediction of the molecular line absorption in other situations. Measurements of the second type of measurement by Woods et al. [8,9] have indicated several inaccuracies in the original AFGL Line Parameter Compilation (see Figure 2). These measurements were made on air-broadened samples of N_2O, HDO, and CH_4 in the DF laser region [8] and on air-broadened H_2O samples in the CO laser region [9]. They indicated that

(1) agreement was excellent for the N_2O line parameters

(2) HDO lines tended to be stronger and wider than calculated (by factors of 50 percent and 25 percent, respectively)

(3) measured CH_4 spectra were many times stronger than calculated and contained many additional lines

(4) Lorentz shape may be more nearly correct than previously thought, if accurate positions, widths, and strengths are used and if the wing cutoff is not restricted to the usual 25 cm^{-1}.

*Sometimes this model is attributed to Zhevakin and Naumov [7].

**The authors wish to acknowledge the helpful discussion of this subject with F. G. Smith of OptiMetrics, Ann Arbor, Michigan.

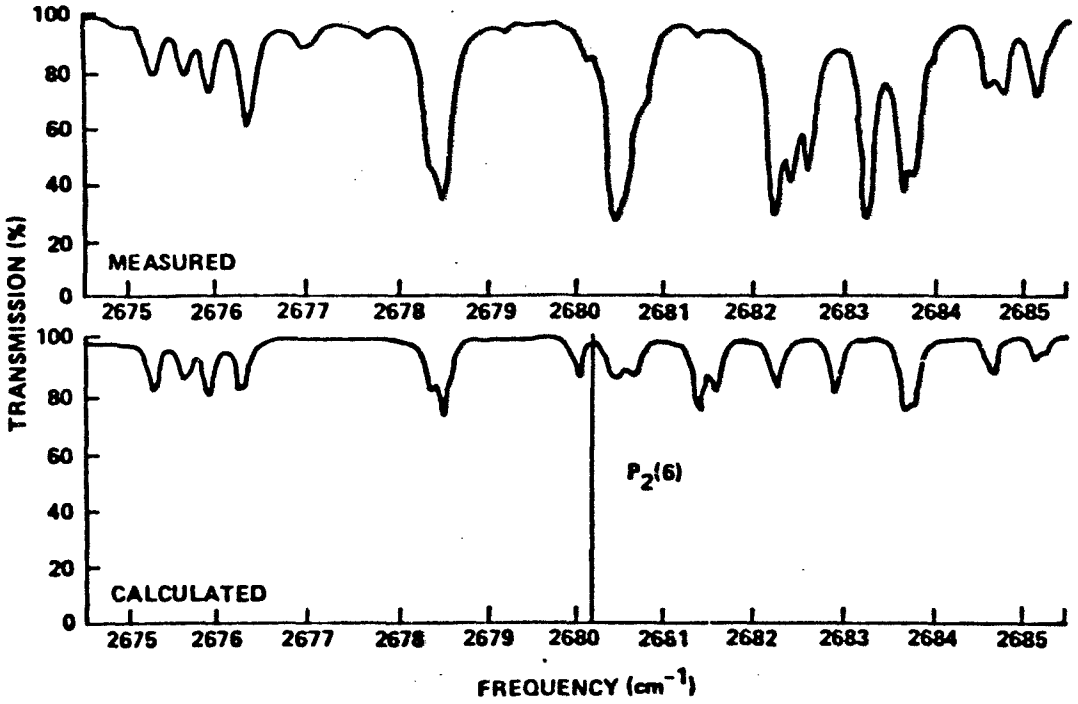

Figure 2. Selected example of measured and calculated spectra in the vicinity of the $P_2(6)$ DF laser line [8].

Measurements of this type were also performed in the HF spectral region [10] and indicated similar results. The conclusions of these latter two references [9,10] were: (1) it is necessary to consider absorption lines in this region as far as 200 cm^{-1} from the laser; and (2) the exponent on the $(\nu-\nu_0)$ term in the denominator of the Lorentz formula should be approximately 1.9 instead of the usual value of 2. The results of the latter measurements seemed to agree better (especially for the weaker absorption lines) with the line strengths given by Flaud and Camy-Peyret [11] than with those of Benedict which are used in the AFGL compilation. The Naval Research Laboratory (NRL) is planning similar measurements using a tunable laser, but the results will not be available for some time.

There have been survey-type spectral scans [12] in spectral regions where the HBr and Xe lasers operate that indicate no apparent discrepancies with the AFGL Line Parameter Compilation; however, the survey did indicate that the commonly quoted value for the position of the Xe laser transition, 2145 cm^{-1}, should actually be 2168 cm^{-1}. This, of course, could drastically change the level of molecular absorption calculated by models. Many discrepancies have been accounted for in subsequent versions of the compilation; however, only a small part of the spectrum (i.e., near the DF, CO, HF, HBr, and Xe laser lines) was investigated. This implies that problems could also exist in other spectral regions where lasers operate.

There have been a number of direct laboratory measurements of the attenuation of radiation from a number of different lasers (i.e., CO_2, CO, DF, HF, and erbium). These measurements were made primarily in multiple-pass White cells or more recently with spectrophones under a variety of experimental conditions (see Table 4). The CO_2 laser is the most popular for this kind of measurement. McCoy et al. [13] made one of the earliest measurements using a 980-m White cell with a mixture of CO_2 and air. They scaled their measured results for the P20 line to standard atmospheric conditions (i.e., 330 ppm CO_2 at 1 atm total pressure) to get an absorption coefficient of 0.0694 km^{-1}, compared with their calculated value of 0.076 km^{-1} based on independent measurements of strength and width. Henry [18] measured an intermediate value of 0.073 km^{-1}. The discrepancy in these basic "dry air" measurements and calculations is as yet unexplained. Actually, the atmospheric extinction of CO_2 laser radiation is usually dominated by the water vapor continuum in this region, as will be discussed in the following section. A number of field measurements of the extinction of CO_2 laser radiation have also been made.

Absorption of the P20 CO_2 laser line radiation by dry air mixtures has been measured by a number of other experimenters (see Table 5). There seems to be good agreement at 300 K for a value near 0.071 km^{-1}, and indications of a reduction in absorption with reduction in temperature. Moskalenko et al. [21] also measured the absorption of the P20

TABLE 4. MAJOR LABORATORY MEASUREMENTS OF MOLECULAR ABSORPTION OF LASER RADIATION

Experimenter	Organization	Date	Laser	Absorbing molecules	Type of measurement	Experimental conditions	Comments	Ref.
McCoy et al.	OSU	1968	CO_2	CO_2 and air	980-m White cell	344 ppm CO_2, 296 K, 700 torr air	$k = 8.39 \times 10^{-4}\ p^2\ km^{-1}$ at 10.59 μm $k = 6.67 \times 10^{-4}\ p^2\ km^{-1}$ at 9.55 μm	13
White et al.	ASL	197'	Erbium	CO_2	480-m path-length, White cell	T = 303 K, P_{CO_2} = 660 torr	Experiment and theory agree	14
Rice	Northrop Corp.	1972	CO	H_2O	71-cm cell	T = 150°C $p(H_2O)$ = 100 - 327 torr $p(N_2)$ = 0,763,1515 torr	19 lines measured; poor agreement with theory	15
Spencer et al.	Aerospace Corp.	1973	DF	CH_4, N_2O, CO_2, NDO	1, 10, 200 cm test cells	Midlatitude summer	24 wavelengths; theory and experiment agree within factor of 2 for all wavelengths	16
Long et al.	OSU	1973	CO		White cell			17
Meyers	General Dynamics/ Convair	-	DF	CO_2			Unpublished	
Henry		1973	CO_2	CO_2 and air			0.073 km^{-1}	18
Deaton et al.		1975	DF	H_2O	Spectrophone	1 - 1000 × atm. conc.	Calibrated to Mills data below	19
Mills	OSU	1976	DF	H_2O, CH_4, CO_2, NDO, H_2O	White cell; 8 laser lines	H_2O: P_{H_2} = 14.3 torr T = 297 K	Absorption coefficients quoted to 5%; compared with midlatitude summer sea-level model; confirm H_2O continuum values obtained from extrapolated Burch data. Theory and experiment agree at the orders of magnitude level for all gases.	20
Watkins et al.	Army-ASL	1978	HF	H_2O				10

TABLE 5. LABORATORY MEASUREMENTS OF DRY AIR ABSORPTION COEFFICIENT FOR THE P20 CO_2 LASER

Experimenter	Temperature (K)	Absorption coefficient (km^{-1})	Reference
Stephenson et al.	295	0.075	22
Oppenheim and Devir	300	0.071	23
Moskalenko et al.	290-300	0.055-0.071	21
Gerry and Leonard	273	0.040	24
McCubbin and Mooney	300	0.071	25
McCubbin et al.	300	0.073	26
Long and McCoy	-	0.029	27

CO_2 laser line in water vapor and showed an increase in absorption with temperature (i.e., absorption coefficients of 0.055-0.071 km^{-1} for T = 290-300 K, respectively), but no details of the experiment were provided.

Extensive laboratory measurements have also been made of the molecular absorption of DF laser radiation by atmospheric gases. Spencer et al. [16] determined the absorption by individual samples of atmospheric gases, considering gases whose line attenuation of DF radiation is the strongest -- HDO, N_2O, CH_4, and CO_2. In Figure 3, the total attenuation indicated by the measurements for a midlatitude winter model is compared with theoretical calculations using the AFGL line parameters. For the 17 DF lines measured, the agreement is within approximately a factor of two. It should be noted, however, that this comparison is for one of the drier model atmospheres and the water vapor continuum is not considered, so much larger uncertainties in the molecular attenuation will be encountered in practice.

More recently, Mills [20] measured the attenuation of eight DF laser lines as a function of the concentration of these same gases. All combinations of laser lines and gases were not considered since some of the lines are not significantly affected by some of the gases. The

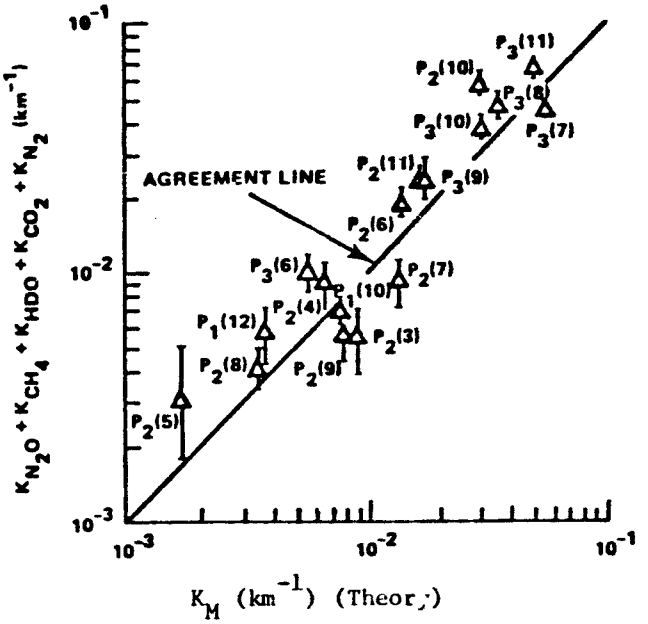

Figure 3. Comparison of experimental and theoretical absorption coefficient values for 17 DF laser lines for the midlatitude winter model atmosphere (H_2O continuum not included). [23]

attenuation of N_2O of five laser lines [i.e. $P_{3-2}(6)$, $P_{3-2}(7)$, $P_{3-2}(8)$, $P_{2-1}(10)$, $P_{2-1}(11)$] was measured to be linear over concentrations ranging from 1-12 ppm up to 50-220 ppm. Attenuation coefficients thus indicated are compared in Table 6 with calculations based on the AFGL line parameters, and with measurements by Spencer et al. [16] and Deaton et al. [19]. Mills' measurements agree best with theory (i.e. generally about 1 percent, but -8.6 percent for one line). Although these measurements were made at higher than normal atmospheric concentrations, the linear behavior indicates that self-broadening effects still are not important and that the results can be scaled accurately to lower concentrations. Deaton's measurements were made at up to 1000 times normal atmospheric concentration and are calibrated to Mills' data. Also shown in Table 6 are similar measurements for CH_4. The differences with theory are much larger for this molecule, but the measurements are more self-consistent, indicating a potential difficulty in the values contained in

TABLE 6. MEASURED AND THEORETICAL N_2O ABSORPTION COEFFICIENTS FOR FIVE DF LASER LINES

Absorbing gas	DF line	Laser frequency (cm^{-1})	Absorption coefficient (km^{-1})			
			Theory	Mills [20]	Spencer et al.[16]	Deaton et al.[19]
N_2O	$P_{3-2}(6)$	2594.198	2.26×10^{-3}	2.27×10^{-3} (+0.4)[a]	2.44×10^{-3} (+8.0)	2.33×10^{-3} (+3.1)
	$P_{3-2}(7)$	2570.522	3.75×10^{-2}	3.73×10^{-2} (-0.5)	3.33×10^{-2} (-11.2)	3.90×10^{-2} (+4.0)
	$P_{3-2}(8)$	2546.375	2.15×10^{-2}	2.14×10^{-2} (-0.5)	2.30×10^{-2} (+7.0)	1.96×10^{-2} (-8.8)
	$P_{2-1}(10)$	2580.097	4.59×10^{-2}	4.53×10^{-2} (-1.3)	4.65×10^{-2} (+1.3)	7.04×10^{-2} (+53.4)
	$P_{2-1}(11)$	2553.953	1.06×10^{-2}	9.69×10^{-3} (-8.6)	1.23×10^{-2} (+16.0)	- -
CH_4	$P_{2-1}(6)$	2680.179	3.051×10^{-4}	1.52×10^{-3} (396.0)	1.98×10^{-3} (547.0)	1.10×10^{-3} (259.0)
	$P_{2-1}(7)$	2655.863	7.147×10^{-4}	1.13×10^{-3} (+58.1)	1.29×10^{-3} (+80.4)	1.14×10^{-3} (+59.5)
	$P_{2-1}(8)$	2631.068	8.458×10^{-4}	8.59×10^{-4} (+1.6)	8.88×10^{-4} (+5.0)	9.79×10^{-4} (+15.8)

[a] ( ) indicates percentage difference from theory.

early versions of the AFGL line compilation. However, the absorption coefficients of Table 6 are typically less than 10^{-2} km^{-1}; hence these coefficients are very small compared with those due to other atmospheric species.

Mills also measured the attenuation of the $P_{2-1}(8)$ DF laser line radiation due to pure CO_2 at pressures of 248, 503, and 761 torr over a 0.7317-km path and found a value of 5.3×10^{-4} km^{-1}, assuming a self-broadening coefficient of unity. He also presented unpublished measurements by Meyers of General Dynamics/Convair (see Table 7) that indicated absorption coefficients of some lines that are four orders of magnitude higher than theory, apparently due to the omission of an isotopic or weak CO_2 band from the AFGL compilation. In any event, this absorption is still small compared with that due to H_2O continuum or HDO lines.

Mills' measurements of HDO absorption of six DF laser lines were fit with a model of the form

$$k = ap + bp^2 \tag{11}$$

where k is the absorption coefficient and p is the partial pressure of HDO-enriched water vapor. These coefficients were then adjusted for normal isotropic abundances of HDO (i.e., 0.03 percent) and the expressions evaluated for the Midlatitude Summer Atmospheric Model (see Table 8). The differences with theory (i.e., calculations with AFGL line parameters) are seen to vary between 30 and 142 percent. These measurements are subject to errors due to unaccounted effects of D_2O as well as possible absorption or condensation of water on the mirrors and/or windows of the White cell.

Measurements of the absorption of CO laser radiation by atmospheric gases are limited. The most extensive measurements have been by Long [17; 28-33] using H_2O vapor broadened by N_2 in a 12-m multipass White cell. Long also made measurements on two of the more highly absorbed lines [32]. His earliest measurements at a H_2O partial pressure of 8.89 torr [30] had considerable scatter, and when compared with theory (i.e., using AFGL line parameters), the mean appeared to vary from a factor of

TABLE 7. MEASURED CO_2 ABSORPTION COEFFICIENTS FOR SIX DF LASER LINES (TAKEN FROM MILLS [20])

DF line	Laser frequency (cm^{-1})	Absorption coefficient (km^{-1})	
		Meyers	Mills
$P_{2-1}(6)$	2680.179	0.19×10^{-4}	-
$P_{2-1}(7)$	2655.863	1.85×10^{-4}	-
$P_{2-1}(8)$	2631.068	9.26×10^{-4}	5.3×10^{-4}
$P_{3-2}(6)$	2594.198	6.85×10^{-4}	-
$P_{3-2}(7)$	2570.522	5.24×10^{-4}	-
$P_{3-2}(8)$	2546.375	4.21×10^{-4}	-

TABLE 8. HDO ABSORPTION COEFFICIENTS EXTRAPOLATED TO 0.03 PERCENT RELATIVE HDO ABUNDANCE

Line	Absorption coefficient (km^{-1})		
	Measured		Theory
	0.03% HDO	14.26 torr H_2O	14.26 torr
$P_{2-1}(6)$	$3.39 \times 10^{-3}p + 2.05 \times 10^{-5}p^2$	5.24×10^{-2} (38)[a]	3.79×10^{-2}
$P_{2-1}(7)$	$5.94 \times 10^{-3}p + 5.24 \times 10^{-5}p^2$	9.54×10^{-2} (30)	7.35×10^{-2}
$P_{2-1}(8)$	$3.38 \times 10^{-4}p + 5.78 \times 10^{-6}p^2$	6.00×10^{-3} (-34)	9.12×10^{-3}
$P_{3-2}(6)$	$1.11 \times 10^{-3}p + 7.62 \times 10^{-6}p^2$	1.74×10^{-2} (142)	7.18×10^{-3}
$P_{3-2}(7)$	$4.71 \times 10^{-4}p + 9.31 \times 10^{-6}p^2$	8.61×10^{-3} (90)	4.53×10^{-3}
$P_{3-2}(8)$	$1.45 \times 10^{-4}p + 1.93 \times 10^{-6}p^2$	2.46×10^{-3} (118)	1.13×10^{-3}

[a] ( ) Indicates percentage difference from theory.

1.15 high at total pressures of 126 torr to a factor of 0.65 low at 767 torr (see Figure 4). His next measurements [31] were not compared with theory, but he did state that the absorption was considerably higher than predicted, in agreement with spectral measurements by Woods et al. [9] that indicate "super-Lorentz" behavior. The reason Long's earliest measurements [30] did not exhibit this behavior (see Figure 4) is thought to be tied to his selection of laser lines. That is, all of the lines were very close to the center of strong absorption lines ($\nu_o \approx \nu_L$), so the different exponent on the $(\nu-\nu_0)$ term is not significant for these lines. The next measurements Long reported [31] had much less scatter, but also displayed this trend. These were also compared to a super-Lorentz shape and found generally in good agreement. Long's latest measurements [32] were on two highly absorbed lines: $P_{10}(10)$ and $P_{11}(12)$. As expected, the latter agreed well with the standard Lorentz model since the laser line is near a strong absorption line (see Figure 5), while the former required the super-Lorentz model because it is farther from any strong lines. Also shown in Figure 5 are spectrophone measurements by Long [32] and measurements by Rice [34] using a short path cell (71 cm). Rice's measured absorption coefficients are below those of Long and Lorentz theory, and have considerable scatter. Rice's earlier measurements [35] have even more scatter, but generally lie above standard Lorentz theory (see Figure 6).

A number of experimenters have made measurements of the attenuation of laser-radiation in the natural atmosphere. Generally these measurements are not as useful as laboratory measurements because of uncertainties in the concentrations of the molecules and aerosols along the path. However, field measurements can, in certain cases, add to the confidence of the theory and laboratory measurements, or possibly indicate shortcomings in them.

An example of field measurements lending credence to laboratory data is shown in Figure 7. The solid curve representing McCoy's laboratory measurements [13] of CO_2 laser absorption (at 330 ppm CO_2) are slightly below most of the field measurements, so consideration of aerosol attenuation could bring them into agreement. The field data from

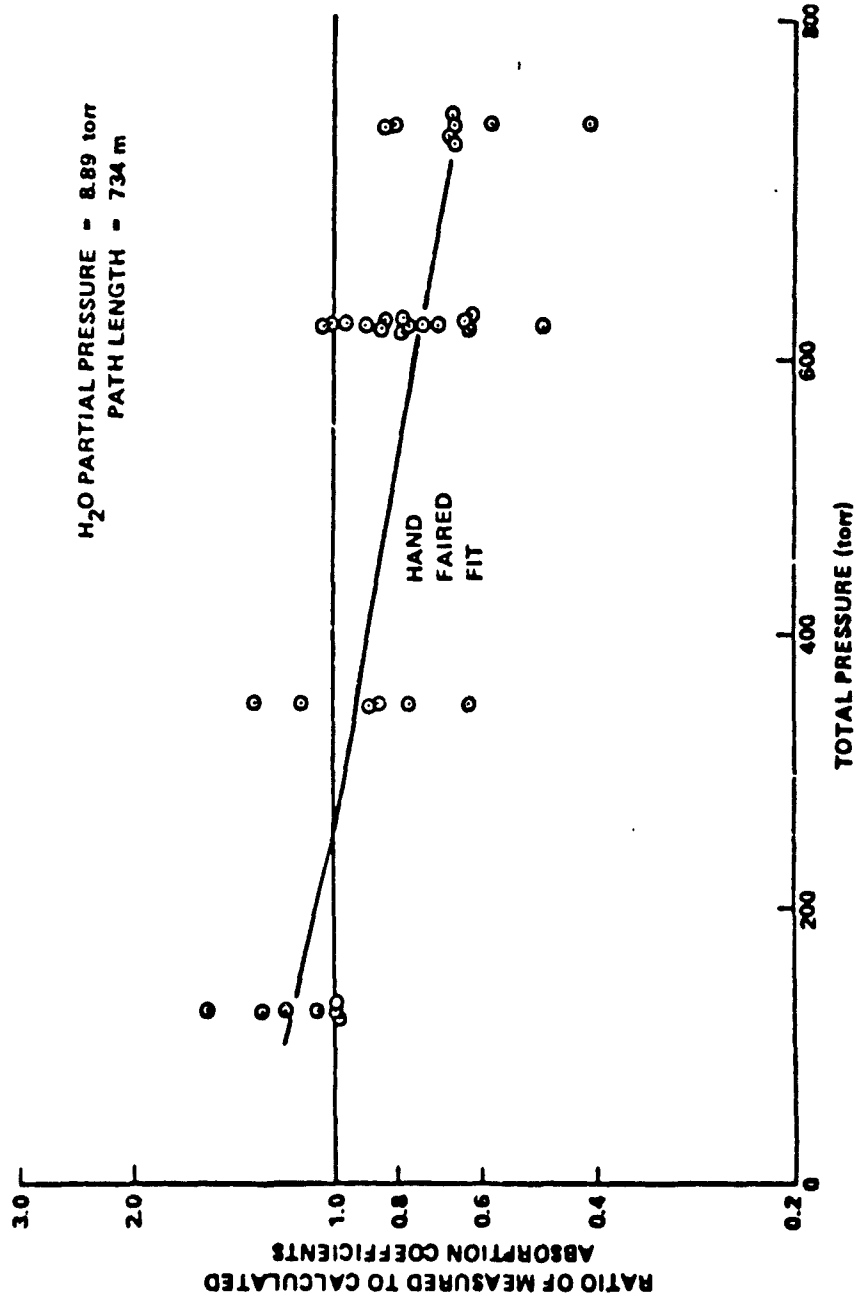

Figure 4. Comparison of measured and Lorentz-calculated absorption coefficients by Long [30].

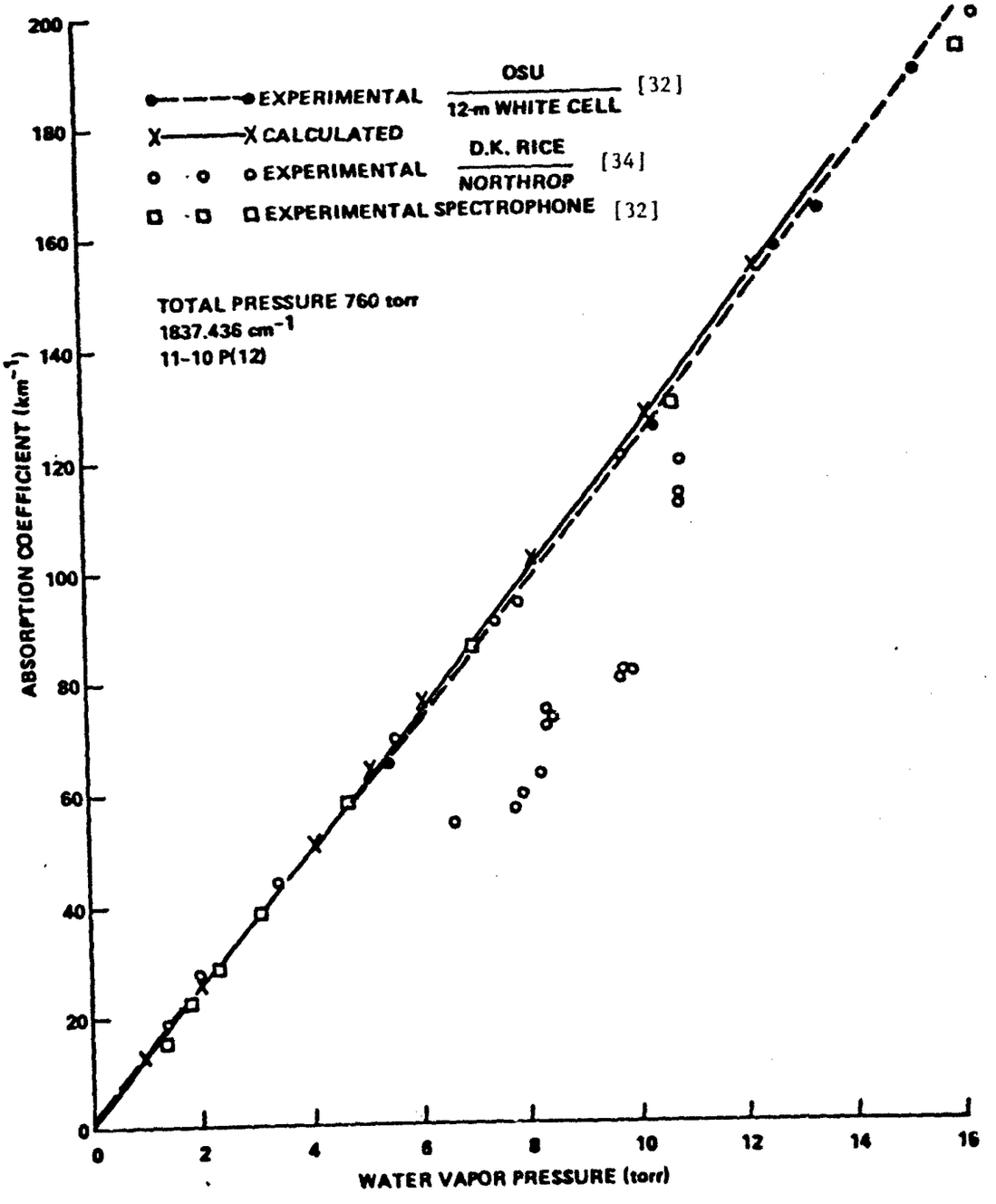

Figure 5. Measured and calculated data for water vapor absorption coefficient at 1837.436 cm^{-1} [32].

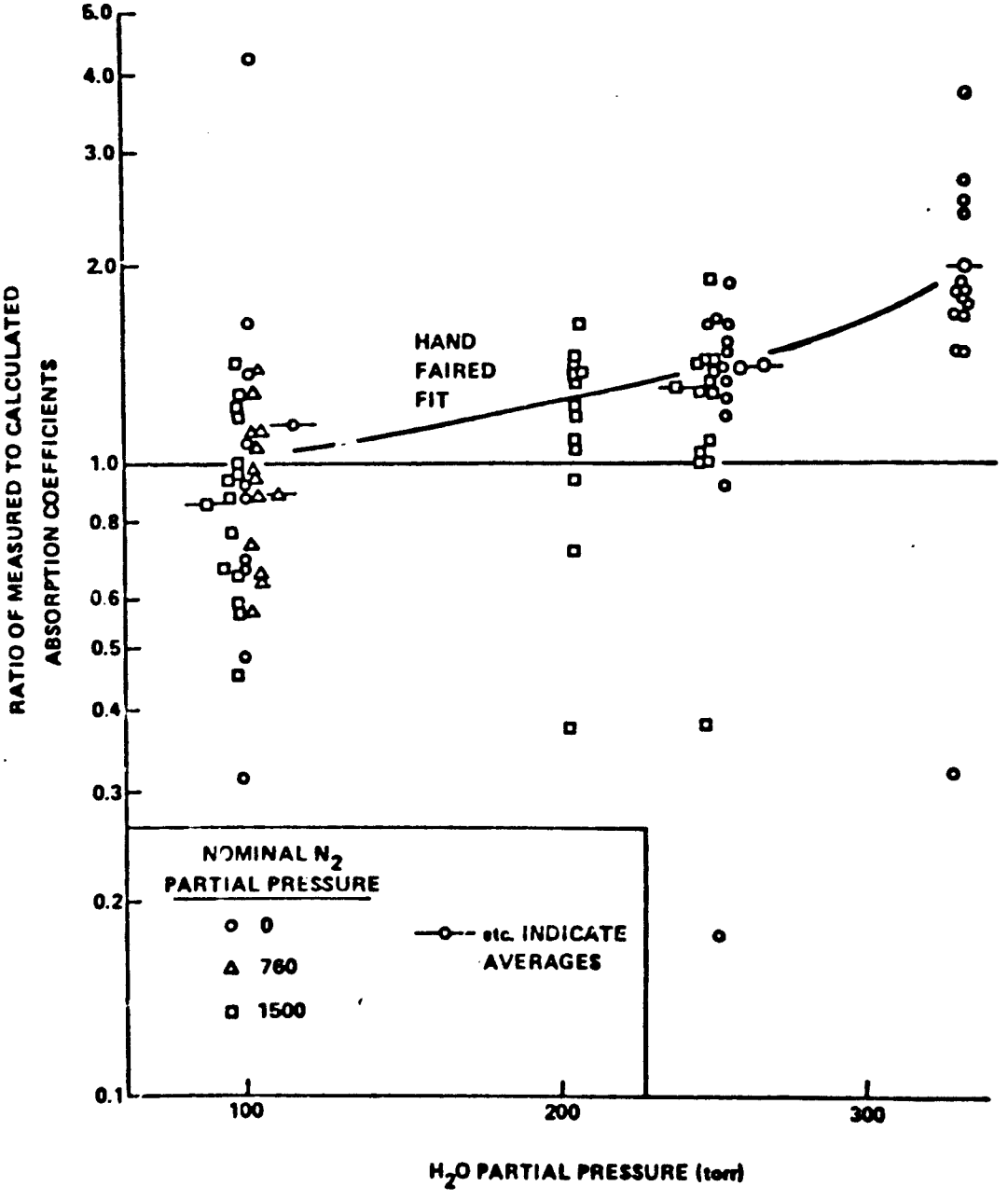

Figure 6. Comparison of measured and Lorentz-calculated absorption coefficients by Rice [35].

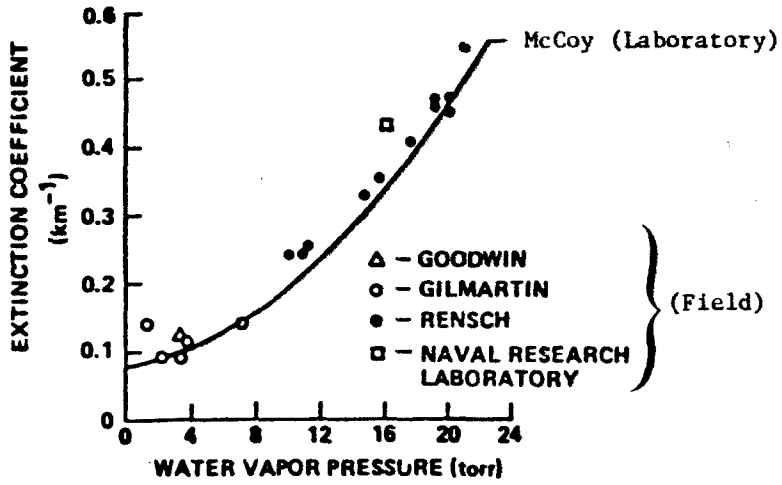

Figure 7. Comparison of laboratory and outdoor extinction data for P20 CO_2 laser line (10.59 μm) [4].

McCoy et al. [13] and unpublished data by Gilmartin of MIT Lincoln Laboratory are in very good agreement with the laboratory measurements and tend to verify the nonlinear dependence on water vapor content. Unfortunately, the source of Figure 7 [4] did not give complete references for the data of Goodwin or of the Naval Research Laboratory; the data attributed to Rensch is apparently a partial set of that given by McCoy et al. [13].

Extensive outdoor measurements of the attenuation of DF laser radiation were conducted by NRL [36] along a 5-km path at the Capistrano test site in California during June to September 1975. In Table 9, these measurements are compared with values calculated by using AFGL line parameters for 22 DF laser lines. It is seen that the measurements are usually about the same as the calculations, or larger (allowing "room" for aerosol attenuation), except for a few lines [i.e., $P_2(8)$, $P_1(9)$, $P_2(4)$, $P_1(7)$, $P_1(6)$, and $P_1(5)$]. Dowling [36] does not discuss this problem, but it is interesting to note that these lines all are near the larger frequency half of the spectral range of the measurements.

Later experiments by NRL [37], at Cape Canaveral Air Force Station during the spring of 1977, measured the atmospheric attenuation of radiation from HeNe, Nd-YAG, DF, CO, and CO_2 lasers. These measurements,

TABLE 9. COMPARISON OF RADC FIELD MEASUREMENTS WITH LABORATORY MEASUREMENTS

DF line	H_2O pressure (torr)	Dew point depression (°F)	Humidity (%)	Laboratory-measured absorption coefficient (km^{-1})	Field-measured absorption coefficient (km^{-1})	Ratio field/lab
$P_{2-1}(8)$	11.23	11	64	3.33E-2	9.5E-1	28.8
	10.14	34	52	3.03E-2	7.82E-1	25.8
	15.76	21	52	4.53E-2	6.83E-1	15.1
	14.9	13.2	62	4.31E-2	6.09E-1	14.1
	4.05	32	37	1.41E-2	1.37E-1	9.7
	4.05	32	37	1.41E-2	9.81E-2	7.0
	4.05	32	37	1.41E-2	9.11E-2	6.5
	4.05	32	37	1.41E-2	7.45E-2	5.3
	4.05	32	37	1.41E-2	7.44E-2	5.3
	3.15	41	29	1.17E-2	1.08E-1	9.2
	3.15	41	29	1.17E-2	2.3E-2	2.0
	3.15	41	29	1.17E-2	3.0E-2	2.6
	3.15	41	29	1.17E-2	1.2E-1	10.3
$P_{3-2}(8)$	9.45	20		4.0E-2	5.9	147.5
	9.45	20		4.0E-2	6.4	160.0
$P_{2-1}(6)$	9.83	14		5.25E-2	8.52E-1	16.2
	8.76	14		4.75E-2	8.14E-1	17.1

over a 5.1-km path near the ocean, were thought to be influenced much more strongly by aerosols than were the California data, probably due to changes in offshore and ocean wind conditions at the Florida site. Analysis of this data is not yet complete.

Another well-controlled measurement of the atmospheric attenuation of the radiation of four DF laser lines was conducted at a 610-m-long outdoor site at Rome Air Development Center [7]. This site is approximately 24 km from the nearest urban environment, so urban and industrial pollution should be small. However, the path extends 0.9-4.6 m above low-lying wet grasslands and wet swampy areas, so the water content in the path was thought to be higher than that monitored at the receiver and transmitter locations; also, high levels of water-type aerosols were suggested. These field measurements are compared to laboratory measurements, showing that they are factors of from 2 to 30 higher than laboratory measurements. In Table 9, this factor seems to correlate well with relative humidity, supporting the above rationalization of these discrepancies. The laboratory measurements used in the comparison were a composite of individual measurements on various atmospheric species from different sources -- Mills [20], Deaton et al. [19], Meyers [38], and Burch et al. [39] -- but do not include the effects of aerosols. However, even after accounting for nominal aerosol attenuation, the field measurements are still generally much larger.

Another field measurement, by Borisov [40] as reported by Adiks et al. [41], suffers from the opposite deficiency. That is, measured atmospheric attenuation of CO_2 laser radiation seems to be well below several laboratory measurements and theoretical calculations. This implies difficulty with this particular field measurement by Borisov, since the other data are in general agreement. In general, however, the existing laboratory and field measurements tend to support the currently accepted theoretical information on molecular line absorption.

Modeling of molecular line absorption is a highly developed procedure; and if the proper input values are available (e.g., line parameters, laser position, molecular concentrations), it generally leads to very accurate results. The procedure is one of simply summing the contributions to the total absorption coefficient due to all the absorption

lines i for each molecular species j:

$$k = \sum_{j=1}^{m} \sum_{i=1}^{n} k_{ij} \tag{12}$$

where k_{ij} is the absorption coefficient as given by the Lorentz, Voigt, or Doppler expressions (depending on the total pressure as discussed earlier in this section) for the ith absorption line of the jth molecular species. Thus, the model simply evaluates a large number of individual absorption coefficients based on equations given earlier and a line parameter compilation and totals them all. The determination of how many absorption lines n to consider is generally based on the location of the absorption line relative to that of the laser. That is, absorption lines are considered one by one, starting at the nearest to the laser, until all lines within some preselected cutoff distance have been considered. This cutoff is generally taken to be 25 cm^{-1} unless there is information to the contrary. Note that this summation is carried out in both spectral directions from the laser line.

Several computer codes have been developed to carry out this calculation, most of them using the AFGL Line Parameter Compilation [3]. Probably the code that is best documented and most widely accepted is the AFGL code LASER [42]. This code is also most likely to be maintained and updated, since such maintenance apparently is one of the charters of the Air Force Geophysics Laboratory. This code is also convenient because it incorporates the most generally accepted models for molecular scattering and continuum absorption, as well as typical models of aerosol extinction.

There are other models available that use an approximate relationship in place of the Lorentz format large distances from the absorption line center. These codes (e.g., SYNSPEC of Science Applications, Inc.) are considerably faster, with little degradation in accuracy; so consideration of absorption lines far from the laser line, as necessary

in some spectral regions (e.g., CO, HF as discussed previously), can be accomplished economically. However, SYNSPEC is neither documented nor widely distributed, so it would probably not be the best choice for the present purposes.

Another class of model has been developed by Tuer [43] which is intended for easy evaluation of molecular absorption for a limited number of laser lines. This model is based directly on the results of other, more sophisticated computer codes, such as LASER or SYNSPEC, by using simple analytic functions of temperature (T) and humidity fitted to their calculated results:

$$k \cong k_0 + \left(k_1 p + k_2 p^2\right) T + \left(k_3 p + k_4 p^2\right) T^2 \qquad (13)$$

where p is the water vapor partial pressure, and k_0, k_1, . . ., k_4 are coefficients determined from the least-squares fit. An example of the results of this model is shown in Figure 8. It is anticipated that such a procedure could easily and effectively be applied to the problem of evaluating the effect of molecules in the atmosphere on laser transmission, for specifying safety considerations. Separate tables of coefficients would be required for various total pressures so that the extinction for paths at altitude could be estimated.

Molecular Continuum Absorption--In certain spectral regions, the primary contributor to the atmospheric molecular absorption of laser radiation is the continuum absorption by atmospheric gases. Therefore, the accuracy with which the continuum absorption can be predicted in these spectral regions has a significant impact on determining the safe laser radiant emittance levels for a given situation. The accuracy with which the infrared transmission in the atmosphere can be calculated has improved slowly since the development in the early 70's of the line-by-line modeling codes by McClatchey et al. [2]. This is due largely to the uncertainties in the level of the continuum in several spectral regions, and how it varies with temperature, pressure, and molecular concentration.

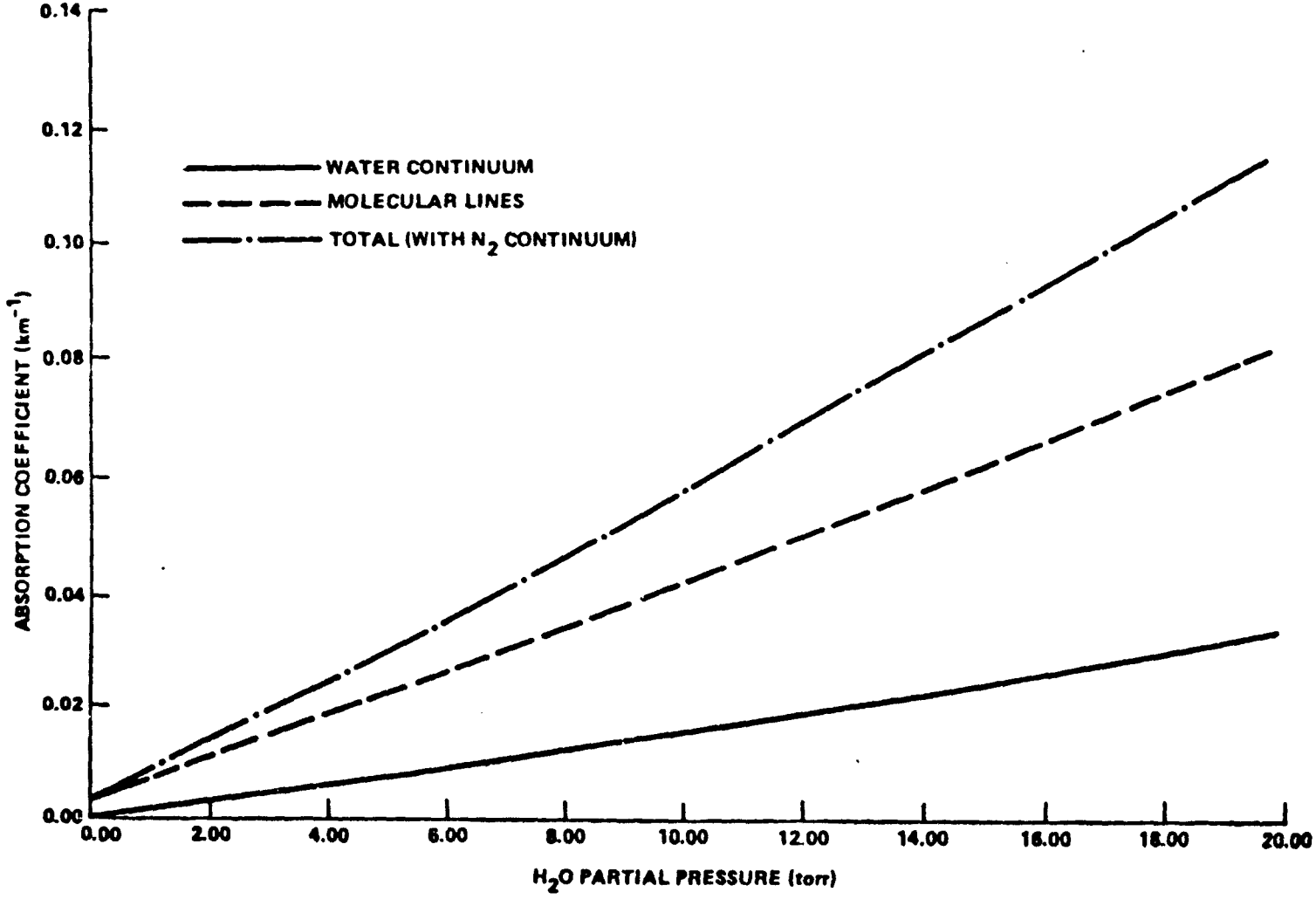

Figure 8. Sample results from model of laser radiation as a function of temperature and humidity, for $P_1(9)$ DF line at 2691.607 cm^{-1}.

In this section, the current state-of-knowledge on theoretical and experimental aspects of infrared molecular extinction is presented. Experiments and data on the water vapor continuum absorption are discussed also. Included is a brief summary of as yet unpublished findings by Burch in the 3-5-μm region at ambient temperature. Recent nitrogen and carbon dioxide continuum absorption experiments are discussed below. Current experiments and models in the areas of continuum absorption by H_2O, N_2, and CO_2 are also compared. Also discussed are the following continuum absorption mechanisms: (1) The combined effects of the far wings of a large number of strong lines; (2) transitions within dimers and larger polymers of water vapor molecules, possibly present in small concentrations in atmospheric paths; and (3) the effects of far wings, such as sub-Lorentzian character of CO_2 lines, and the self-broadening effects of water vapor on far line wings. Finally, in Appendix A, recent measurements of molecular continuum absorption are summarized.

Temperature dependence of the continuum absorption of water vapor and nitrogen and accurate determination of the spectral shape of the CO_2 continuum absorption are areas of major interest in infrared laser absorption experiments. Data are available for spectral regions 3-5 μm and 8-12.5 μm for water vapor, 3.7-4.8 μm for N_2, and 5-12.9 μm and 1.41-1.47 μm for CO_2. Of primary concern in current experiments is the temperature dependence of the H_2O continuum absorption in the 3-5-μm and 8-12.5-μm regions. Reliable quantitative data in these spectral regions at realistic atmospheric conditions will lead to more reliable attenuation predictions, and possibly to an understanding of the mechanism responsible for the absorption in these regions.

The continuum absorption in the 3-5-μm spectral region is thought to be simply far-wing absorption of the strong water vapor lines that are a few hundred wavenumbers away [37]. The investigation of the pressure and temperature variation of the weak vapor absorption in the 3-5-μm window has tended to follow the experimental approach of Burch et al. [44]. Cosden et al. [37] present data in the 3-5-μm region on the temperature and pressure variation of the self-absorption coefficient of

H_2O, and of the ratio of the foreign to self-broadening coefficients at three temperatures -- 338, 384, and 428 K. Briefly, the conclusions of their work were: (1) Absorption due to water vapor in the far wings is quadratic in the water vapor pressure (i.e., $k \propto p^2$); (2) In the presence of a foreign gas, additional "broadening" is observed which varies linearly with the foreign gas pressure, giving the continuum absorption coefficient in this region the form:

$$k \propto \frac{P_{H_2O}}{T} C_{H_2O} \left[P_{H_2O} + B\left(P_t - P_{H_2O}\right) \right] \tag{14}$$

where

P_{H_2O} = Pressure in atmosphere of water vapor

P_t = Pressure in atmosphere of water vapor and foreign gas

C_{H_2O} = Wavelength-dependent coefficient obtained by Burch (see Figure 9)

B = Foreign broadening coefficient;

and (3) Continuum absorption decreases as the temperature (T) is increased, following the form exp(-const./T).

Since this early work, major efforts have been made by Damon et al. [45], Mills [20], White et al. [46,47], and Watkins et al. [10] to verify and extend Burch's data. These groups utilized deuterium fluoride (DF) lasers having 26 lines in the 3-5-μm window. Damon et al. [45] present spectrophone measurements of the absorption coefficient as a function of water vapor partial pressure up to approximately 15 torr, with each sample buffered to a total pressure of 760 torr with artificial air (80 percent N_2/20 percent O_2). To extract the H_2O continuum absorption coefficient at 14.3 torr, the measured HDO absorption and the calculated (AFGL tape) H_2O absorption from nearby lines were subtracted from the total extinction. The results for the absorption coefficient at six wavelengths are reproduced in Table 10 and plotted in Figure 10.

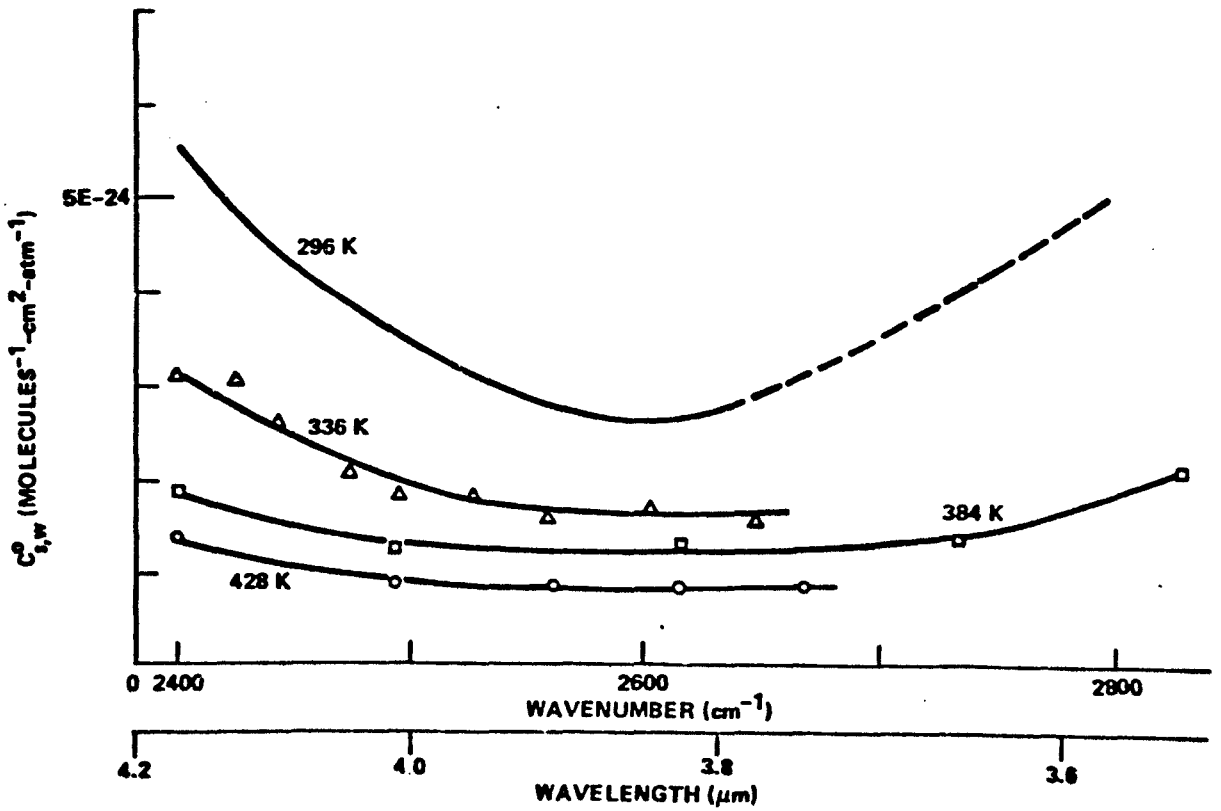

Figure 9. Measurements of self-broadened coefficient of water vapor continuum absorption at three temperatures, and an extrapolation to 296 K [44].

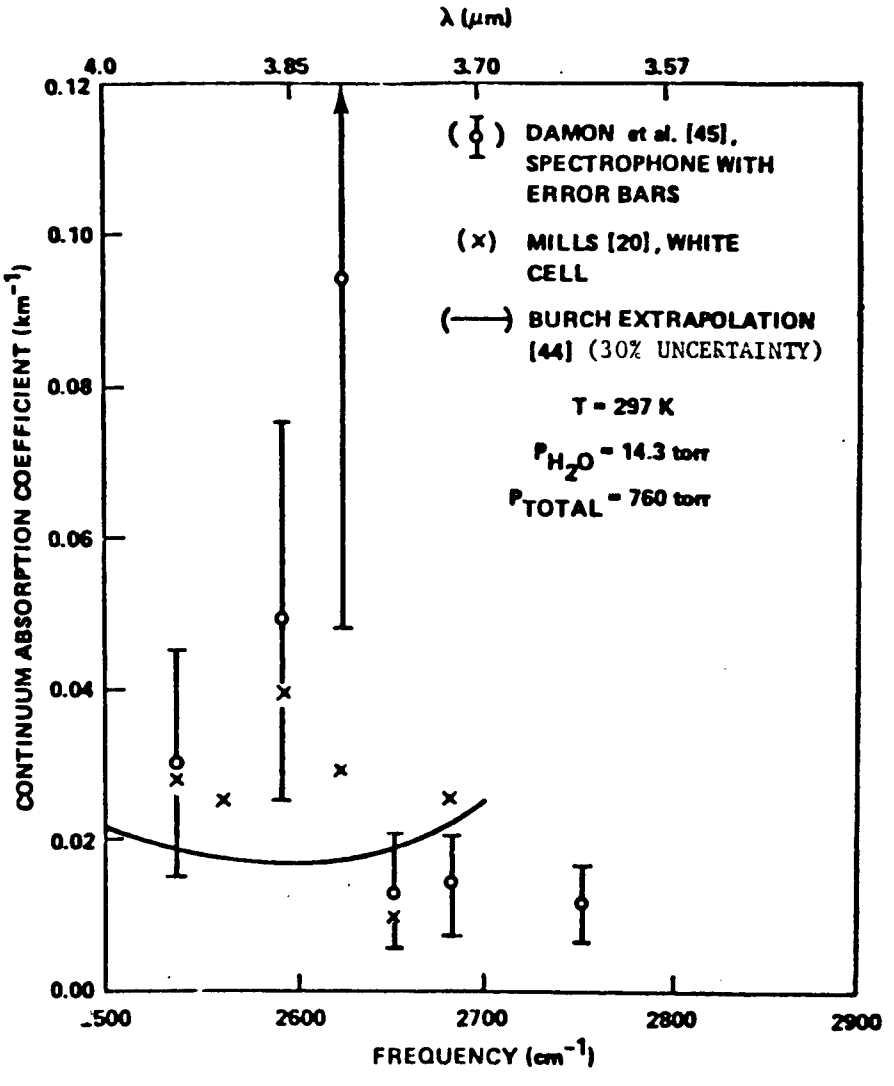

Figure 10. Measured H_2O continuum absorption coefficients as a function of frequency compared to Burch extrapolation.

These authors quote a water vapor continuum absorption coefficient at these wavelengths of k=0.04±0.02 cm^{-1}; however, the data indicate a somewhat larger spread in uncertainty. Note that this is for isotropically pure H_2O at a partial pressure of 14.3 torr and a temperature of 297 K. In Figure 10, we have compared their results with an absorption coefficient obtained by extrapolating the Burch data given in Figure 9.

Using the values of the self-broadening coefficient from Figure 9 in Eq. 14, we obtain extinction coefficients that range between 0.02 and 0.03 km^{-1} in the wavenumber range of 2600 to 2800 cm^{-1}. The agreement in this spectral range is good and lends support to the Burch extrapolation; however, the support is weak at best because the quoted error in the spectrophone data is so large (±50 percent).

Also shown in Table 10 and Figure 10 are data from two White cell (1.34-km pathlength) measurements, by Damon [45] and Mills [20], at 14.3 torr water vapor pressure, 760 torr total pressure (buffered with N_2), and at a temperature of 297 K. The uncertainty presented in Table 10 for the spectrophone data is that quoted by the experimenters for their average absorption coefficient. Mill's White cell and Damon's spectrophone values differ from each other by 2.5 standard deviations at the lower frequency. At the higher frequency, the two measurements are in better agreement, although they are not within one standard deviation.

The most recent data available on water vapor absorption in the 3-5 μm window are from White et al. [46,47] and Watkins et al. [10]. White et al. measured the water vapor absorption coefficient at 25 DF lines in a White cell at 338 K, with a water vapor partial pressure of 72 torr. White cell and spectrophone data are also presented for T=296 K and 14.3 torr water vapor. All samples were buffered to a total pressure of 760 torr with a 4:1 mixture of N_2 to O_2. The nitrogen continuum was experimentally subtracted. The 338 K, p_{H_2O} = 72 torr data were taken to allow a direct and unambiguous comparison with Burch's data taken under similar conditions, and to provide data beyond the frequency range covered by Burch at this temperature and pressure. The continuum absorption coefficients were derived by subtracting the HDO and H_2O line contributions from the total water vapor absorption. Their high-temperature results are compared in Figure 11. The calculated HDO and H_2O line contributions were based on the January 1976 updated AFGL data tape. Considering the 30 percent uncertainty contained in the Burch results, the two sets of data in Figure 11 are consistent in this high-temperature, high-pressure region.

TABLE 10. H_2O EXTINCTION COEFFICIENT MEASURED BY DAMON [45] AND MILLS [20] WITH CALCULATED H_2O LINE ABSORPTION AND MEASURED HDO ABSORPTION SUBTRACTED (p_{H_2O} = 14.3 torr; p_T = 760 torr; T = 297 K)

$$\left\{k_{H_2O}^{(meas)} - \left[k_{HDO}^{(meas)} + k_{H_2O\text{-line}}^{(calc)}\right]\right\} \ (km^{-1}) \times 10^{-2}$$

DF line	Frequency (cm^{-1})	Damon [45]		Mills [20]
		Spectrophone	White cell	White cell
$P_{3-2}(8)$	2546	3.15 ± 1.57		2.85 ± 0.001
$P_{3-2}(7)$	2570			2.64 ± 0.004
$P_{3-2}(6)$	2594	4.92 ± 2.46		3.92 ± 0.023
$P_{2-1}(8)$	2631	9.44 ± 4.72[a]	3.8 ± 0.5	2.73 ± 0.002
$P_{2-1}(7)$	2656	1.38 ± 0.69	10.3 ± 1.0	0.76 ± 0.01
$P_{2-1}(6)$	2680	1.26 ± 0.63		2.24 ± 0.001
$P_{2-1}(3)$	2750	1.04 ± 0.52		

[a]Calibration questionable.

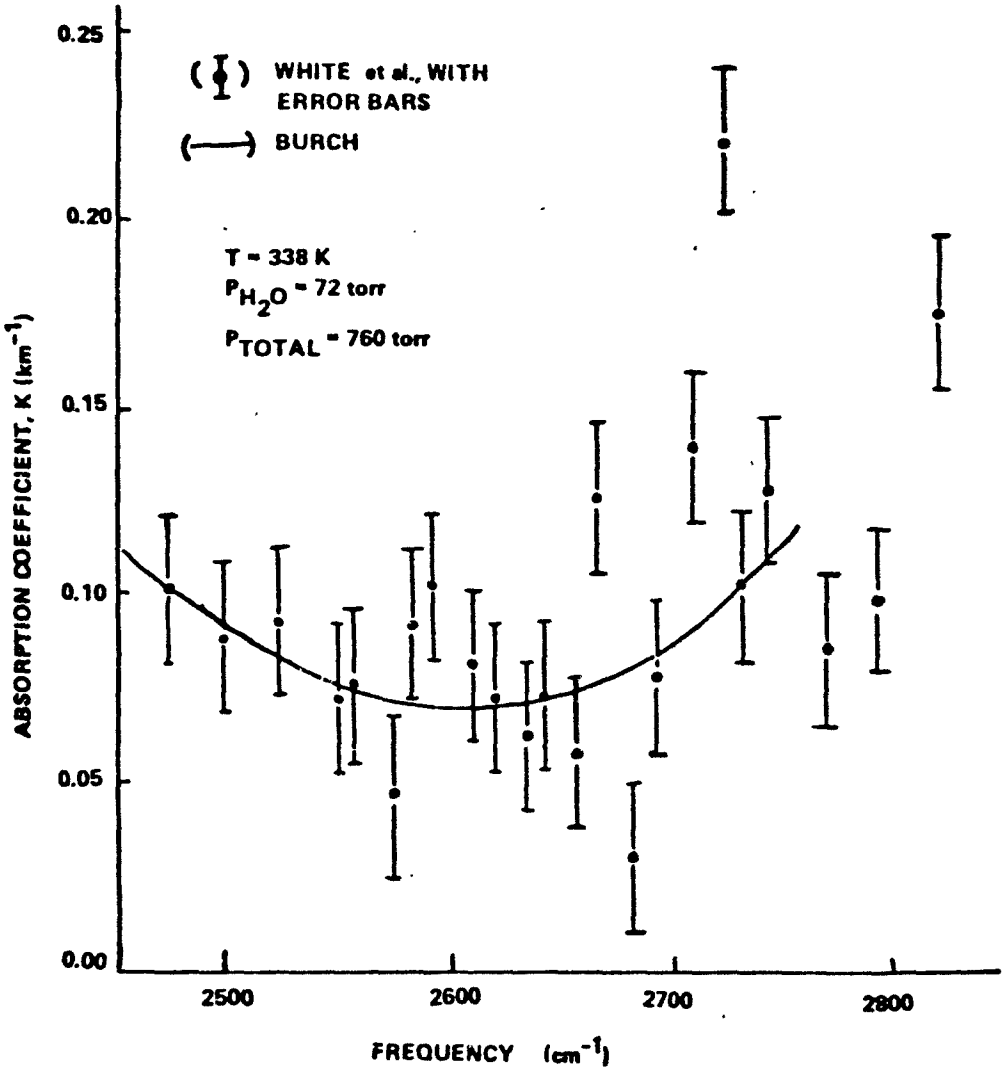

Figure 11. Water vapor continuum measured by White et al. [46,47] and Burch [44].

Additional continuum data by White et al. [47] are presented and compared in Figure 12 with the Burch extrapolations for nominal atmospheric conditions (i.e., T=296 K and p_{H_2O}=14.3 torr). One set, from spectrophone and White cell measurements, represents absorption by natural water vapor, from which the AFGL calculated HDO and H_2O line contribution have been subtracted. The second set is White cell data from HDO-depleted (2 percent of natural abundance) water vapor samples. For ease in comparing data, the error bars on the HDO-depleted data and

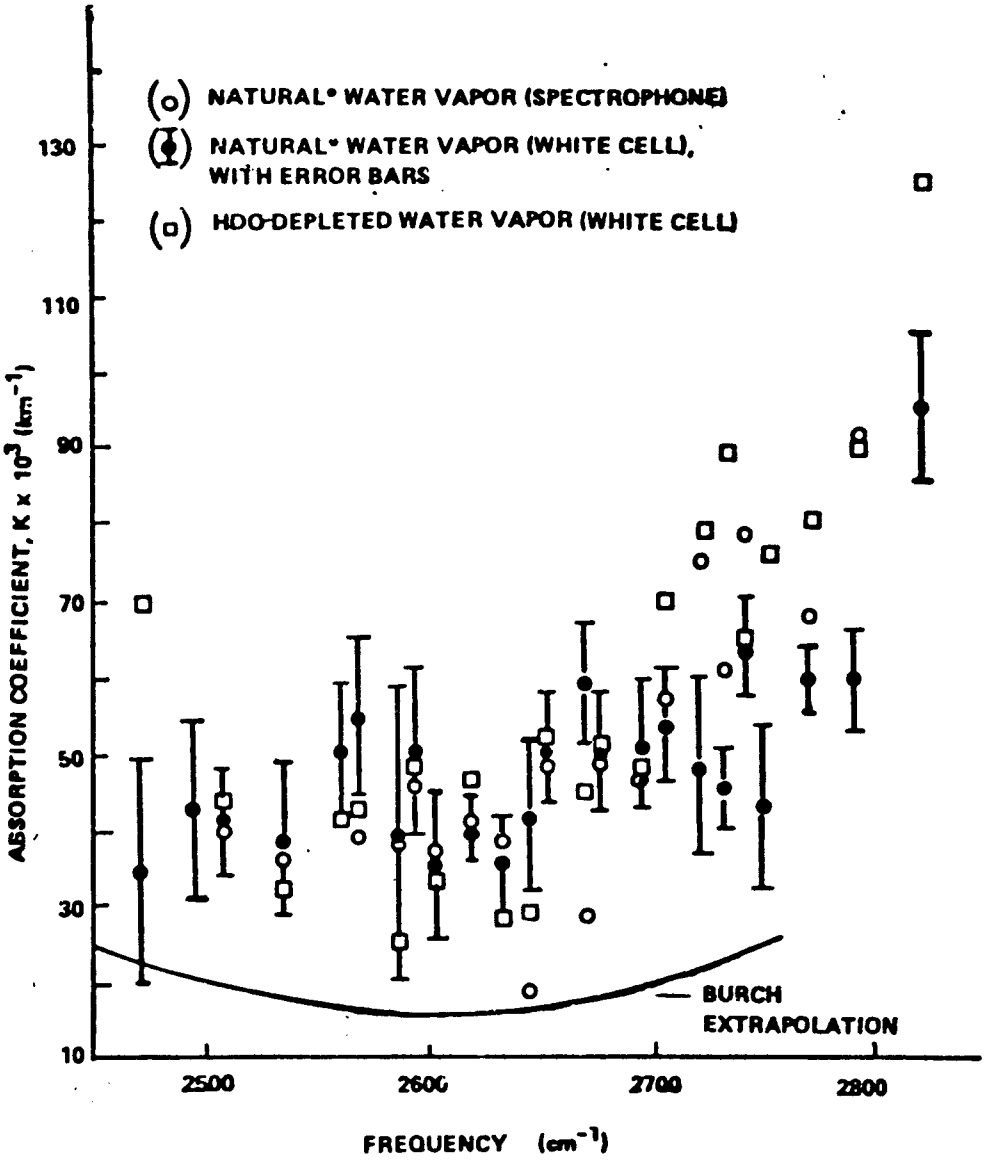

*CALCULATED HDO LINE ABSORPTION HAS BEEN SUBTRACTED.

Figure 12. Water vapor continuum measured by White et al. [46,47] compared with the extrapolated Burch continuum; T = 296 K, p_{H_2O} = 14.3 torr.

the spectrophone data were omitted. Their error bars were comparable to those shown. These data were averaged by White et al. and then compared to the Burch result. From this comparison, they concluded that the Burch extrapolation underestimates the continuum in the 3-5-μm region.

We conclude the discussion of the state-of-knowledge in 3-5-μm experiments with a summary of the sequel to this last work (by White), in which Watkins et al. [10] present new White cell data at 298 K, 14.3 torr water vapor, and several different foreign-broadening gas pressures. Their data for 764.3 torr total pressure is in general agreement with the earlier data by White [46] (i.e., falls within the error bars of White's earlier data presented in Figure 12), but lies systematically closer to the Burch extrapolation at this temperature. These authors also present (see Figure 13) new determinations for the ratio of foreign- to self-broadening coefficients (C_f/C_s) at 26 DF laser frequencies. Their weighted average value for this ratio is $C_f/C_s=0.011$, at T=298 K and $p_{H_2O}=14.3$ torr. The weighted average is formed by weighting the individually measured values of C_f/C_s with the measured extinction coefficients at zero-broadening pressure and normalizing to the sum of extinction coefficients. This weighted average is expressed in the following form:

$$\frac{\overline{C_f}}{C_s} = \sum_{j=1}^{26} \left(\frac{C_f}{C_s}\right)_j k_j(p_f = 0) \Bigg/ \sum_{j=1}^{26} k_j(p_f = 0) \qquad (15)$$

where the $k(p_f=0)$ is the extinction coefficient extrapolated to zero foreign gas pressure. This ratio of foreign- to self-broadening is more than an order of magnitude smaller than the value obtained by Burch [44] at 338 K (i.e., $C_f/C_s=0.12$).

Based on their result for the ratio C_f/C_s, Watkins et al. propose a somewhat ad hoc model for the water vapor continuum absorption coefficient at these frequencies. By assuming a third contribution to the continuum absorption coefficient, which is independent of foreign-broadening pressure, and reanalyzing their data, they obtained the value

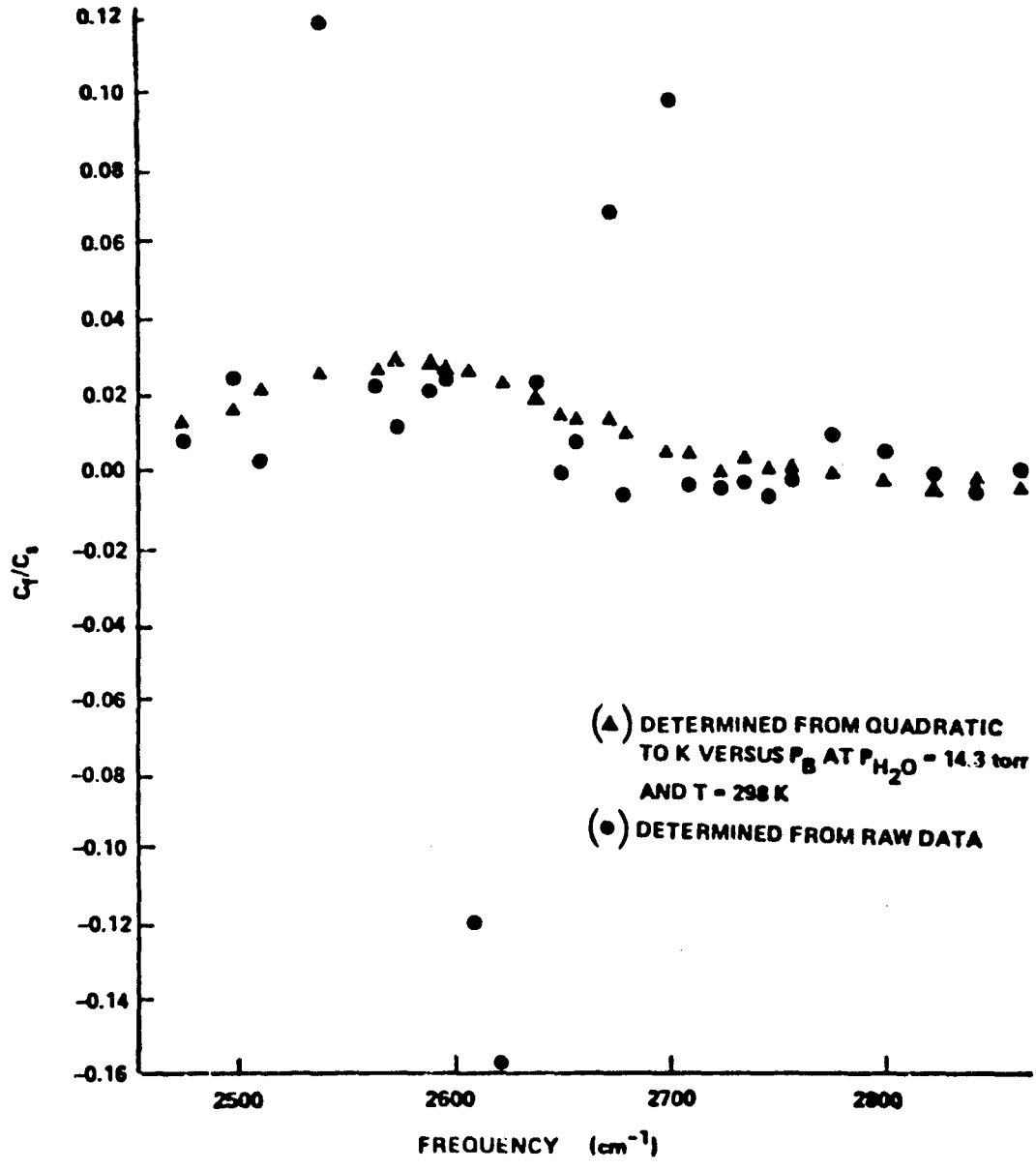

Figure 13. Ratio of foreign- to self-broadening coefficients at 26 DF laser lines before (●) and after (▲) curve fitting the measured absorption coefficients, Watkins et al. [10].

of this third contribution. This additional absorption term is hypothesized to result from water vapor dimers. With this assumption and the additional assumption that the Burch extrapolation is valid and represents only far-wing absorption, the Burch continuum is subtracted from their data at each wavelength. So by hypothesis, what remains is the water vapor dimer absorption coefficient. The temperature dependence of this term is under investigation by Watkins et al. [10].

Burch has completed a new experiment in the 3-5-μm region on the water vapor continuum at both high and ambient temperatures [48]. His high-temperature data (338 K) agree with his earlier data, and hence with the 338-K data of White et al. [47]. His low-temperature (near 296 K) data, however, fall below those of White et al. Burch has found that heating the mirrors in White cells during ambient temperature experiments can produce increases of up to an order of magnitude in the transmittance. He attributes this to absorbed water vapor on the mirror surfaces. McClatchey indicated [48] that the new version of LOWTRAN, LOWTRAN V, will use a water vapor continuum in the 3-5-μm region based on recommendations by Burch. The new model will probably be lower than White's data [49].

In concluding the state of the 3-5-μm water vapor continuum measurements, it is worth noting that in 1971, Burch [44] reported that the transmitted signal slowly decreased over a period of several hours following the filling of his White cell. He attributed at least part of this anomalous absorption to a water vapor film that formed on the mirror surfaces. He also found that the signal could be retrieved by complete evacuation of the cell. These early results of Burch and his recent attention to the temperature dependence of this absorption lead to the reasonable conclusion that until this large systematic error is quantified, good low-temperature White cell data on water vapor continuum absorption are accurate to approximately ±30 percent in this wavelength region. This is the error quoted by Burch [44] in 1971 for his low-temperature data.

In the 8-12-μm region, early field data by Kondrat'yev et al. [50], taken at three elevations (sea level, 310 m, and 3100 m) under carefully monitored atmospheric conditions, show the general dependence of the continuum absorption coefficient on wavelength (Figure 14). Considering the lack of control over such factors as temperature and aerosol content inherent in their experiment, the data can only be regarded as qualitative.

One of the earliest experiments claiming to provide evidence for the H_2O dimer contribution to continuum absorption in the 8-12-μm window is that of Varanisi [51]. The absorption coefficient for p_{H_2O} = 1 atm at three rather high temperatures (400, 450, and 500 K) is plotted in Figure 15 as a function of frequency. To obtain a semiempirical estimate of the dimer-binding energy, Varanisi first defines what he terms "an average absorption coefficient per particle" by the relation:

$$\bar{k}(\nu)T \quad [\text{Sum of intensities (in cm-g}^{-1}\text{) of all the lines between 600 and 1000 cm}^{-1}]/400 \text{ R} \qquad (16)$$

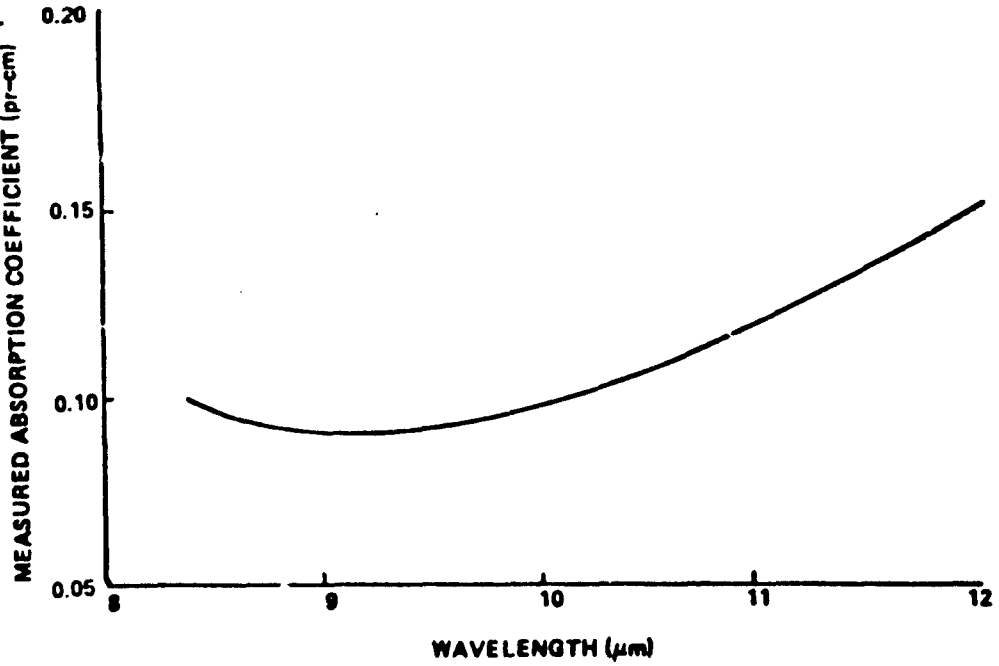

Figure 14. Qualitative shape of wavelength dependence of H_2O continuum absorption coefficient from data of Kondrat'yev et al. [50].

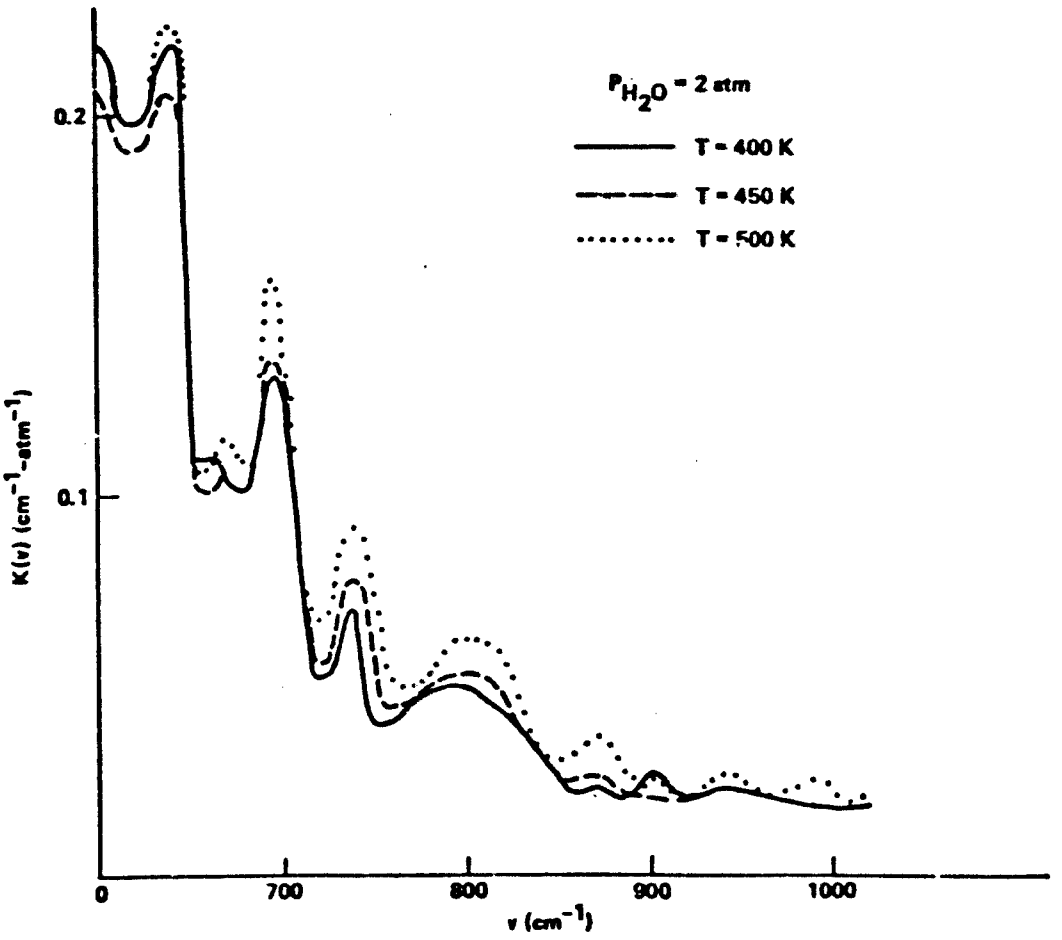

Figure 15. Plot of the absorption coefficient from Varanisi [51] for p_{H_2O}=2 atm at three elevated temperatures.

where R is the gas constant per gram. Using tabulated values (Benedict and Kaplan [52]) for the line intensities with a temperature dependence assumed to be described by:

$$S \propto \frac{N}{P} T^{-3/2} e^{-(E/RT)} \qquad (17)$$

where $T^{-3/2}$ is the temperature dependence of the rotational partition function, Varanisi plots $\ell n(T^{3/2}[\overline{TK}]_{Theory})$ versus T^{-1}. The tabulated line intensities used are for temperatures of 220, 260, and 300 K. This

plot yields a straight line which can be extrapolated to obtain a theoretical estimate of an average absorption coefficient, $[\overline{kT}]_{Theory}$, at the experimental temperatures of interest. We assume that the difference

$$\Delta(kT) = (\overline{kT})_{measured} - (\overline{kT})_{Theory} \tag{18}$$

between the measured average absorption coefficient (reduction of this quantity from Varanisi's data is unclear) and the theoretical average absorption coefficient is proportional to the number of hydrogen bonds with a Boltzmann temperature dependence:

$$\Delta(kT) \propto e^{-E_{H-H}/RT} . \tag{19}$$

Then a value of 5 kcal/mole is derived for the hydrogen-bonding energy, E_{H-H}, from the data plotted in Figure 15 (taken at p_{H_2O}=2 atm). By increasing the pressure to p_{H_2O}=10 atm, a value of 3 kcal/mole was determined. Varanisi concludes by asserting that his results for E_{H-H} do not change significantly when allowance for far-wing absorption of strong distant lines is made.

McCoy et al. [13] present White cell data on foreign- and self-broadening H_2O absorption at 10.59 and 9.55 μm at a temperature of 298 K. A least-squares fit at λ=10.59 μm to a plot of -ℓn(transmittance) versus $p^2_{H_2O}$ was used to obtain a self-broadened extinction coefficient, given as a function of $p^2_{H_2O}$ by

$$k(10.59\ \mu m) = 8.39\times10^{-4}\ p_{H_2O}(km^{-1}) . \tag{20}$$

Their estimated error was ±0.587x10^{-4} in the coefficient; p_{H_2O} was in torr. At 9.55 μm, these authors obtained

$$k(9.55\ \mu m) = 6.67\times10^{-4}\ p^2_{H_2O}(km^{-1}) \tag{21}$$

with an error of $\pm 0.8 \times 10^{-4}$. Further data are presented for the 10.59-μm transmittance in the presence of foreign gas. In these experiments, the H_2O vapor pressure was varied while a constant total pressure of 700 torr was maintained. A fit of the equation

$$k(10.59\ \mu m) = \alpha \rho_{H_2O}\left[P_T + (B-1)p_{H_2O}\right] \tag{22}$$

to their transmittance data yielded

$\alpha = 4.32 \times 10^{-6}$

B = Self- to foreign-broadening coefficient = 194

P_T = Total pressure

with an estimated error of ±10 percent in α. Using these coefficients and expressing the attenuation in units of $dB\text{-}km^{-1}$ at a total pressure of 760 torr, the absorption loss at sea level was given by McCoy et al. as

$$\text{Loss} = 1.43 \times 10^{-2}\ p_{H_2O} + 3.62 \times 10^{-3}\ p^2_{H_2O}\ dB\text{-}km^{-1}\ . \tag{23}$$

To test this result, field data were taken at 10.59 μm over a 1.95-km outdoor path. The measurements were made at temperatures ranging from 15° to 30°C, and relative humidities of 50 to 90 percent. The field data are plotted in Figure 16, along with the calculated loss using Eq. 23 plus a constant 0.47 $dB\text{-}km^{-1}$ (445 ppm CO_2) loss due to CO_2 absorption (solid curve). The authors point out that the 445 ppm CO_2 is higher than the 330 ppm CO_2 (see dashed line in Figure 16) usually assumed for a standard 25°C atmosphere; however, this higher-than-average CO_2 content was substantiated by measurement of the CO_2 concentration. By virtue of the agreement between the field data and the calculated attenuation based on Eq. 23, McCoy et al. conclude that the absorption

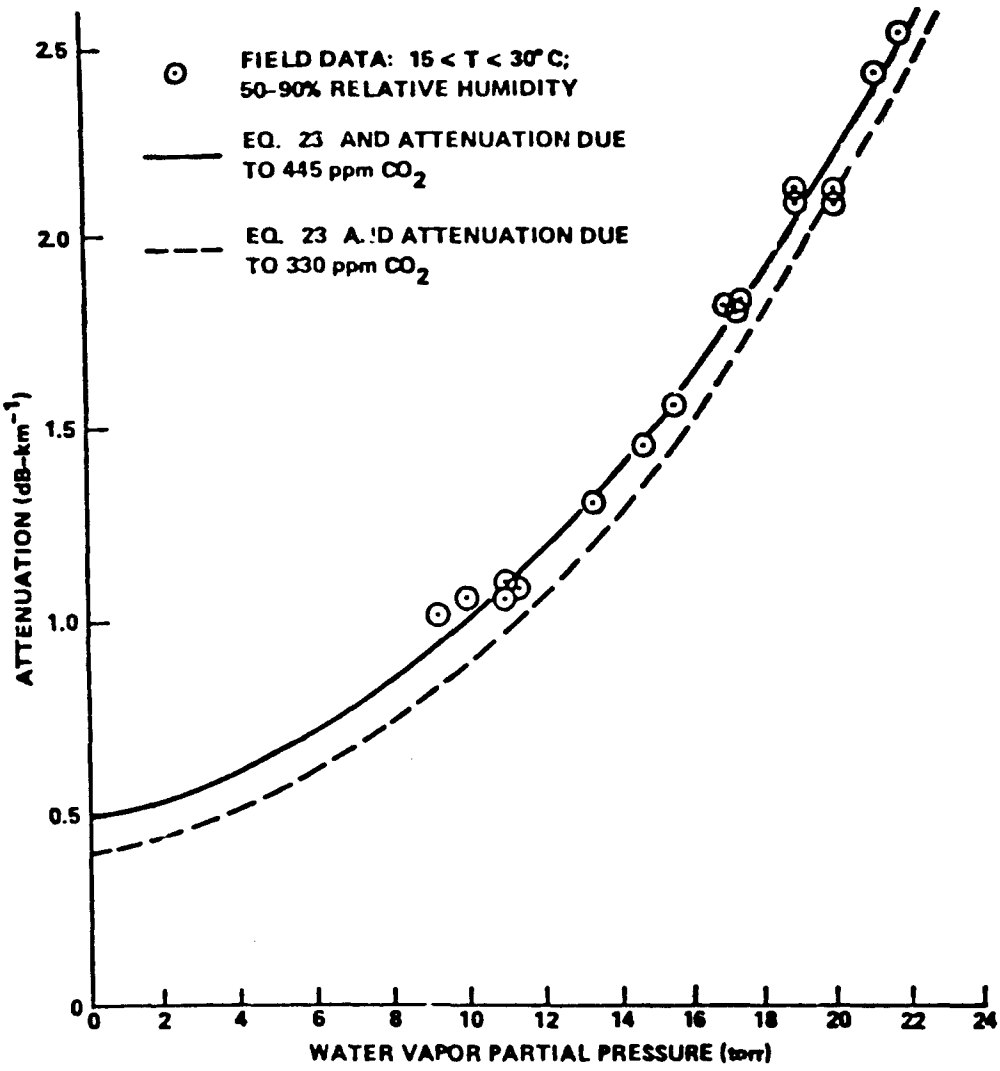

Figure 16. Field data of McCoy, et al. [13], at 10.59 μm compared with calculated attenuation based on Eq. 23 text.

loss is not highly temperature sensitive over the temperature range of their data (15° to 30°C).

Bignell [53] presents water vapor absorption at several wavelengths in the 8-12-μm range. To extract the quoted values of the self-broadening coefficient, the author removed the foreign-broadening contribution from his raw data without quoting the values or the source of the foreign-broadening coefficient used.

Measured absorption coefficients by Moskalenko et al. [54], at 10.6 μm as a function of temperature are displayed in Figure 17. These authors give no interpretation or possible explanation for their observations. The behavior of the water vapor absorption coefficient as a function of temperature reported by these authors has not to date been corroborated by other researchers in this field.

In 1976, Gryvnak et al. [55] reported data at three temperatures in the 8-12-μm region, which modified slightly their earlier results [39] for C_s°, the water vapor self-broadening coefficient. In some cases, the changes in C_s° were as great as 20 percent. These later results are plotted in Figure 18 for all three temperatures — 296, 392, and 430 K. The authors quote an upper bound of ±10 percent for the error in the 392 and 430 K data. The sharp increase in C_s° with increasing frequency above 1150 cm^{-1} (8.70 μm) is attributed by these authors to an increasing contribution from the lines centered just above this frequency. However,

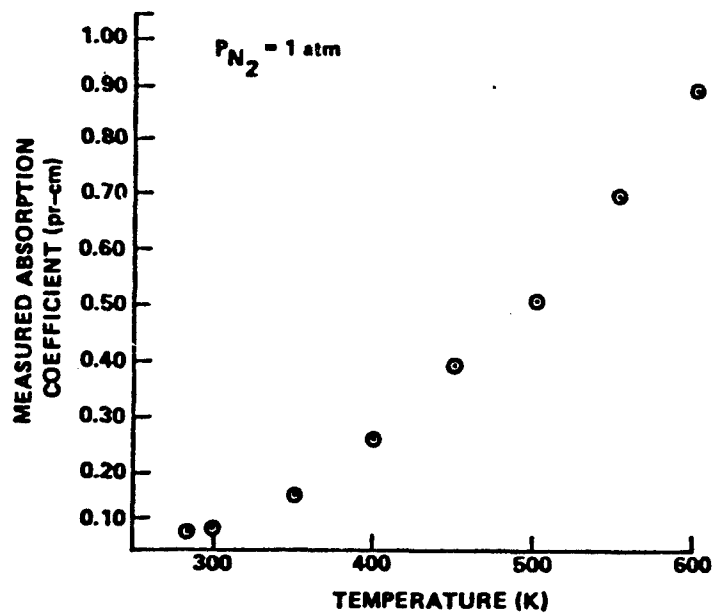

Figure 17. Measured water vapor absorption coefficients as a function of temperature [54].

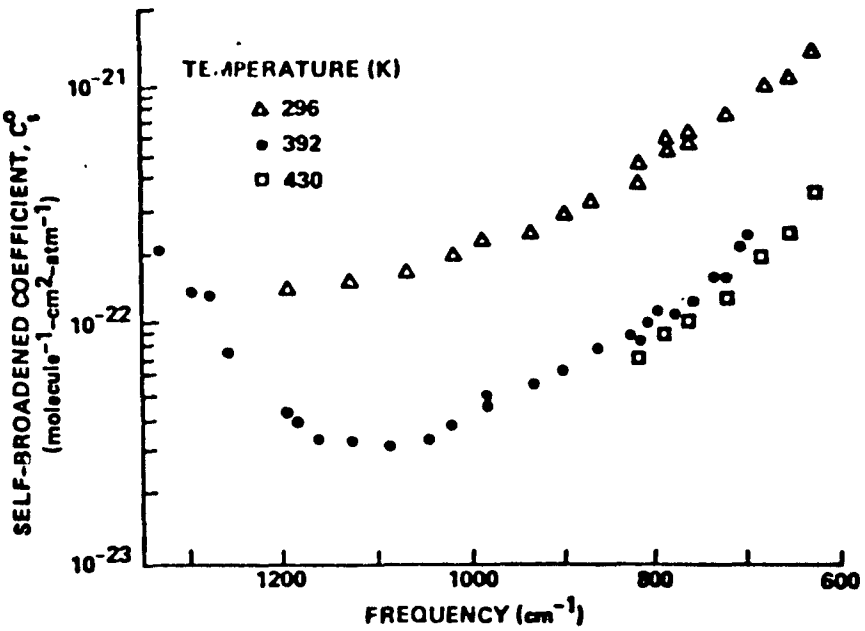

Figure 18. Water vapor self-broadening coefficient, C_s°, as a function of wavelength at three temperatures [55].

they assert that a large portion of the continuum below 1100 cm^{-1} (above 9.1 μm) is probably due to the extreme wings of the very strong lines centered below 600 cm^{-1} (above 16.7 μm). This could account for the increase in the self-broadening contribution with decreasing wavenumber below 1100 cm^{-1}. The conclusion was unchanged from the earlier (1970) report by these authors [39] that the ratio of foreign- to self-broadening coefficient, C_n°/C_s°, is less than 0.005 near 296 K.

Shumate et al. [56] measured H_2O extinction coefficients at 49 wavelengths within two CO_2 laser bands, one centered at 9.4 μm and one at 10.4 μm. These measurements were taken with a spectrophone at three water vapor partial pressures buffered with air to a total pressure of 760 torr, at a temperature of 300 K (see Tables 11 and 12). Direct comparison with the measurements of McCoy et al. [13] at 10.59 μm, discussed earlier, is given in Table 13. The agreement is fair according to Shumate et al. We can compare the data of Gryvnak et al. [55] in this wavelength region with the data from Shumate et al. To make a

TABLE 11. ABSORPTION COEFFICIENTS OF WATER VAPOR IN AIR AT THREE WATER VAPOR PARTIAL PRESSURES: 10.4-μm BAND OF THE $C^{12}O_2^{16}$ LASER [56]

Laser line (001-I)	Frequency (cm^{-1})	Absorption coefficients[a] (10^{-4} cm^{-1})		
		5.0 Torr	10.0 Torr	15.0 Torr
P(32)	932.960	1.39,[b] 0.30[c]	2.32,[b] 0.82[c]	3.63,[b] 1.93[c]
P(30)	934.895	0.36,[b] 0.30[c]	0.95,[b] 0.87[c]	2.01,[b] 1.92[c]
P(28)	936.804	0.33, 0.30[c]	0.87	1.85
P(26)	938.688	0.37, 0.34[c]	0.89	1.78
P(24)	940.548	0.36	1.00	1.92
P(22)	942.383	0.37	0.94	1.97
P(20)	944.194	0.41	1.15	2.18
P(18)	945.980	0.38	1.00	1.97
P(16)	947.742	0.49,[b,d] 0.45[c,d]	1.23,[b] 1.18[c]	2.66,[b] 2.60[c]
P(14)	949.479	0.45,[b] 0.40[c]	1.27,[b] 1.19[c]	2.50,[b] 2.41[c]
P(12)	951.192	0.35,[b] 0.31[c]	1.01,[b] 0.95[c]	2.10,[b] 2.03[c]
P(10)	952.881	0.32	0.91	2.19
R(8)	967.707	1.96,[b] 0.41[c]	3.08,[b] 0.88[c]	4.53,[b] 2.03[c]
R(10)	969.139	0.40,[b] 0.34[c]	0.81,[b] 0.74[c]	1.55,[b] 1.46[c]
R(12)	970.547	1.00,[d,b] 0.97[d,c]	2.12,[b] 2.07[c]	3.32,[b] 3.27[c]
R(14)	971.930	0.97,[d,b] 0.92[d,c]	1.81,[b] 1.75[c]	2.63,[b] 2.56[c]
R(16)	973.289	0.78[d]	1.70	2.59
R(18)	974.622	0.61[d]	1.22	1.88
R(20)	975.930	5.49[d]	11.0	16.8
R(22)	977.214	0.84[d]	1.66	2.67
R(24)	978.472	0.50	1.12	1.90
R(26)	979.705	0.49	1.03	1.78
R(28)	980.913	0.40	0.92	1.66
R(30)	982.096	0.46[d]	1.07	1.97
R(32)	983.252	0.40	1.09	1.96

[a] Measured at 760-torr total pressure, 300-K temperature.

[b] Significant absorption from ammonia observed at this frequency.

[c] Corrected by subtracting the ammonia contribution.

[d] Significant absorption from water lines predicted at this frequency.

TABLE 12. ABSORPTION COEFFICIENTS OF WATER VAPOR IN AIR AT THREE WATER VAPOR PARTIAL PRESSURES: 9.4-μm BAND OF THE $C^{12}O_2^{16}$ LASER [56]

Laser line (001-II)	Frequency (cm^{-1})	Absorption coefficients[a] (10^{-3} cm^{-1})		
		5.0 Torr	10.0 Torr	15.0 Torr
P(32)	1035.474	0.42,[b] 0.39[c]	0.85,[b] 0.82[c]	1.47,[b] 1.43[c]
P(30)	1037.434	0.39	0.77	1.39
P(28)	1039.369	1.30[d]	2.72[d]	4.46[d]
P(26)	1041.279	0.41	0.77	1.37
P(24)	1043.163	0.41,[b] 0.37[c]	0.93,[b] 0.89[c]	1.57,[b] 1.52[c]
P(22)	1045.022	0.47,[b] 0.44[c]	0.96,[b] 0.92[c]	1.62,[b] 1.58[c]
P(20)	1046.854	0.51,[b] 0.36[c]	1.09,[b] 0.88[c]	1.69,[b] 1.44[c]
P(18)	1048.661	0.37,[b] 0.35[c]	0.89,[b] 0.86[c]	1.43,[b] 1.40[c]
P(16)	1050.441	0.47,[b,d] 0.45[c,d]	1.02,[b,d] 1.00[c,d]	1.58,[b,d] 1.56[c,d]
P(14)	1052.196	0.41,[b] 0.38[c]	1.03,[b] 1.00[c]	1.58,[b] 1.55[c]
P(12)	1053.924	0.43,[b] 0.36[c]	0.86,[b] 0.77[c]	1.50,[b] 1.40[c]
P(10)	1055.625	1.15[d]	2.82[d]	3.86[d]
R(10)	1071.884	0.35	0.83	1.25
R(12)	1073.278	0.44[d]	1.17[d]	1.88[d]
R(14)	1074.646	1.48[d]	3.51[d]	5.24[d]
R(16)	1075.988	1.53,[b,d] 0.57[c,d]	2.88,[b,d] 1.60[c,d]	3.54,[b,d] 2.10[c,d]
R(18)	1077.303	0.43	0.99	1.45
R(20)	1078.591	0.40	0.93	1.41
R(22)	1079.852	0.40	0.91	1.38
R(24)	1081.087	0.39	0.95	1.47
R(26)	1082.296	0.36	0.84	1.35
R(28)	1083.479	0.41,[b] 0.38[c]	0.97,[b] 0.93[c]	1.42,[b] 1.38[c]
R(30)	1084.635	6.21,[b] 1.40[c]	8.25,[b] 1.65[c]	9.36,[b] 1.93[c]
R(32)	1085.765	0.58[d]	1.27[d]	1.85[d]

[a] Measured at 760-torr total pressure, 300-K temperature.

[b] Significant absorption from ammonia observed at this frequency.

[c] Corrected by subtracting the ammonia contribution.

[d] Significant absorption from water lines predicted at this frequency.

TABLE 13. COMPARISON OF MEASURED WATER VAPOR ABSORPTION COEFFICIENTS AT 10.59 μm

P_{H_2O} (torr)	Absorption coefficient (km^{-1})	
	Shumate et al. [56]	McCoy et al. [13]
5	0.041	0.038
10	0.115	0.117
15	0.218	0.235
20	0.353	0.396

comparison, we assume C_n°/C_s°=0.005 [55], and p_{H_2O}=15 torr with a total pressure of 760 torr. This comparison is given in Table 14. While the agreement is poor, it must be remembered that the comparison is dependent upon the assumption of a constant foreign- to self-broadening ratio of 0.005. A choice of smaller values would naturally yield a more favorable comparison.

TABLE 14. COMPARISON OF MEASURED WATER VAPOR ABSORPTION COEFFICIENTS AROUND 10 μm (p_{H_2O}=15 torr, P_{total}=760 torr, T=300 K)

Frequency (cm^{-1})	Absorption coefficient (km^{-1})	
	Gryvnak et al. [55]	Shumate et al. [56]
935	0.274	0.192
981	0.262	0.166
1072	0.190	0.125

Coffey [57] presents field-measured water vapor attenuation at 10.7 and 11.6 μm, recorded during flights over sea environments. He analyzed his results by writing the water vapor absorption coefficient in terms of the observed transmittance τ as follows:

$$k(g^{-1}cm^2) = -1/u \ln \tau \qquad (24)$$

where τ is the measured transmission and u is the absorber amount. Coffey then writes k as the sum of two terms:

$$k = k_1\left(p_{N_2} + \beta p_{H_2O}\right) + p_{H_2O}k_2 \qquad (25)$$

where p_{N_2} and p_{H2O} are the nitrogen and water vapor partial pressures in atmospheres, respectively, and β is the self-broadening coefficient, assumed by Coffey to be 6, based on Reference 58. In order to extract from k the values of k_2, Coffey performs a line-by-line calculation to obtain k_1 which was then subtracted from the data. The line-by-line calculations were based on McClatchey's 1973 line data [3] (portions of these HDO line parameters underwent major revisions in 1976). The general trend of the results of this analysis is to confirm the negative temperature dependence of the water vapor absorption observed by Burch et al. [39]. Any quantitative comparison would suffer from uncertainties in (1) the computed values for k_1, and (2) the assumed value for the ratio of foreign- to self-broadening coefficients. Comparing the slope from a $\ell n(k_2)$ versus T^{-1} plot with the temperature coefficient obtained from the second virial coefficient of steam, Coffey concludes that water vapor dimers are responsible for absorption in the 10-12-μm region.

Montgomery [59] presents measurements of the temperature dependence of the self-broadening coefficient, C_s, near 8.33 μm, using a lead-tin-telluride diode laser and a 40.5-m-pathlength White cell. The temperature used ranged from 333 to 473 K. Montgomery first measured the total extinction as a function of the water vapor partial pressure at each temperature. A typical example of this data is plotted in Figure 19, where the error bars indicate fluctuations in laser intensity during the measurements. The straight line is a fit of the data to k/p^2_{H2O}=Const. The result of this fitting at each temperature is then used in the expression

$$k/p^2_{H_2O} = C_s^\circ/k_{Boltz}T \qquad (26)$$

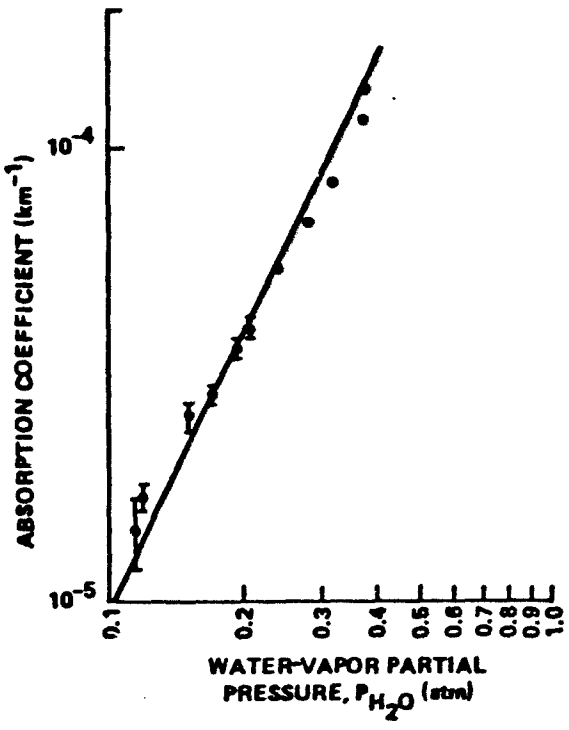

Figure 19. Pressure dependence of the water vapor absorption coefficient at 423 K, from Montgomery [59].

to arrive at a self-broadening coefficient. Montgomery's results for C_s as a function of temperature are plotted in Figure 20, along with values from Gryvnak et al. [55] for comparison. It is reasonable to say the two sets of data are in general agreement.

Nordstrom et al. [60] present water vapor absorption measurements at room temperature (295.5 ± 0.5 K) for five CO_2 laser wavelengths in the 10.4-μm band. Three gases, pure nitrogen and two nitrogen-oxygen mixtures (80:20 and 60:40), were used to buffer the water vapor samples to a total pressure of 760 torr. Transmission measurements were made over a range of water vapor partial pressures from 0 to 15 torr for each buffer gas. These authors analyze their data at each of the five wavelengths in terms of an extinction coefficient of the form:

$$k = w\left(C_s P_{H_2O} + C_n P_n + C_0 P_0\right) \qquad (27)$$

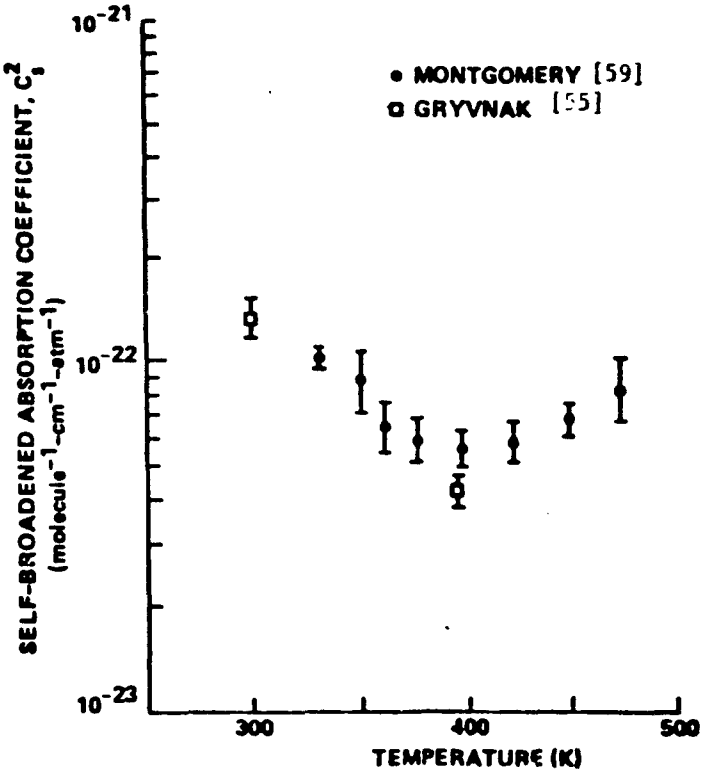

Figure 20. Comparison of measured water vapor self-broadening coefficients near 8.33 μm as a function of temperature.

where C_s and C_n are the usual self- and foreign-broadening coefficients and C_0 is an oxygen foreign-broadening coefficient. Since one of the laser lines [R(20), λ=10.2466 μm] is so very near a water line, the authors used this line to determine C_0. This value for C_0 was assumed to apply to all lines investigated. A Lorentz line shape with a width given by:

$$\alpha = \alpha_0[P+(C_0/C-1)\overline{p_0}] \qquad (28)$$

where $\overline{p_0}$ is the average oxygen pressure and P is the total pressure, leads to an absorption coefficient given by:

$$k(\nu \approx \nu_0) \propto \frac{p_{H_2O}}{P+\left(C_0/C_n-1\right)p_0} \quad . \tag{29}$$

A least-squares fit to k versus p_{H_2O} yielded a value for the ratio C_0/C_n of 0.75; i.e.,

$$C_0/C_n = 0.75 \tag{30}$$

which Nordstrom et al. interpret as strong evidence that oxygen is not so efficient a broadening gas as nitrogen. The results for the self-broadening coefficient and the ratios of the foreign- to self-broadening coefficients are tabulated in Table 15 along with the results from Gryvnak et al. [55] for comparison. These authors conclude by pointing out that the small values of C_n/C_s force a fit of Lorentzian wings to the observed absorption; i.e., the Lorentz line shape is not adequate to model absorption in the wings of strong water lines.

TABLE 15. COMPARISON OF MEASURED SELF-BROADENING COEFFICIENTS AND FOREIGN- TO SELF-BROADENING RATIOS FROM NORDSTROM et al. [60] WITH THOSE FROM GRYVNAK et al.[55]

ν (cm^{-1})	C_s° (cm^2-atm^{-1} - $molecule^{-1}$) $\times 10^{22}$		C_n°/C_s°	
*******	Nordstrom	Gryvnak	Nordstrom	Gryvnak
936.804	2.20	1.25	0.005	0.005
944.194	2.11	2.19	0.003	0.005
977.214	1.84	2.18	0.009	0.005
980.913	1.75	2.00	0.003	0.005

The most recent data on water vapor nitrogen attenuation coefficients are from Peterson et al. [61], who present self-broadening coefficients and ratios C_n/C_s at several CO_2 laser frequencies. Spectrophone and White cell data were concluded to be in good agreement. As the spectrophone data were not at a single temperature, only the White cell data on the pressure-broadened water vapor extinction coefficient are plotted in Figure 21. These room-temperature data were for a water vapor partial pressure of 14.6 torr, buffered by nitrogen to a total pressure of 760 torr. Also plotted for comparison in Figure 21 are data from Nordstrom et al. [60] and McCoy et al. [13]. Peterson et al. concluded from the strong quadratic pressure of the absorption coefficient and the assumed Lorentz-line shape of the far wings, that self-broadening (H_2O-H_2O interactions) is much more important in its contribution to absorption at these wavelengths than is foreign-broadening (H_2O-N_2 interactions).

The systematic uncertainties discussed in the conclusion to the previous paragraphs on 3-5-μm continuum are of course present in these measurements in the 8-14-μm region. However, the characteristic continuum water vapor absorption in this region is roughly an order of magnitude greater than that in the 3-5-μm region. Thus, a conservative error to associate with continuum data in the 8-14-μm region is ±10-15 percent.

The proper model for the temperature dependency has been a problem for some time. Early workers either neglected the temperature effect entirely or assumed the same temperature function for both the self- and foreign-broadening terms. Kunde and Maguire [62] seem to be the first to point out that the self- and foreign-broadening terms should have different (indeed inverse) temperature dependencies, as shown in Figure 22.

$$k\left(P, p_{H_2O}, T\right) = k_1(T)P + k_2(T)p_{H_2O} \tag{31}$$

They used the modified Van Vleck-Weisskopf line shape for the rotational lines at 400 cm^{-1}, and the self-broadened Lorentz line for the lines of

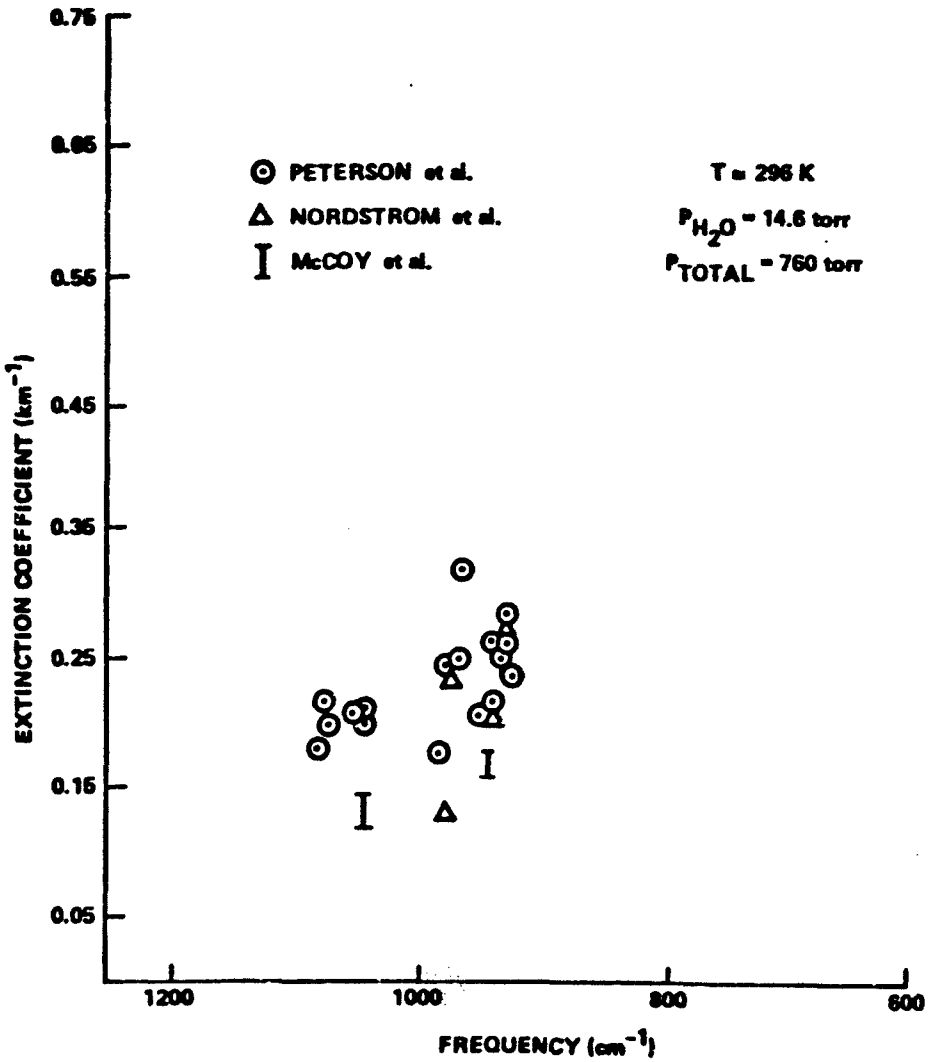

Figure 21. Extinction coefficients from Peterson et al.[61], Nordstrom et al.[60], and McCoy et al.[13].

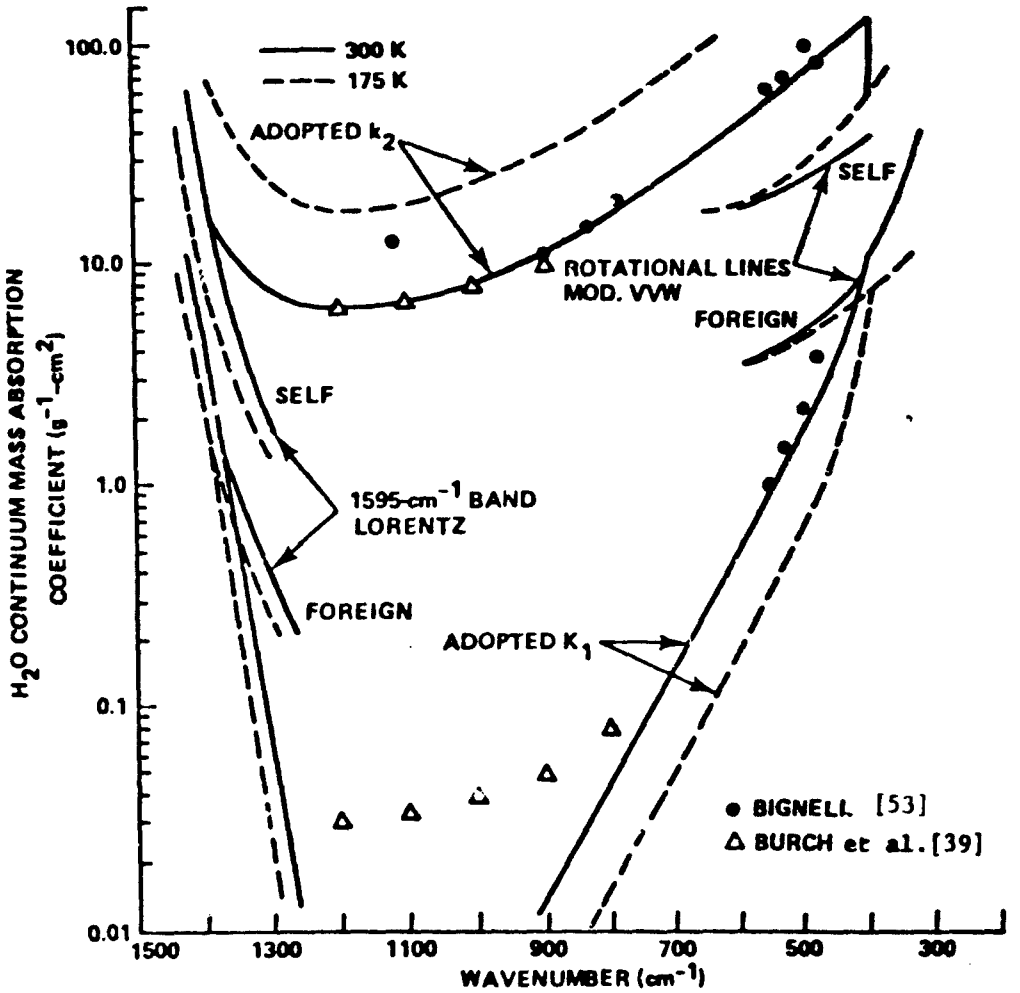

Figure 22. Water vapor continuum absorption coefficient for the 400-1400-cm^{-1} region [62].

1595-cm^{-1} H_2O band at 1400 cm^{-1}. The k_1 component is normalized in a similar fashion to the foreign-broadened water vapor components at 400 and 1400 cm^{-1}. These temperature dependencies were indicated by Tuer [63] as shown in Figure 23, where LOWTRAN II had no temperature dependence (except through the density variation at constant pressure); and Roberts et al. [64] suggested using the same functional dependence for k_1 and k_2.

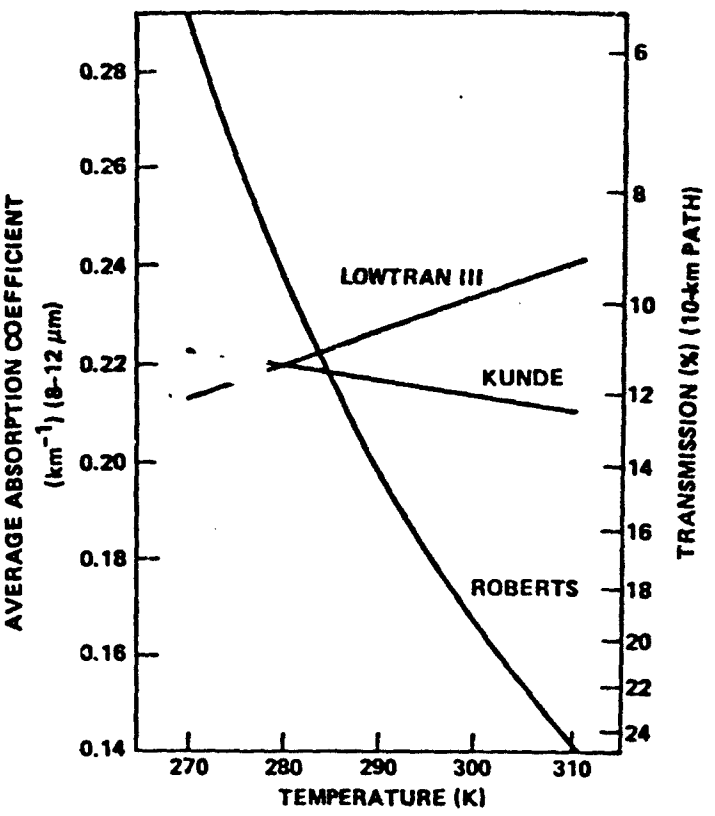

Figure 23. Comparison of various 8-12-μm water continuum models [water content (14 g/m^3) and total pressure (1 atm) correspond to midlatitude summer model] [63].

Very recently, Burch and Gryvnak [65] presented some new data on H_2O continuum absorption just beyond 5 μm where the CO laser operates. By working in the wing just below the strong 6.3 μm H_2O band, they investigated the "shape factor," χ, for nitrogen-broadened versus self-broadened lines. They concluded that both foreign- and self-broadened H_2O lines absorb more over a large portion of the wings than do Lorentz-shaped lines, and that, in the wings, self-broadened lines absorb more than nitrogen-broadened lines.

Besides the above data and the CO_2 and N_2 continua already mentioned that were measured by Burch and have been incorporated in the AFGL Laser Code, there have been other continua discussed in the

literature. (For example, Ashcheulov et al. [66] and Bolle [67] measured continuum from 8 to 25 μm; and Gates [68] measured water vapor continuum from 0.872 to 2.537 μm.) However, these continua measurements seem largely unsupported, and for conservatism in safety standards probably should be neglected for present purposes.

Molecular Scattering--Scattering of laser radiation depends strongly on the size of the particle relative to the wavelength of the radiation. When the particle size is much smaller than the wavelength, as it is for molecules, the Rayleigh theory gives a good representation of the scattering process. The volume-scattering coefficient for Rayleigh scattering can be expressed as:

$$\sigma_R = \frac{\left(4\pi^2 NV^2/\lambda^4\right)\left(n^2-n_0^2\right)^2}{\left(n^2+2n_0^2\right)^2} \tag{32}$$

where

N,V,n = The number density, the volume, and refractive index of the molecules

λ = Wavelength of the radiation

n_0 = Refractive index of the medium in which the molecules are suspended.

McClatchey and d'Agati [42] propose a semiempirical expression based on the equation for σ_R, obtained by fitting molecular-scattering coefficients published by Penndorf [69]. This expression is given in terms of the pressure (atm) and temperature (K) of the atmosphere and the frequency of the laser ν (cm^{-1}):

$$\sigma_m = 2.677\times10^{-17}\ p/T\nu^m \tag{33}$$

where m is 4.0117 and σ_m is in units of km^{-1}. It is interesting to note that the exponent m is slightly larger (i.e., approximately 0.3 percent) than Rayleigh theory.

It appears that this expression, which is contained in the AFGL LASER Code, should provide an adequate representation of the extinction due to molecular scattering for the present purposes. This extinction will be negligibly small for most lasers of interest, as indicated in Figure 24.

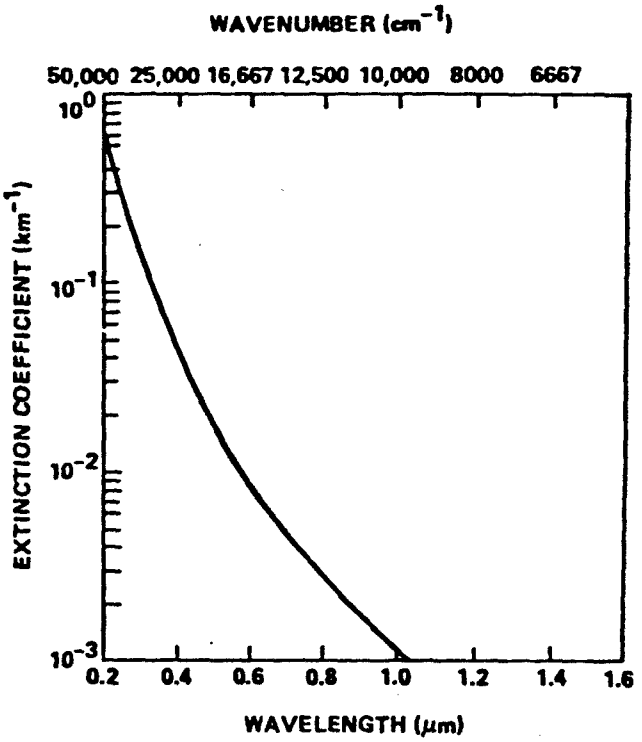

Figure 24. Model for extinction coefficient due to molecular scattering as a function of laser frequency at STP [42].

Laser Attenuation Due to Atmospheric Aerosol Extinction

In this section, the basic electromagnetic radiation scattering equations are reviewed and current predictive attenuation models are evaluated. For lower power laser radiation, molecular and aerosol absorption and scattering are the principal attenuation. Currently, the aerosol attenuation of laser radiation is so poorly predictable from easily obtained atmospheric parameters such as wind speed, relative humidity, and visibility, that clear-air laser energy density limits should be employed for safety considerations..

Theory--Scattering is defined as the process by which a particle, solid or liquid, continuously extracts energy from an incident electromagnetic wave and reradiates that energy into a solid angle centered at the particle. Absorption can also occur whereby some of the energy is converted to heat and reradiated as broadband thermal infrared radiation. The combined effects of scattering and absorption are referred to as extinction. Scattering of an incident beam of radiation requires that the index of refraction of the particle be different from that of the surrounding medium. As one might expect, the distribution pattern of scattered radiation strongly depends on the ratio of the particle size or radius to the wavelength of the incident radiation (see Figure 25). The three primary parameters of scattering phenomena are, therefore, the refractive index and radius of the particle and the wavelength of the incident radiation. The scattering of radiation by particles much smaller than the wavelength of the incident radiation (air molecules, for instance) is termed Rayleigh scattering, while the scattering of radiation by particles of radius/wavelength ratios of approximately 0.1 and greater is referred to as Mie scattering.

Since atmospheric particle sizes cover a range from 10^{-4} μm to 10 mm (Table 16), and the radiation wavelength of interest is typically from approximately 0.3 μm to 20 μm, both types of scattering mechanisms are, in general, present.

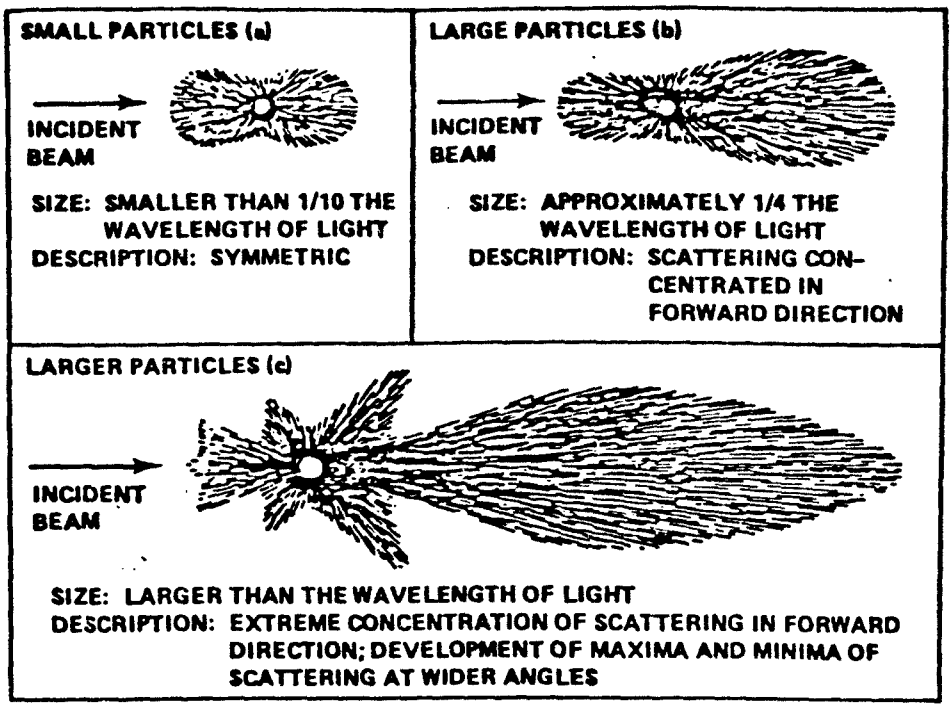

Figure 25. Angular patterns of scattered intensity from particles of three sizes: (a) small particles, (b) large particles, and (c) larger particles [70].

TABLE 16. PARTICLES RESPONSIBLE FOR ATMOSPHERIC SCATTERING [70]

Type	Radius (μm)	Concentration (cm^{-3})
Air molecule	10^{-4}	10^{19}
Aitken nucleus[a]	$10^{-3} - 10^{-2}$	$10^{2} - 10^{4}$
Haze particle[b]	$10^{-2} - 1$	$10 - 10^{3}$
Fog droplet	$1 - 10$	$10 - 100$
Cloud droplet	$1 - 10$	$10 - 300$
Raindrop	$10^{2} - 10^{4}$	$10^{-5} - 10^{-2}$

[a] Salt, dust, pollen, etc.

[b] Small fog droplet.

The general approach to analytically modeling scattering phenomena in the atmosphere has been to:

- Calculate the spectral scattering due to a single particle of radius r and index of refraction n.
- Determine (or postulate) a size distribution of particles in the atmosphere as a function of altitude.
- Calculate the aggregate effect of all the particles in a particular radiation path.

The attenuation of small-diameter laser beams can, in general, be determined to sufficient accuracy by considering only single scattering effects. Multiple scattering effects are much more difficult to model and calculate.

The basic equation for the scattering process begins with a definition for the angular scattering cross section of a single particle:

$$\sigma_{p\lambda}(\theta) = \frac{I_\lambda(\theta)\, d\lambda}{E_\lambda\, d\lambda} \text{ cm}^2\text{-sr}^{-1} \tag{34}$$

where

$\sigma_{p\lambda}(\theta)$ = angular scattering cross section for a single particle at wavelength λ

$I_\lambda(\theta)$ = spectral radiant intensity at wavelength λ and angle (θ) - symmetry about the propagation axis is assumed (w/sr^{-1})

E_λ = spectral irradiance at wavelength λ (w/cm^{-2}).

The total scattering cross section for a single particle is given by the integral of the angular scattering cross section over 4π sr:

$$\sigma_{p\lambda} = \int_0^{4\pi} \sigma_{p\lambda}(\theta)\, d\omega \text{ cm}^2 \tag{35}$$

where $d\omega$ = element of solid angle. $\sigma_{p\lambda}$ can be thought of as the equivalent area of an elemental surface that completely scatters a portion of the incident irradiance $E_\lambda d\lambda$.

If the scattering aerosol consists of identical particles uniformly distributed with a density of N particles/cm^3, then a scattering coefficient can be expressed by:

$$\beta_\lambda = N\sigma_{p\lambda} \ cm^{-1} \ . \tag{36}$$

β_λ can be regarded as a coefficient that expresses the fraction of a unit area that effectively scatters an incident irradiance $E_\lambda d\lambda$ per unit pathlength. The primary assumption here is that the dimensions are chosen such that the medium is optically thin in a unit pathlength (i.e., $\beta \lesssim 0.2$).

One might intuitively speculate that the maximum value $\sigma_{p\lambda}$ can take on is πr^2, the geometric cross-sectional area of a particle of radius r. Such is not the case. An efficiency factor (Q_λ) is defined as the ratio of the effective cross-sectional area to the geometric cross-sectional area:

$$Q_\lambda = \frac{\sigma_{p\lambda}}{\pi r^2} \ . \tag{37}$$

This function is strongly dependent on the ratio of the particle radius to the wavelength (λ) of the scattered radiation (Figure 26). As can be seen, the function Q takes on a maximum value, near 4, for r/λ ratios near 1. The feature that is particularly interesting, however, is the rapid increase of this efficiency factor from r/λ values of less than 0.5 to r/λ values near 1. This means that the attenuation due to scattering can vary by a factor of 5 to 10 for a relatively small increase in particle diameter. This is particularly important under growing fog conditions.

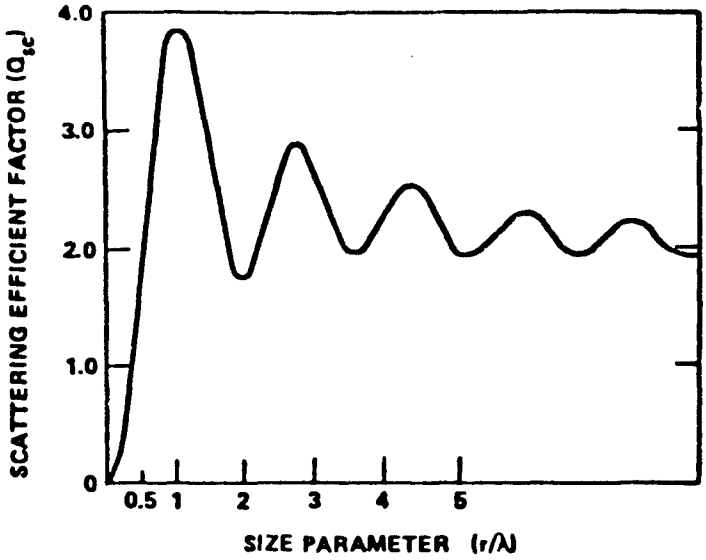

Figure 26. Scattering efficiency factor versus size parameter for water droplets [70].

For polydispersions of scattering aerosol, β_λ can be expressed as an integral over a size-distribution density function n(r) multiplied by the total cross-sectional area:

$$\beta_\lambda = \int_0^\infty n(r)\sigma_\lambda(r)\, dr \quad . \tag{38}$$

This scattering coefficient can also be expressed in terms of the efficiency factor Q_λ:

$$\beta_\lambda = \int_0^\infty \pi r^2 Q_\lambda(r) n(r)\, dr \quad . \tag{39}$$

In general, only a range of particle radii r_1-r_2 is of interest; therefore:

$$\beta_\lambda = \pi \int_{r_1}^{r_2} Q_\lambda(r) n(r)\, dr \tag{40}$$

where n(r) is the number of particles per unit volume and per unit interval of radius. The total number of particles (N) in a unit volume is given by:

$$N = \int_0^\infty n(r)\, dr \quad . \tag{41}$$

Several particle-size distribution models n(r) have been proposed to describe observed distributions analytically. The most generalized, currently popular, distribution model is one proposed by Deirmendjian [71] and is referred to as the Deirmendjian model. This analytical model has the form:

$$n(r) = a r^\alpha e^{-b r^\gamma} \tag{42}$$

where r is the particle radius and a, b, α, and γ are positive constants.

For a particular choice of α and γ, the other two constants, a and b, can be determined from a count of the total number of particles in a unit volume, and the mode radius r_{mode}, where the particle concentration is a maximum (i.e., curve derivative is zero). Then:

$$b = \frac{\alpha}{\gamma r_{mode}^\gamma} \tag{43}$$

and

$$a = \frac{N\gamma}{b^{\frac{-(\alpha+1)}{\gamma}}\,\Gamma\frac{\alpha+1}{\gamma}} \tag{44}$$

where Γ is a gamma function. Typical haze distributions predicted by this model are shown in Figure 27.

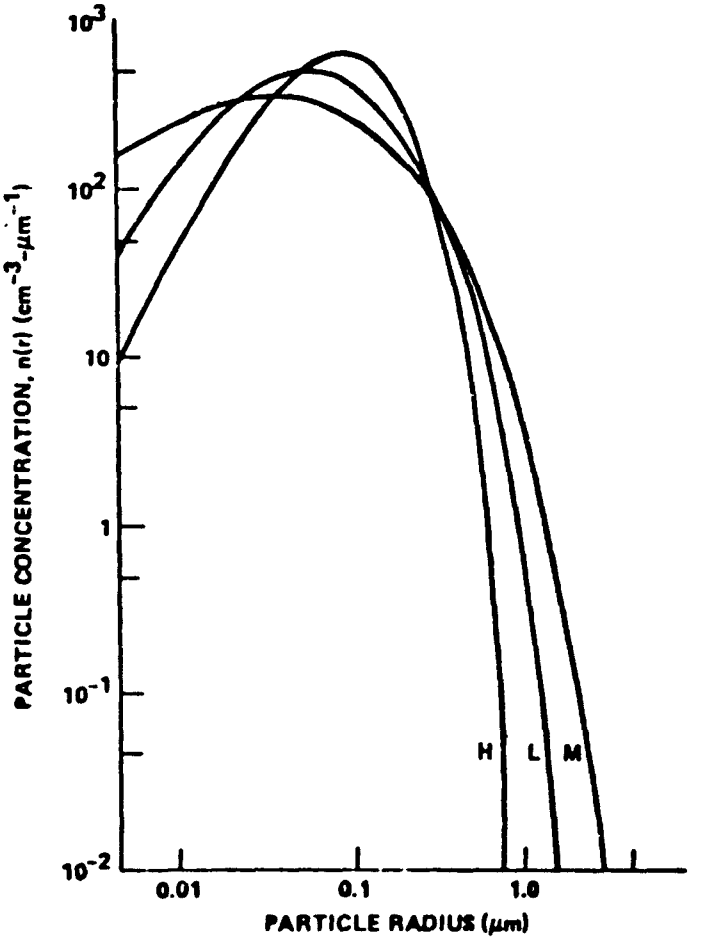

Figure 27. Particle-size distributions for various haze models [71]: H -- high-altitude stratospheric dust particles; L -- continental aerosols; and M -- maritime types of aerosols.

A second, less general size distribution function was proposed by Junge [72], and is referred to as a power law size distribution function. This model has the form:

$$n(r) = cr^{-v} = \frac{dN}{d(\log r)} \tag{45}$$

where c and v are constants. The model assumes a power law relationship between the change in particle concentration and the change in the log of the radius, or is valid for only the straight-line portion of the [dN/d(log r)] versus log (r) curve (Figure 28).

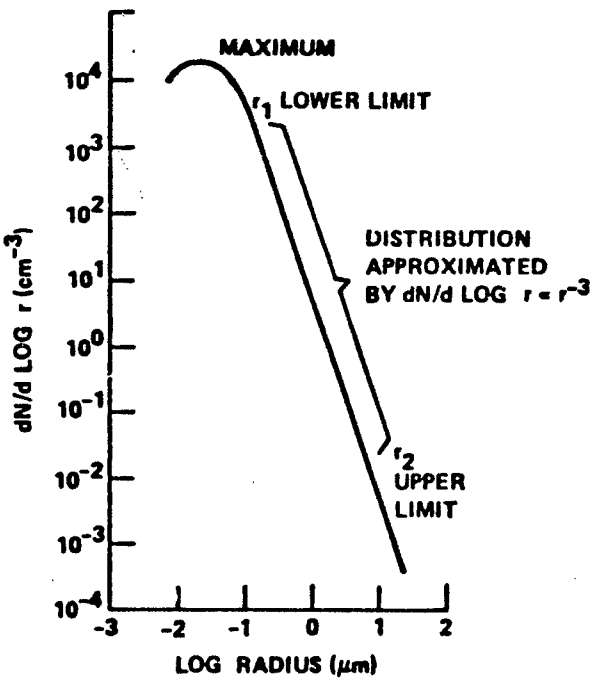

Figure 28. Particle-size distribution showing range of the power law relationship [72].

The constant (-v) is determined from the slope of the straight-line portion of the curve, and C can be determined from a total particle count in a unit volume (N) by the following equation:

$$C = \frac{-vN}{0.434\left(r_2^{-v} - r_1^{-v}\right)} \quad . \tag{46}$$

Current Prediction Models--A number of current prediction models for aerosol extinction were evaluated with regard to their application to low-power laser transmission through the atmosphere. The salient features of the models are briefly reviewed here. Published sources of the model descriptions are also included.

The overwhelming evidence from the OPAQUE measurement program is that the aerosol extinction coefficients cannot be predicted with acceptable accuracy by using easily measured atmospheric parameters as inputs. Since all of the models reviewed use the easily measured parameters, such as relative humidity, wind speed, and visibility, as inputs, none of them would be adequate predictive models from a safety standpoint. The six models reviewed are referred to as Barnhardt and Streete, Wells-Gal-Munn, Hänel, LOWTRAN IV, Roberts, and Science Applications.

The Barnhardt and Streete model [73] was one of the early attempts to predict the effects of aerosol scattering on the optical transmittance in the infrared. The aerosol size distribution models used were a combination of a continental model by Junge:

$$\frac{dn(r)}{dr} = 0.434\ Cr^{-(\gamma+1)} \tag{47}$$

and a maritime model by Deirmendjian:

$$\frac{dn(r)}{dr} = \frac{0.434}{r}\ be^{-ar} \tag{48}$$

where n(r) is the particle concentration in particle/cm^3, r is the particle radius, and a, b, c, and γ are the constants.

The relative humidity is included in a growth factor (F) with the following assumptions:

- A particle of any radius will undergo the same fractional growth for the same change in relative humidity.
- All particles grow at the same rate.
- The dry nuclei have an index of refraction of n=1.54.
- The dilute water droplet is assumed to have a refractive index of n=1.33.

The refractive index is assumed to vary between these values as a function of the relative humidity:

$$n = 1.54 + 0.03 \ln(1-RH) \quad . \tag{49}$$

The growth factor is given by the expressions:

$$r = r_0 F \tag{50}$$

$$F = 1 - \frac{1}{\beta r_0} \ln(1-RH) \tag{51}$$

where r_0 is the particle radius of 0 percent relative humidity, and β is the constant for a particular species of condensation nuclei. The scattering coefficients were determined by assuming a particular combination of continental and maritime aerosols and relative humidity and then calculating, with a digital computer program, the scattering coefficients as a function of wavelength, using Mie scattering theory.

This Barnhardt and Streete model does not apply to atmospheric conditions where the relative humidity is approaching 100 percent or for supersaturated cases. It therefore has limited utility for low-visibility or fog-formation conditions.

The Wells-Gal-Munn (WGM) maritime aerosol attenuation model [74] generates a particle-size distribution that is a function of particle radius (r), relative humidity (RH), altitude (h), visibility (v), and wind velocity (U).

The overall particle-size distribution model is a combination of the Deirmendjian size distribution model for maritime aerosols and Junge's size distribution model for continental aerosols.

The Deirmendjian size distribution model used for the maritime aerosols was of the form:

$$n(r) = ar^{\alpha} e^{-br^{\gamma}} \tag{52}$$

where r is the particle radius for the original Deirmendjian model, and a, b, α, and γ were constants. In the WGM model, a and γ are functions of the wind velocity (U):

$$a = C_1 + C_2 U^d \tag{53}$$

$$\gamma = d + pU^q \ . \tag{54}$$

An aerosol growth factor (f) is included that is a function of relative humidity (RH):

$$F = 1 - 0.9 \ln(1-RH) \ . \tag{55}$$

The Junge size distribution model is used for the continental aerosols:

$$n(r) - k_1 r^{k_2} \ . \tag{56}$$

A normalization parameter is included to define low-wind conditions, and a mixture parameter is included to define the ratio of maritime/continental aerosols present in the atmosphere under consideration.

Exponential scale height multipliers are used to describe the particle-size distributions as functions of altitude. These are selected from a table look-up. Separate (different) tables are provided for the continental and maritime distribution.

Finally, the function dependence on visibility (V) is included as multiplier β that is inversely proportional to V:

$$\beta = \frac{3.91}{K_{0.55}V} . \tag{57}$$

A Mie scattering computer code is then used to determine the extinction coefficients as functions of wavelength. The index of refraction of the particles is based on the assumption that all of the particle nuclei are NaCl.

While this model does consider wind velocity as a factor, the fact that the assumed coefficients have a discontinuity at a particular wind velocity is an indication that the relationship between particle density and wind velocity is complex and not easily predictable.

The decrease in particle density and optical attenuation with altitude is not a realistic model for conditions of low-hanging clouds and certain types of fogs.

The growth of atmospheric models as a function of nuclei size, chemistry, relative humidity, and previous history is an exceedingly complex phenomenon. Therefore, the simple relationships assumed are subject to substantial uncertainties in low-visibility, high-relative-humidity situations. Further, as will be demonstrated later in this report, large variations in infrared extinction can occur with regard to constant λ=0.55 visible ranges.

The Hänel Model [75] provides a theoretical evaluation of aerosol particle mass, size, mean density, and mean refractive index as functions of relative humidity. The model is rigorous and considers the curvature (radius) and dissolved nucleation-site material in the aerosol particle, and the equilibrium partial vapor pressure over the

particle. Particle growth (or shrinkage) as a function of particle radius and dissolved salts is considered and discussed in detail. This model, however, has its primary application to relatively stable light-haze conditions, since thermodynamic equilibrium was assumed in the analytic derivations. The nonequilibrium conditions associated with the formation or disintegration of clouds or unstable fogs were not considered. The OPAQUE measurement data [76,77] and the laser transmission data of Chu and Hogg [78] have shown optical transmittance variations of two to three orders of magnitude for essentially the same humidity conditions (RH≈1). The theoretical aerosol growth modeling of Neiburger and Chien [79] has also shown that the particle concentrations in the 1-10-μm-radius range can increase by two orders of magnitude in five-minute periods under nonequilibrium, saturation conditions.

The AFGL LOWTRAN series of atmospheric transmittance codes were generated initially to predict molecular absorption effects on the atmospheric optical transmittance and radiance in the spectral region from 0.25 to 28.5 μm. The inclusion of scattering effects on optical transmittance has been a recent addition [80].

The spectral volume aerosol extinction and absorption coefficients are calculated for several "standard" aerosol atmospheres (maritime, continental, urban, and rural) for visual ranges of 23 km and 5 km. The spectral aerosol extinction and scattering coefficients for an arbitrary visual range (V) are determined by simple interpolation:

$$\sigma(\lambda,V) = \sigma(\lambda,V_1) + \frac{\left(\frac{1}{V} - \frac{1}{V_1}\right)}{\left(\frac{1}{V_2} - \frac{1}{V_1}\right)} [\sigma(\lambda,V_2) - \sigma(\lambda,V_1)] \qquad (58)$$

where V_1 is the 23-km visual range and V_2 is the 5-km visual range.

A functional dependence is also provided for an altitude correction. This model assumes the same spectral dependence for all aerosol distributions included. The model will provide calculations for visual ranges less than 5 km; the results, however, should be applied with caution.

The model apparently is not meant to be used under low-visibility fog conditions. Specific aerosol distributions cannot be included in the model, or specific dependence on relative humidity. Since the LOWTRAN IV model code is, by far, the most popular atmospheric transmission predictive code used currently, it is unfortunate that a more realistic low-visibility aerosol predictive capability is not included.

The R. E. Roberts (Institute for Defense Analysis) attenuation model [81] is based on a simple phenomenological approach to aerosol optical extinction modeling. Basically, the model correlates the spectral extinction coefficients due to aerosols with the relative volume of particulates in an atmospheric path. Several measured and theoretical particle-size distributions were integrated to determine the relative water content. The attenuation coefficients at several wavelengths in the visible and infrared were calculated for these particle-size distributions, using Mie scattering theory. The calculated extinction coefficients were then related to the relative water content. Log-log plots of the extinction coefficient (for λ's = 1.0, 4.0, and 10.0 μm) in km^{-1} versus relative water content in g/m^3 were relatively straight lines and with approximate data spread of less than a factor of two.

For wavelengths greater than the particle radius, Roberts suggested that the extinction cross section should be proportional to the radius cubed, or

$$\alpha_{ext} \sim r^3 , \tag{59}$$

and for particle radii much greater than the wavelength, Mie scattering would predict a relationship:

$$\alpha_{ext} \sim r^2 . \tag{60}$$

Therefore, it was argued that the relationship between the λ = 1.0-μm extinction coefficient and the λ = 10.0-μm extinction coefficient would be of the form:

$$\beta_{(10.0\ \mu m)} = C_\lambda \beta^{3/2}_{(1.0\ \mu m)} \tag{61}$$

or that the $\beta_{(10.0\ \mu m)}$ would increase as a function of relative water content at a faster rate than the $\beta_{(1.0\ \mu m)}$ extinction coefficient.

The calculated data generated by Roberts, in general, support this hypothesis, with the plotted data showing a relationship:

$$\beta_{(10.0\ \mu m)} = C_\lambda \beta^{1.49}_{(1.0\ \mu m)} \cdot \tag{62}$$

While this approach of attempting to relate the optical attenuation due to aerosols to a parameter such as the total water/unit area in a given path is an improvement over attempts to correlate attenuation with relative humidity, some problems still remain. Specifically:

- The problem of determining the water/particulate content in a path. Direct measurements are not easy.
- If visibility is used as a parameter to determine water content, then the model is subject to all previously discussed pitfalls with regard to using visible radiation attenuation as a measure of infrared attenuation.
- The OPAQUE measurement data [77] indicate that large variations can be expected in attempting to correlate visible extinction coefficients (λ = 0.55 μm) with the infrared window band extinction coefficients ($\Delta\lambda$ = 3-5 and 8-12 μm).

The SAI aerosol attenuation model [82] uses two basic types of input data: (1) the ground-level visibility, and (2) the aerosol-mass content. This approach has the unique feature of not being functionally dependent on relative humidity. The relative humidity, while rather easily measured at lower values, becomes increasingly difficult to accurately measure as it approaches one and reaches supersaturation values. Further, it has been shown, theoretically and experimentally, that relative humidity is a poor indicator of infrared extinction under low-visibility conditions. However, although the aerosol-mass content may be a more useful parameter for predicting infrared extinction accurately, determining the mass content from measurable parameters is not simple and straightforward.

This aerosol-mass-content parameter is determined in the SAI model by calculating the Mie scattering extinction coefficients as a function

of wavelength for measured particle-size distribution. The size distributions are integrated to determine the aerosol-mass content (assumed to be water). The volume optical extinction coefficients are log-log plotted as a function of the aerosol mass (liquid water content) in g/m^3. From these plots, the slopes and intercepts are determined for analytically correlating the extinction coefficients with liquid water content. The visible volume extinction coefficient (λ=0.55 μm) is related to the surface horizontal visibility range by the inverse relationship:

$$k_{(\lambda=0.55\ \mu m)} = 3.912\ V^{-1} \quad . \tag{63}$$

Therefore, the visibility (V) is used to determine the surface aerosol-mass/water content.

Measurements were made at Grafenwöhr, West Germany, to determine the vertical profile of the aerosol mass. In the SAI model, the vertical profile is approximated by exponential functions of the form

$$W_{(z)} = W_0 e^{pz} \tag{64}$$

where z is the vertical height above Earth's surface. Changes in the profile due to increasing or decreasing aerosol-mass density are handled by discrete changes in the factor p. The total liquid water per unit along a slant path is determined by integrating the altitude density profile along the slant path. From this information, the aerosol extinction coefficients are determined and the spectral transmittance functions are calculated.

This SAI aerosol attenuation model is an improvement over previous models that used relative humidity as an input parameter, and is best suited for predicting attenuations under hazy conditions. However, this model has substantial deficiencies with regard to accurate prediction of infrared attenuation under low-visibility conditions. Determination of the infrared attenuation is functionally dependent on the

visible range (at λ=0.55 μm) through the aerosol-mass content. OPAQUE data [77] and the laser transmittance data of Chu and Hogg [78] have shown that the visibility can vary by two orders of magnitude for a relatively constant IR transmittance. Further, in the model the surface visibility and the vertical aerosol-mass density in mass/unit area (referred to as the liquid water column density) are regarded as independent input variables. Smith's comment [82] that "there is probably some correlation between the two in actual situations" appears to be a gross understatement.

Measurement Results--A number of predictive models for infrared attenuation have attempted to correlate radiative extinction in the two primary atmospheric window regions (3-5 μm and 8-14 μm) with visibility (i.e., transmission in the visible portion of the spectrum). The hazards in attempting such correlations were demonstrated by some very careful measurements by Chu and Hogg [78] (Figure 29). In the measurement data shown, the visibility (0.63 μm) radiation degenerates drastically (more than three orders of magnitude) as the fog becomes denser, while the 10.6-μm transmittance is relatively unattenuated and the 3.5-μm radiation is only slightly decreased. The upper curves show the transmission in the 3.5-and 0.63-μm regions improving as a fog dissipates. As might be expected, as the fog droplets shrink in size, the 3-5-μm transmission improves first as the mean droplet radius passes through 3.5 μm. The visible transmittance then improves drastically after the mean radius shrinks below 0.6 μm.

Theoretical work by Neiburger and Chien [79] has predicted rapid changes in the size distribution function for increasing fog conditions. A change of two orders of magnitude in the concentration at 5 μm over a five-minute interval is shown (Figure 30). A bimodal distribution is also predicted for certain development stages. Since fog development occurs under essentially saturated or supersaturated conditions (RH = 100 percent), large changes in the visible and near-infrared transmittance can occur for essentially constant high-relative-humidity conditions. This variability is graphically demonstrated by the results of

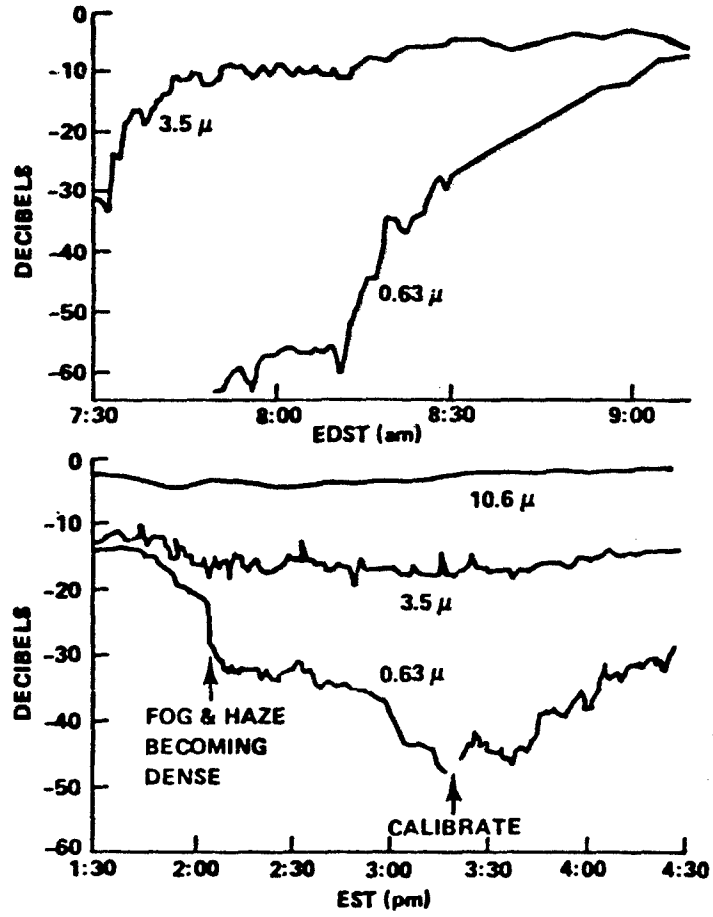

Figure 29. Measurement of 2.6-km transmission loss in light fog; 0-dB-signal level in clear weather [78].

the extensive OPAQUE measurement program [77] (Figure 31). As shown, the visible extinction coefficient (0.55 μm) varies by nearly two orders of magnitude for high humidity conditions. The difficulties in attempting to use visibility in predicting 3-5-μm and 8-12-μm extinction coefficients are also demonstrated by the OPAQUE data (Figure 32). As the data show, it is not possible to reliably predict the infrared extinction coefficient to within a one-half order of magnitude given visible extinction values.

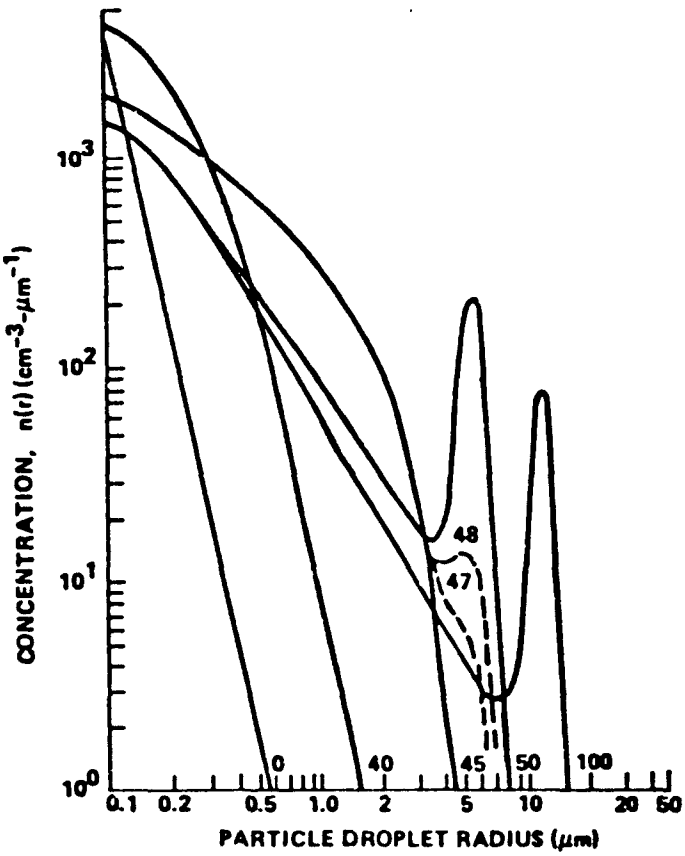

Figure 30. Theoretical size distribution of fog droplets as a function of elapsed time. The time in minutes after start is shown for each curve [79].

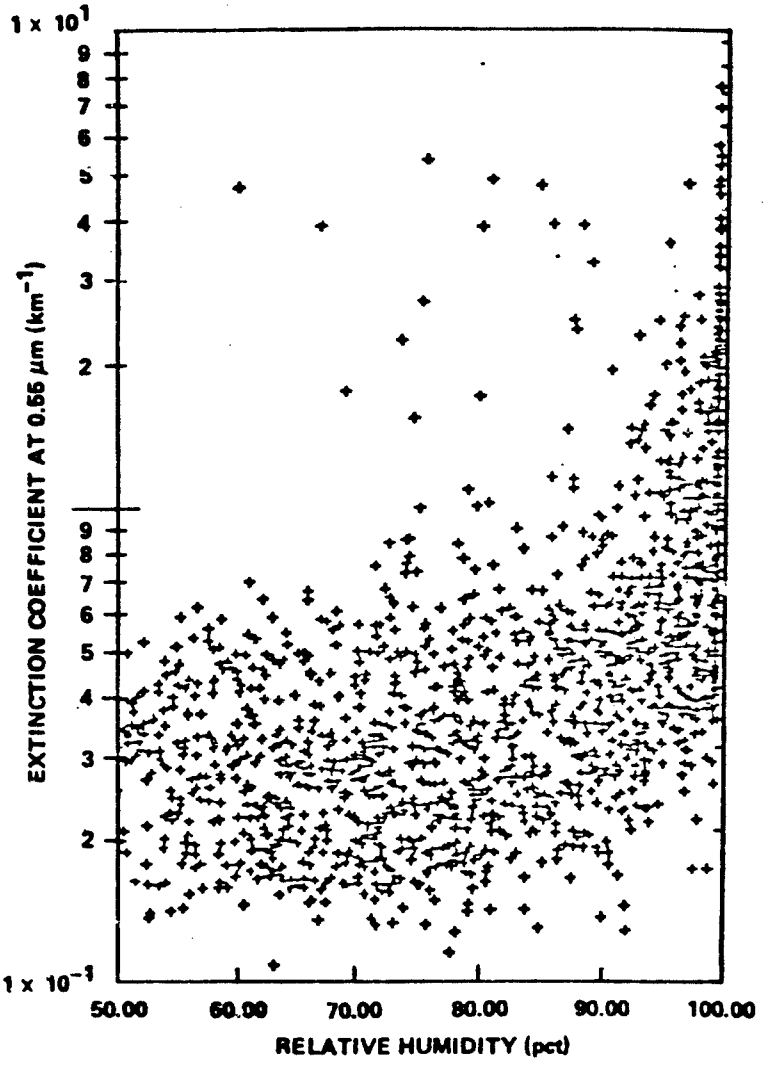

Figure 31. Variation of visible-aerosol extinction coefficient with relative humidity. Derived from OPAQUE Netherlands 3/77-5/77 data [77].

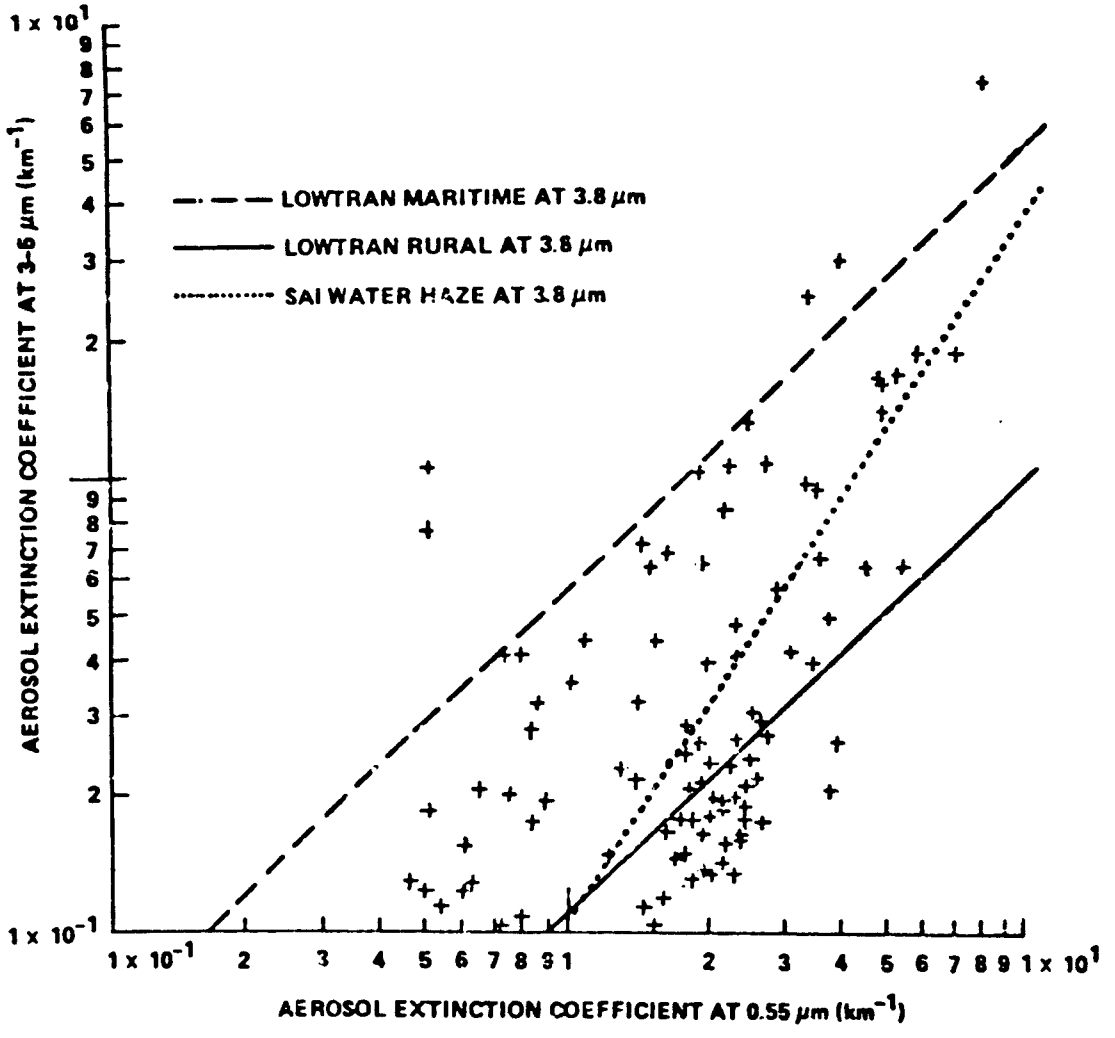

Figure 32. Comparison of various aerosol models with OPAQUE data. Aerosol extinction coefficient at 0.55 μm versus aerosol extinction coefficient at 3-5 μm. Derived from OPAQUE Netherlands 3/77-5/77 data [77].

Atmospheric Turbulence Effects

Turbulence in the atmosphere can cause random variations in the optical properties of the atmosphere, which affect the statistical atmospheric transmission characteristics for laser radiation. This effect has long been a limiting factor in the resolution achieved by ground-based astronomical observatories, and is commonly referred to as atmospheric scintillation or twinkling. Laser radiation can be similarly influenced by atmospheric turbulence in the path between the transmitter and the receiver, with random temporal and spatial variations in the received irradiance. With regard to safety considerations, these statistical variations imply the possibility of local bright spots whose irradiance can be as much as five times larger than the average. In addition, the turbulence can cause random spreading of the laser beam that would reduce the irradiance (per unit area of collector). For these reasons, it is important to investigate both of these atmospheric turbulence effects on the transmission of laser radiation, and to determine the best models for predicting the level of atmospheric turbulence and its effects on laser transmission.

The level of turbulence in the atmosphere typically varies strongly with time of day, wind, cloud cover, local terrain features, and altitude. The discussion in the following paragraphs evaluates the available information on the theories, experiments, and models pertinent to the expected turbulence levels in the atmosphere as a function of these and other pertinent parameters. The section entitled "Turbulence Effects" presents an evaluation of the available information on the effects of such turbulence that are important to personnel safety. This evaluation also addresses the theories, experiments, and models relevant to these effects.

Atmospheric Turbulence Levels--Turbulence in the atmosphere is the result of several mechanisms such as wind shear over terrain, vegetation, and buildings, and the result of thermal nonequilibrium between various layers in the atmosphere or with the ground. Transient and/or spatially

nonuniform heating of the ground due to the sun (i.e., sunrise, sunset, and broken cloud cover) is the main source of the local nonequilibrium between the ground and the air just above it.

In these paragraphs, the theory, measurements, and models overlap so much that they were not called out in separate headings. However, as much as possible, the topic is addressed in that order: a general historical discussion of turbulence comes first, followed by specific theory and measurements on atmospheric turbulence. Low-altitude turbulence will be discussed first and then high-altitude turbulence.

Turbulence in a fluid has long been the subject of theoretical and experimental investigations. The origin of turbulence and the mechanism affecting the transition from laminar to turbulent flow are of fundamental importance for the entire field of fluid mechanics. Fluid dynamists traditionally characterize the flow of gases by the Reynolds number, which can be thought of as the ratio of the inertial forces to viscous forces acting on the fluid. They have found, in controlled experiments, that there is a sudden transition from laminar to turbulent conditions as the Reynolds number passes some critical number (approximately 2300).

In the open atmosphere over the ground there are a number of complicating factors, such as the ground heating or cooling faster than the air, which produce convective currents. These unstable conditions (sometimes called active conditions) are frequently quantified by the Richardson number:

$$R_i = (g/\bar{T}) \frac{\partial\bar{\theta}/\partial Z}{|\partial\bar{U}/\partial Z|^2} \qquad (65)$$

where

g = acceleration due to gravity

$\bar{T}$ = mean absolute air temperature

$\bar{U}$ = mean horizontal wind

Z = altitude.

The gradient in θ is given as:

$$\frac{\partial\bar{\theta}}{\partial z} = \frac{\partial\bar{T}}{\partial z} + \gamma \qquad (66)$$

where γ is the adiabatic lapse rate of a parcel of dry air (9.8×10^{-3} K/m). Unstable conditions are characterized by negative values of R_i, and stable conditions by positive values. Nighttime conditions are usually stable, since convection is inhibited by warmer air above the cooler surface air.

The parameter generally used as a measure of the level of turbulence is the temperature structure constant (C_T^2), which is related to the expected value of the square of the temperature difference between two points (r_1 and r_2) separated by a small distance (r):

$$C_T^2 = r^{-2/3}\left\{[T(r_2) - T(r_1)]^2\right\} \quad . \qquad (67)$$

Wyngaard and Izumi [83] developed an expression for C_T^2 near the ground in terms of a function of R_i:

$$C_T^2 = z^{4/3}(\partial\bar{\theta}/\partial z)^2 f(R_i) \quad . \qquad (68)$$

Measurements of C_T^2 over a variety of conditions at heights of 5.66, 11.3, and 22.6 m, were correlated to the Richardson number, as shown in Figure 33. Note that the turbulence is shown to become very small for $R_i > 0.2$. Turbulence does develop even under these highly stratified conditions, although at present there is no adequate treatment for these situations.

The variation of C_T^2 with altitude was also investigated theoretically and experimentally by Wyngaard and Izumi [83]. They show semiempirical relations for C_T in the surface layer (i.e., up to approximately 25 m) in terms of the Monin-Obukhov length L and a parameter T_* (see Figure 34). These parameters are defined by:

$$L = -U_*^3\bar{T}/kgQ \qquad (69)$$

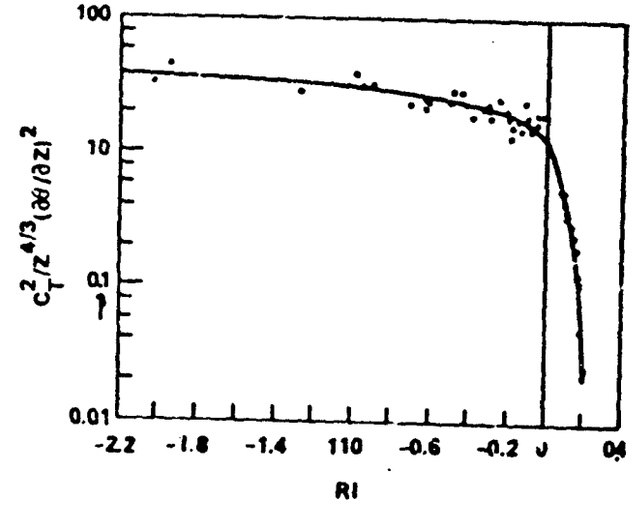

Figure 33. The dimensionless temperature-structure parameter versus Richardson number [83].

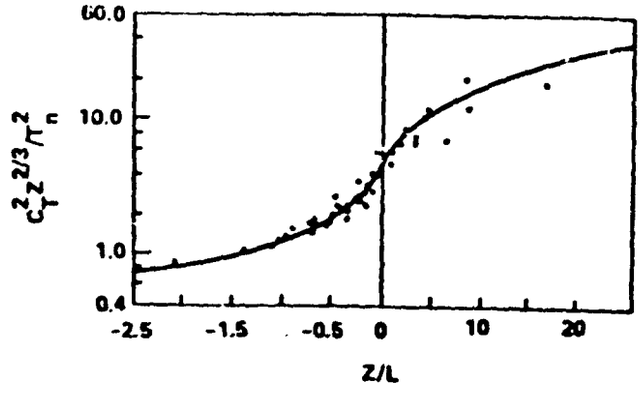

Figure 34. Correlation for C_T^2 as a function of altitude based on measurements [83].

and

$$T_* = -Q/U_* \quad , \tag{70}$$

where U_* is the kinematic surface stress (i.e., the stress per unit air density exerted by the wind on the surface in cm^2/sec^2), Q is the surface temperature flux (in K cm/sec), and k is von Karman's constant (traditionally taken to be 0.4). The functional form in this figure is given by:

$$C_T^2 = T_* Z^{-2/3} g_3(Z/L) \tag{71}$$

where

$$g_3 = 4.9(1 - 7Z/L)^{-2/3} \quad \text{for } Z/L \leq 0$$

and

$$g_3 = 4.9(1 + 2.74Z/L) \quad \text{for } Z/L \geq 0 \ .$$

This indicates a transition from a $Z^{-2/3}$ decay at low altitudes to a $Z^{-4/3}$ decay at higher altitudes occurring a few meters above the ground. The $Z^{-4/3}$ relationship has been experimentally substantiated up to altitudes in the 100- to 500-m range [84]. Unfortunately, this expression involves the parameters T_* and L which are not easily obtainable. Hufnagel [85] recasts the expression for the thermally active region (i.e., $Z/L \leq 0$) into a more convenient form:

$$C_T^2 = 2\text{x}10^{-3} \, Q^{4/3} \, Z^{-4/3} \left(1 + \frac{14000 \, U_*^3}{hQ} \right)^{-2/3} \tag{72}$$

and gives approximate relationships:

$$U_* \cong 0.35Z\left(\frac{\partial U}{\partial Z}\right) \text{ m/s} \tag{73}$$

and

$$Q = Q_0 \sin \zeta - 50 \text{ w/m}^2 \tag{74}$$

where ζ is the solar zenith angle and Q_0 is as given in Table 17 for various conditions.

TABLE 17. REPRESENTATIVE VALUES OF Q_0 VERSUS TERRAIN AND CLOUD COVER [85]

Type of terrain	Q_0 Continuously clear sky	Q_0 Overcast sky
Dry sand or lava	500	200
Dry field or brush	400	150
Wet fields	200	70

There are a large number of measurements of the turbulence level near the ground (see Table 18). Several of these measurements are represented in Figure 35 in the form of an index of refraction structure "constant," C_n^2, as a function of altitude. This structure function is directly related to that of temperature and is the parameter used to relate the turbulence levels to their effects on laser beam propagation. Considerable scatter is seen in the measured data as might be expected due to the random nature of the phenomena. However, the general levels and trends of most of the data seem roughly self-consistent, with the possible exception of Subramanian's measurements that seem high, and Wright and Schutz's minimum that seems low.

For comparison with models, the above data were replotted in Figure 36, and the turbulence levels predicted by Hufnagel's model [85] for extremes in solar heating and wind speed were superimposed. The maximum solar-heating case (i.e., clear sky, sun at zenith over dry sand or lava) produces high-turbulence levels as reported by Subramanian,

TABLE 18. LOW-ALTITUDE MEASUREMENTS OF REFRACTIVE INDEX STRUCTURE PARAMETER

Experimenter	Date	Description	Altitude (m)	Time of day	Conditions	Comments	Ref.
Fried et al.	1967	Ground-level measurements of C_n^2 over 8-km path $C_n^2 \sim 5 \times 10^{-15}\ m^{-2/3}$	15	0600-2200	Overcast-clear	"It is our opinion that use of a value of $5 \times 10^{-15}\ m^{-2/3}$ ... is reasonable ... 10-100 m above ... ground." Some correlation with lapse rate.	86
Subramanian	1972	Profiles of C_n^2 to 300 m using tethered balloon-retro-reflector laser transceiver $3.6 \times 10^{-15} < C_n^2 < 1.6 \times 10^{-13}\ m^{-2/3}$	0-300	?	Clear-partly cloudy	No meteorological data available. Higher values than Fried et al.	87
Wyngaard & Izumi	1968	Measurements of C_T^2 near the ground					83
Wright & Schultz	1967	Hot wire anemometers near ground measured C_T^2; C_n^2 derived 5- and 10-min. averages	2	0900-2200	?	Meteorological data missing.	88
Lawrence et al.	1970	Hot wire anemometers near ground and in A/C measured $C_T^2 C_n^2$ derived. Large variations in C_n^2 with altitude.	0-3300 2	00-2400	Partly cloudy and sunny day; night	Meteorological data missing. "No simple model can describe variations with altitude."	89
Ochs & Lawrence	1969	2-m data from temperature probes; 100- to 1000-m data from optical measurements over Boulder, Colorado.	2-1000	Evening, noon, and dusk	Varied	Agrees reasonably well with Hufnagel's 1966 model.	90
Tatarski	1961	Measurements not presented in terms of C_n^2 or C_T^2.	Near earth	00-2400			91

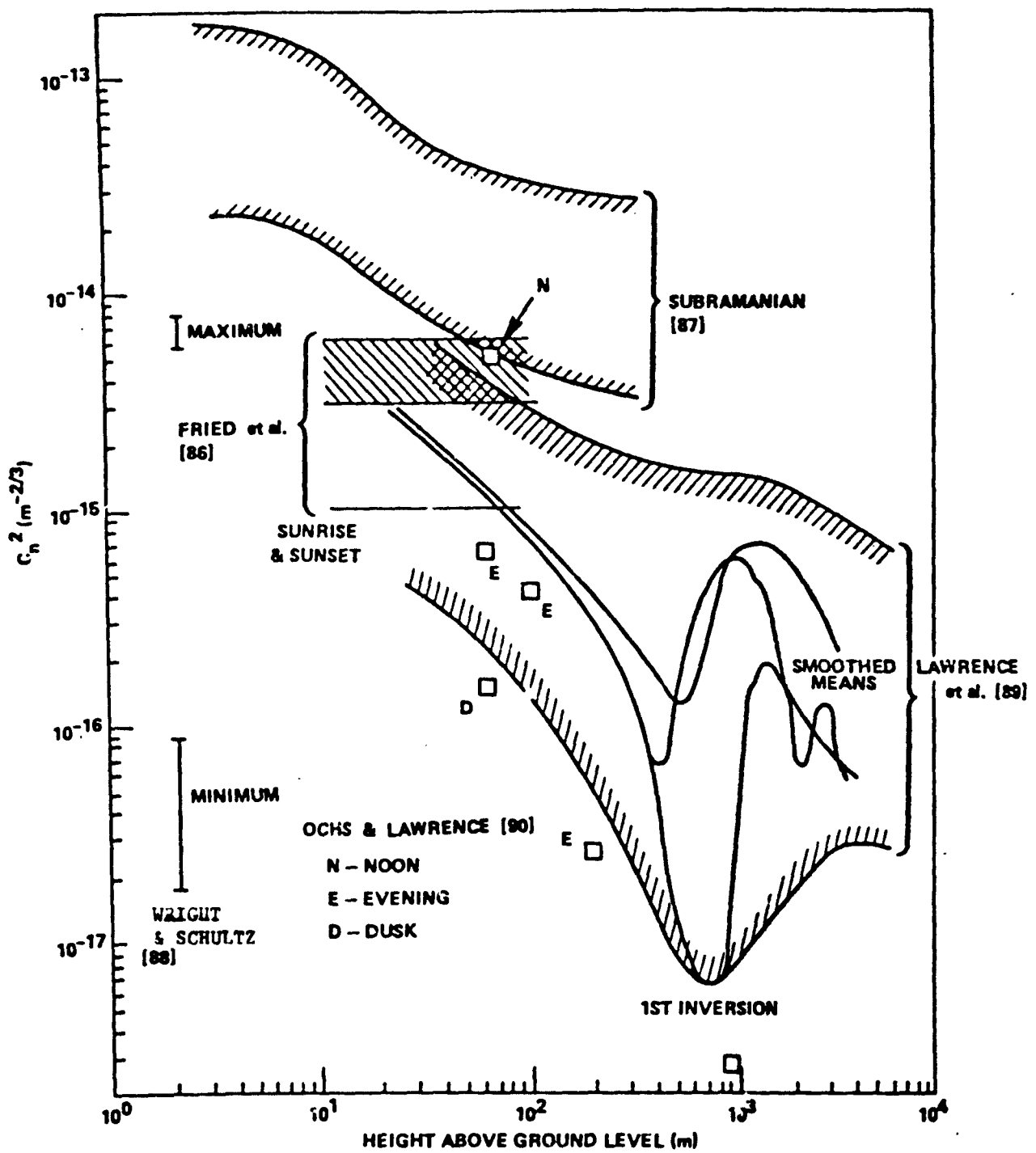

Figure 35. Comparison of turbulence models with measurements - low altitude.

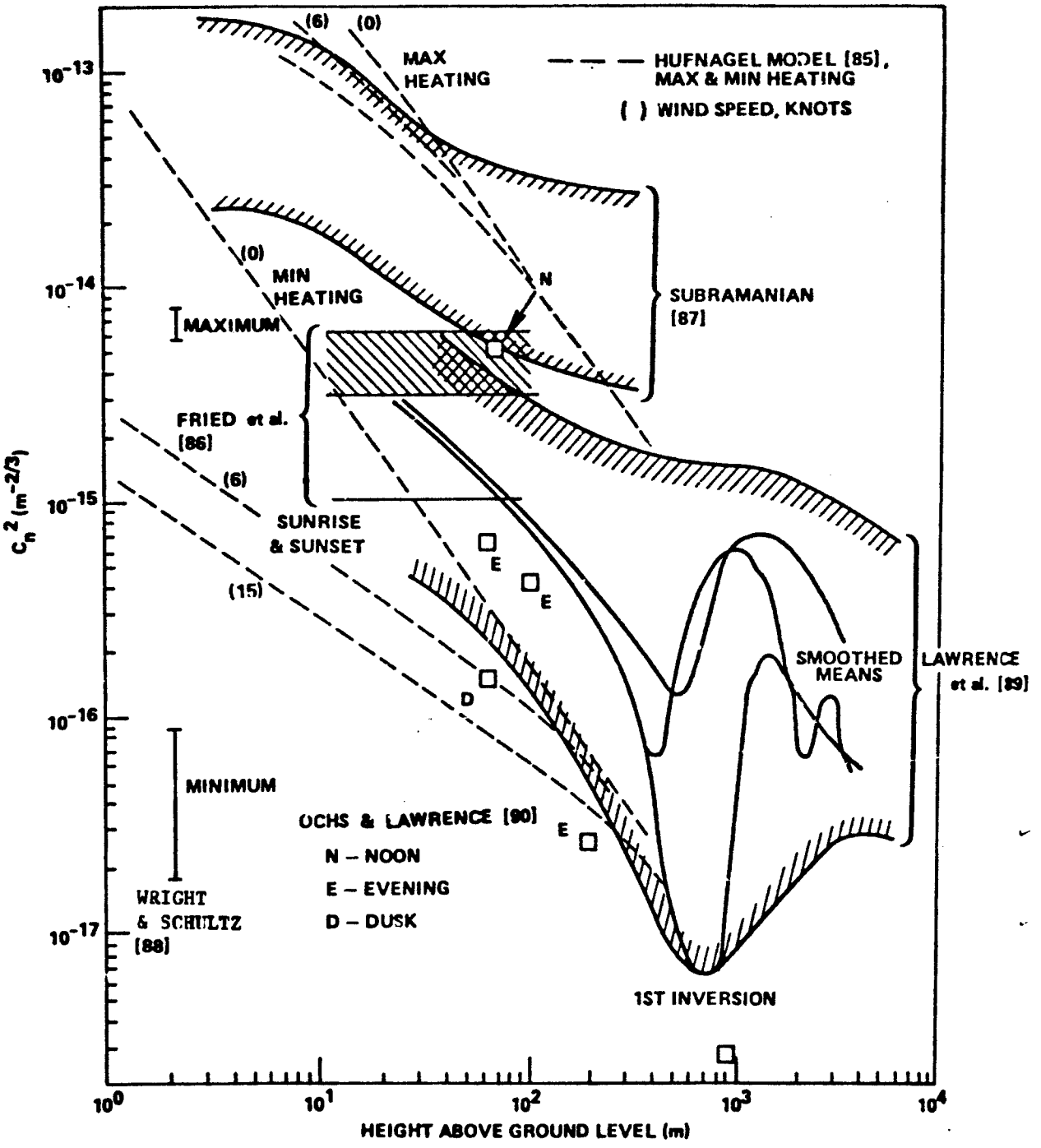

Figure 36. Comparison of turbulence models with measurements - low altitude.

but has a much faster decay rate with altitude than those measurements. The turbulence decay rates for both maximum and minimum illumination conditions with no wind, however, appear in general agreement with the rest of the measurements shown. Wind reduces the turbulence levels much more for the minimum heating condition than the maximum, according to this model.

It should be realized that the structure constant is very sensitive to local winds and local terrain features, so the large spread in the measurements should not be unexpected. For these same reasons, a simple model such as Hufnagel's cannot be expected to give more than general indications of the levels of turbulence that can be expected. For safety considerations, the upper models (i.e., maximum insolation) should probably be used in all situations to be conservative, since the phenomena are not completely understood at the present time and detailed empirical verification of the models is lacking.

At higher altitudes, the turbulence theory is poorly understood and strongly influenced by the nonstationarity of the entire boundary layer [85]. However, there have been numerous measurements (see Table 19) and several basically empirical models fit to the data. Some of these measurements and models are compared in Figure 37. The solid curves on the figure are various models by Hufnagel and by Fried. There is a considerable spread in the measured turbulence levels at high altitudes, but most of the spread originates in the extensive aircraft measurements by Morris [93]. Morris' data also indicate turbulence levels that are approximately an order of magnitude larger than any of the other measurements or models. Such aircraft-borne measurements would seem very difficult to make and particularly sensitive to bias.

A number of models have been developed for the high-altitude region. Hufnagel and Stanley [95] made one of the first attempts to semi-empirically model the observed variation of the structure constant with altitude. The expression they give is:

$$C_T^2 = \alpha^2 \, E^{2/3} \, \gamma^2 / \beta^2 \qquad (75)$$

TABLE 19. HIGH-ALTITUDE MEASUREMENTS AND MODELS OF REFRACTIVE INDEX STRUCTURE PARAMETER

Experimenters	Date	Description	Altitude (m)	Time of day (hr)	Conditions	Comments	Ref.
Tsvang	1969	Measurements of C_T^2 $(°C)^2(cm)^{-2/3}$	50, 100, 200, 250, 500, 750, 1000, 2000, 3000, and 4000 Few to 100-500	700-1430 1600-1800	Clear and cloudy	Model $C_T^2 = kz^{-4/3}$ for developed convection, based on his measurements.	84
Bufton et al.	1972	Measurements of C_n^2 indicate several stable layers but no well-defined tropopause. General agreement with Hufnagel's model [101]	1000-15,000	Dawn		"No simple model can describe layer structure, but could envelope"	92
Morris	1973	Measure C_n^2 with airborne laser; shows strong turbulence persists up to at least 10 km	1500-10,500			Much higher than Hufnagel's model or Fried model	93
Barletti et al.	1976	Radiosonde measurements of C_T^2 converted to C_n^2. Comparison with Hufnagel's 1974 model and Fried model	0-25,000		Clear?	Astronomical seeing survey	94
Hufnagel & Stanley	1964		1.5-1500 extrapolated to 65,000	Daytime		Model based on experimental data by Tatarski, Zwang, and Cossard	95
Hufnagel	1966	Models for normal conditions and disturbed conditions	$1-3 \times 10^4$	a) Sunny day b) Clear night c) Dawn-dusk min. d) Disturbed layers			99
Brookner	1971	Fits Ref. 99 formula to Ref. 95 models a-c	0-2000				100
Fried	1967	Model based on Ref. 95				$C_n^2 = C_{n_0}^2 h^{-b} \exp(-h/h_0)$ $b = 1/3$, $h_0 = 3200$ m, $C_{n_0}^2 = 4.2 \times 10^{-14}$ $m^{-2/3}$	98
Hufnagel	1974		3000-24,000			Model includes wind and a random variable for fine structure	101

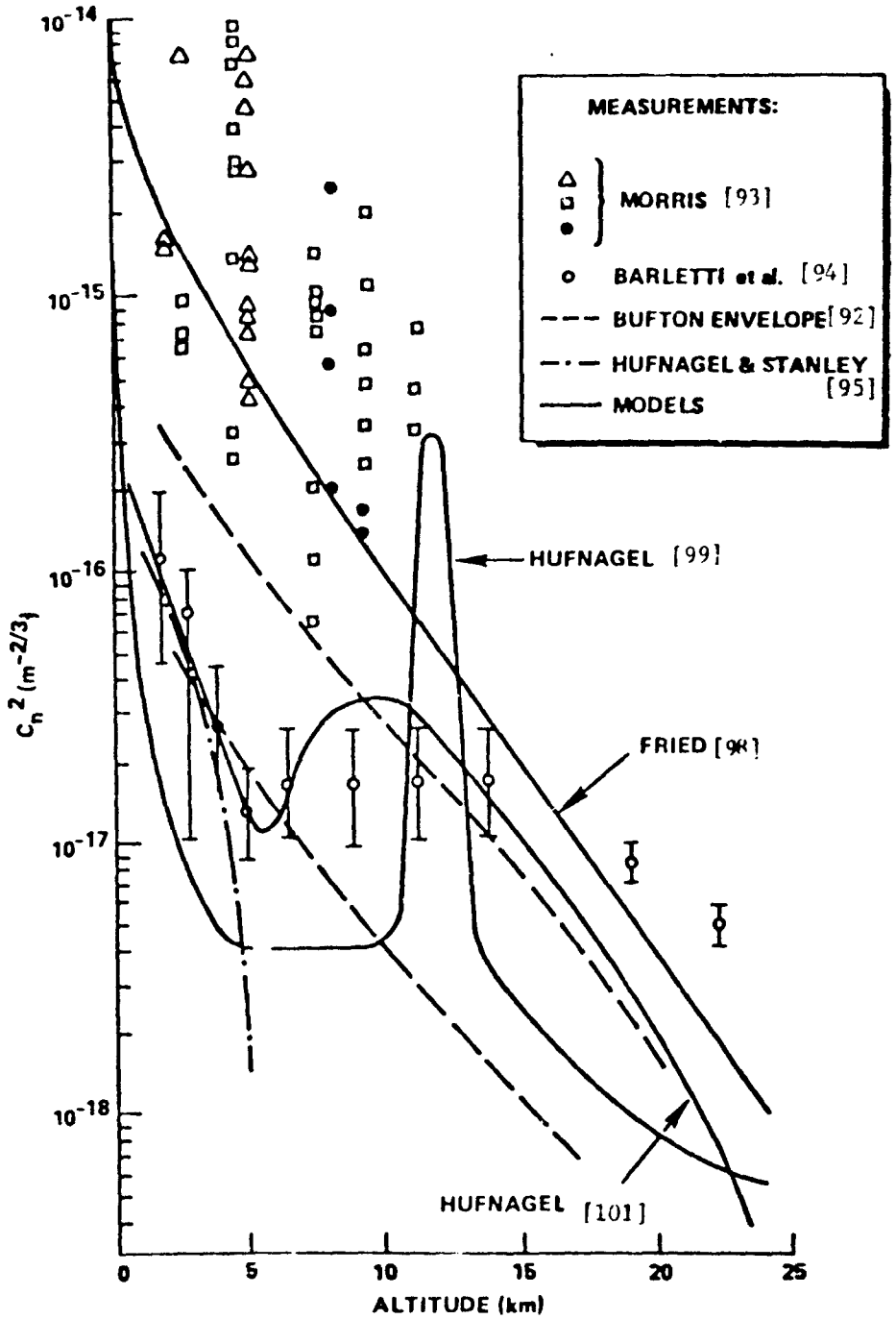

Figure 37. Comparison of turbulence models with measurements - high altitude.

where

α = Constant

E = Rate of energy per unit mass dissipated by viscous friction

γ = Vertical gradient of the potential temperature

β = Average shear rate of the wind.

In their paper, Hufnagel and Stanley [95] present average relationships for the parameters of Eq. 75 as a function of altitude from various sources that were used in their model. This model is indicated by the broken curve in Figure 38. The solid curve was not discussed by them, but presumably it is a fit to data of the form $Z^{-1/3}$ as predicted at low altitudes by Tatarski [91]. Measured data (with and without variability bars) are from Tatarski [91], Zwang [96], and Gossard [97]. Fried [98] later provided the expression:

$$C_n^2 = C_{n_0}^2 \; h^{-\beta} \exp(-h/h_0) \tag{76}$$

with $C_{n_0}^2 = 4.2 \times 10^{-14}$, $\beta = 1/3$, $h_0 = 3200$ m, and C_n^2 given in units of $m^{-2/3}$, which is intended to represent Hufnagel's model [95].

In 1966, Hufnagel updated this model [99] and included the ability to model distributed layers in the atmosphere (see Figure 39). Brookner [100] extended Eq. 76 to obtain an analytical expression of this Hufnagel model [99] (including the disturbed layer):

$$C_n^2 = C_{n_0}^2 \; h^{-\beta} \exp(-h/h_0) + C_n^+ \, \delta(h-h_p) \tag{77}$$

where C_n^+ is a random quantity with a mean value of $4.3 \times 10^{-13} \; m^{1/3}$ and a standard deviation factor of (ℓn 2) greater than that; δ is the delta function. This expression does not adequately represent Hufnagel's model over a very large altitude regime, however, and so does not seem to be of much value for the present problem.

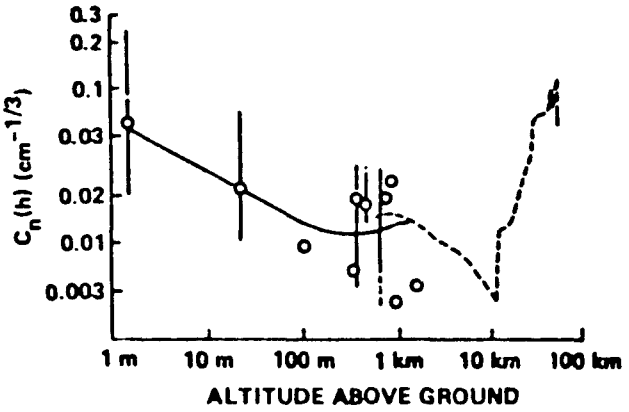

Figure 38. Early model of temperature structure constant versus altitude by Hufnagel and Stanley compared with measurements [95].

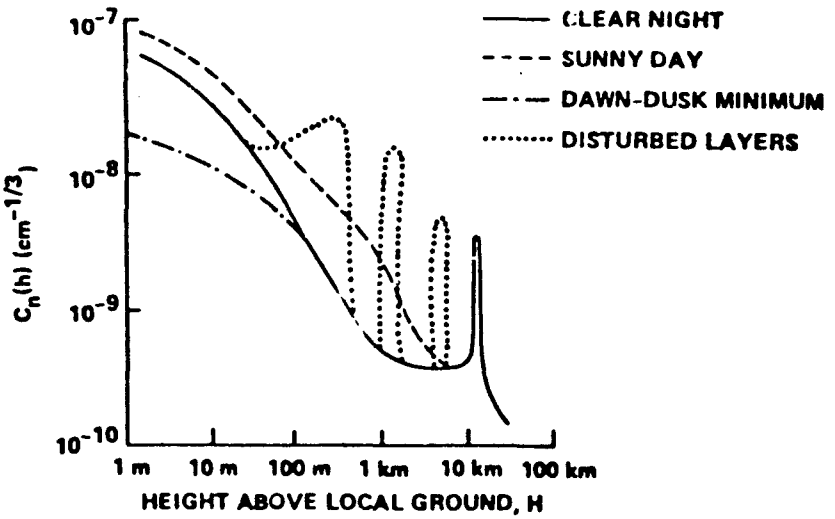

Figure 39. Hufnagel's 1966 model for index of refraction structure constant C_n [99].

Hufnagel later proposed another model [101], valid between 300 and 2400 m above ground, which is similar in form to Brookner's but more representative of nature:

$$C_n^2 = 2.2\times10^{-53}\, h^{10}\, (U/27)^2\, \exp(-h/1000) + 10^{-16}\, \exp(h/1500)\, e^{r(h,t)} \quad . \tag{78}$$

This expression contains a factor, U, which is the root-mean-squared (RMS) wind speed from 5 to 20 km, and also allows for the generation of fine structure by the Gaussian random variable r, with zero mean and a variance of $\sqrt{2}$. For those not interested in the fine structure, the random exponential factor can be replaced by the constant e (i.e., 2.7183). Hufnagel also provides a typical value for U (i.e., RMS wind speed U=18 m/sec). He presents a sample of random-generated atmospheric turbulence function which aesthetically, at least, looks similar to real data (see Figure 40). Hufnagel [85] recently gave an equation equivalent to Eq. 78 except without the random factor (which he said could be added if desired). In this last discussion, however, he also suggests that U can be represented by a Gaussian random variable that varies from day to day, with a mean of 27 m/sec and a standard deviation of 9 m/sec.

These more prominent models of high-altitude atmospheric turbulence discussed above were compared in Figure 37 with the previously presented measurements. Hufnagel's 1974 high-altitude turbulence model [101] appears to match the measured data shown, except for Morris', quite well. This model can be evaluated in three different ways. The first and easiest is to simply use a nominal average value for U in the 5-20-km region (e.g., 27 m/sec) (as was done for the curve shown in Figure 40a). The second method is to use radiosonde measurements of the wind speed for the actual conditions and altitude of interest. The third produces a random atmospheric value by using a random sample from a Gaussian distribution of speeds with a nominal mean and standard deviation to get the day-to-day variability (e.g., 27 and 9 m/sec, respectively). Such random fluctuations are frequently observed in high-resolution measurements at altitudes above the first inversion (see Figure 40b). However,

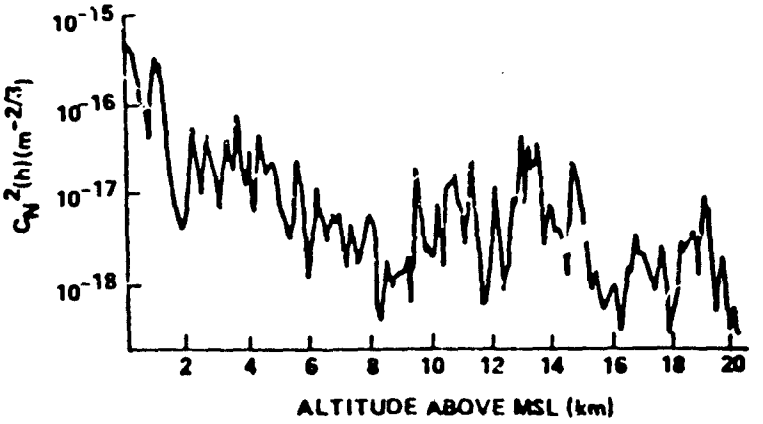

Figure 40a. Sample of atmospheric turbulence calculated with Hufnagel's random model (with W = 18 m/sec) [101].

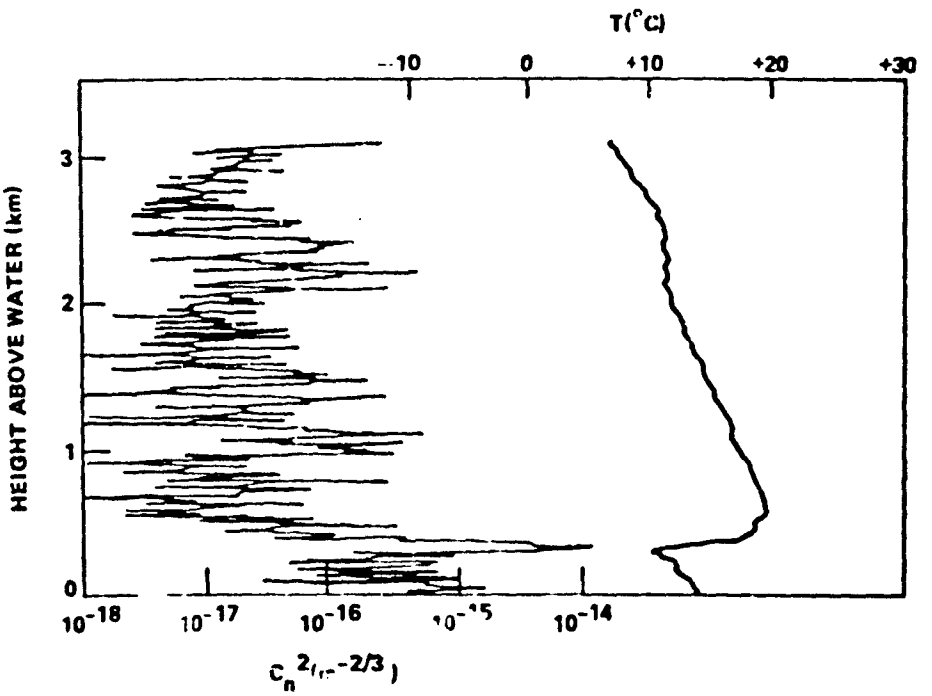

Figure 40b. Measured atmospheric turbulence and air temperature as a function of altitude over the ocean [85].

the third method would not be the best from a conservative safety viewpoint. The second method is, of course, the best of the three, but the first should be satisfactory if a safety margin were added. This could be accomplished simply by multiplying the coefficient of the second term (i.e., 2.7×10^{-16}) by a factor (e.g., 1.1).

Turbulence Effects--Atmospheric turbulence in the path of a laser beam causes temporal and spatial variations in its radiation field. The variations produce localized regions of intensification that can possibly enhance significantly the probability of laser eye damage. Existing theories, measurements, and models relevant to these effects are reviewed here to assess the state of information in this field and make recommendations for predictive models to aid in setting comprehensive safety standards.

As a field of study, the effect of turbulence on optical transmission has had a relatively long and active history due in part to its importance in astronomical observations. In 1952, Chandrasekhar [102], estimated the amplitude scintillation caused by atmospheric turbulence, using a geometric optics approach. In 1955, Muchmore and Wheelan [103] extended Chandrasekhar's work by calculating the variance and spectral correlation functions for the amplitude, phase, and angle of arrival of the laser radiation, using the geometric optics formulation. The Born approximation (i.e., method of small perturbations) was used by Wheelan [104] to solve the scalar-wave equation including diffraction effects. Obukhov [105] in 1953 apparently first applied a method proposed by Rytov [106] to consider atmospheric turbulence effects in sound and light propagation; however, this work did not receive wide circulation until it was translated in 1960 [107,91]. The Rytov method is similar to that of Born in that they are both perturbation techniques; however, Rytov's method includes multiple scattering, while Born's method treats only single scattering and is more widely used to correlate measured turbulence effects. Rytov's method is much more severely limited in the range of applicability than originally thought.

Rytov's theory results in the following equation relating the variance in the log of the amplitude of the laser irradiance (σ_T) at a point in space to the atmospheric turbulence structure function (C_n^2):

$$\sigma_T^2 = 0.56(2\pi/\lambda)^{7/6} \int_0^L C_n^2(x)(x/L)^{5/6} (L-x)^{5/6} dx \qquad (79)$$

where the integral is carried out over the entire path (i.e., x running from zero to L). If the turbulence is uniform over the path, this can be integrated to yield [108]:

$$\sigma_T^2 = 0.124(2\pi/\lambda)^{7/6} L^{11/6} C_n^2 . \qquad (80)$$

This relationship has been verified by several experiments (e.g., see Figure 41), within the limit of the scatter in the measurements. The set of data by Johnson et al. [109] (Figure 41) indicates excellent agreement with linear theory up to and slightly beyond log intensity standard deviations of unity. Their measurements were taken over a 460-m range, and the refractive index structure constant was derived from differential thermometer data. A data set by Kerr [110] (Figure 42), which is a composite of measurements at different wavelengths, indicates similar agreement with Rytov's theory (σ_T^2) but seems to drop away from the linear behavior early (i.e., at lower turbulence levels).

Gracheva and Gurvich in 1965 [111] were the first to demonstrate experimentally that the variance in the irradiance does not continue to increase linearly with the level of turbulence as characterized by C_n^2, the so-called saturation effect (e.g., see Figure 43). This was soon verified by other experiments [12-15]. In 1970, both Gracheva et al. [113] and Kerr [110] measured the supersaturation effect, where the variance of the irradiance actually grows smaller as the turbulence level is increased still more beyond the linear region (see Figure 44). Reviews of several reported measurements indicate that the maximum standard deviation always seems to lie below a value of 1.6, as shown in Figure 45.

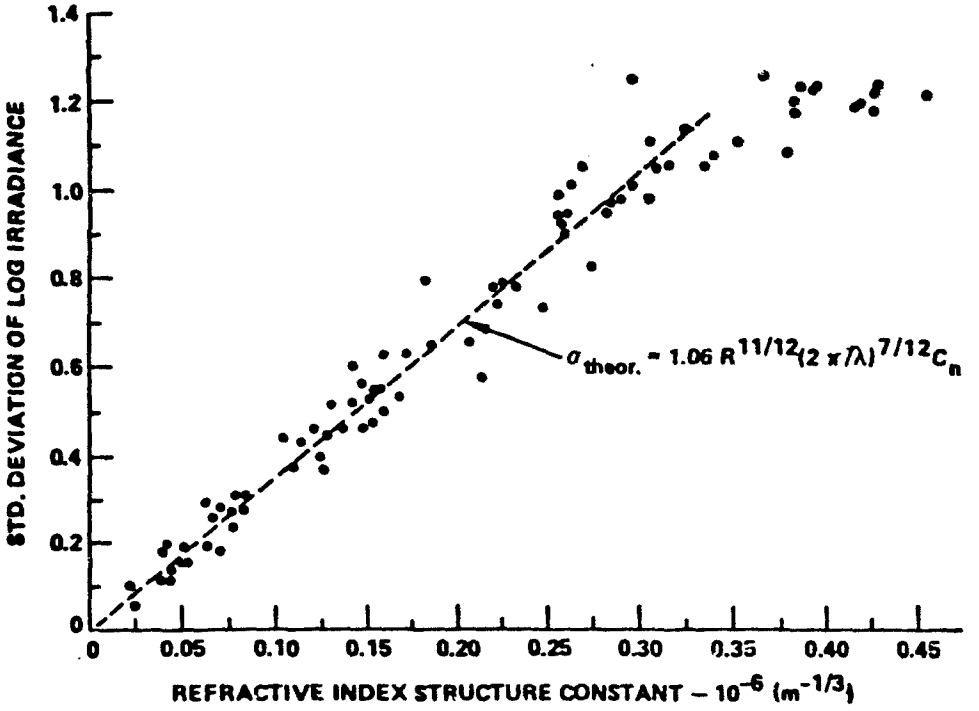

Figure 41. Observed irradiance statistic versus measured structure constant (linear scintillation region) [109].

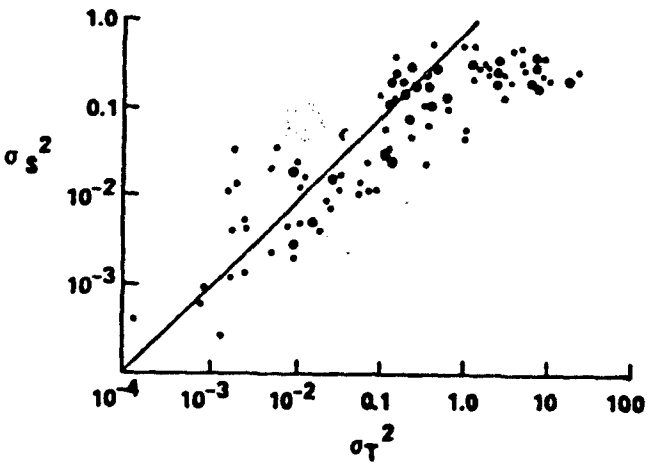

Figure 42. Experimental versus theoretical log-amplitude variance for 4880 Å, 1.15 μm, and 10.6 μm combined [110].

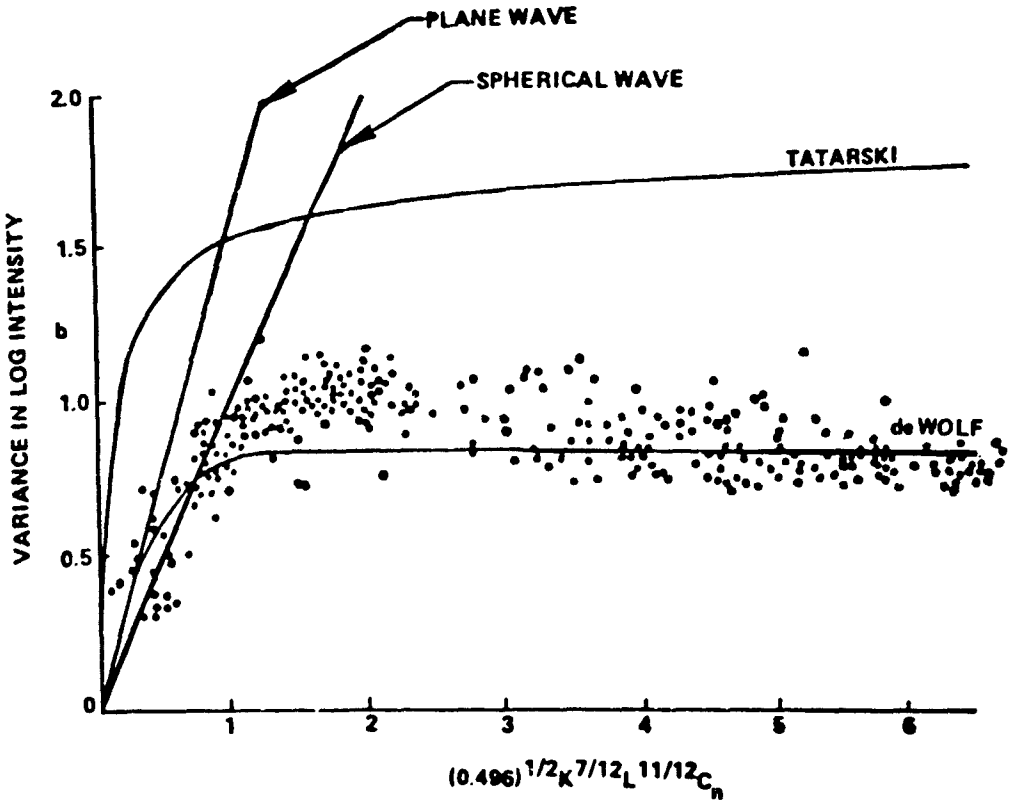

Figure 43. Measurements of variance in log intensity as a function of the turbulence level, showing the saturation effect [112].

There has been some controversy over the type of statistical distribution function that best represents these irradiance variations. It is generally taken to be log-normally distributed, but some authors have preferred the Rice-Nakagami distribution. It currently appears that the consensus is with the log-normal distribution. This distribution appears to apply even outside the range of linear effects into the saturation region [112].

A number of empirical models have been developed to predict the functional behavior of the standard deviation, but there is no consensus as to the best. It appears that the model by Johnson et al.[109] fits his data very well (see Figure 44), and seems to have the general shape of the other measurements (see Figure 45):

$$\sigma_m = \frac{\sigma_t}{1+0.16\sigma_t^2} \tag{81}$$

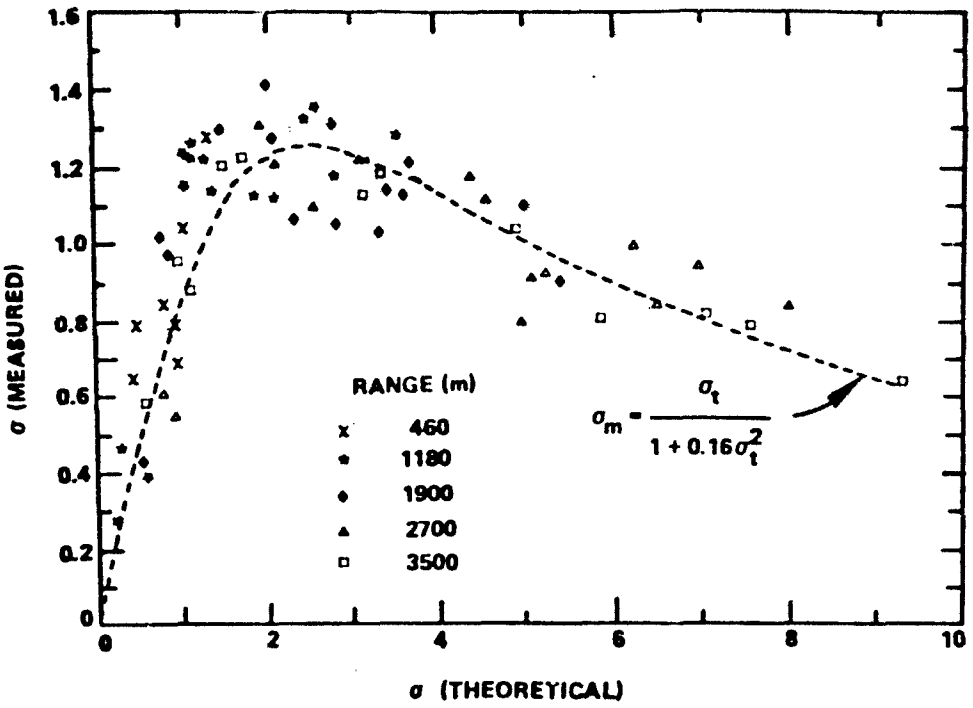

Figure 44. Observed relationship between the theoretical standard deviation (using linear theory) and measured standard deviation; shows the effect of supersaturation [109].

where σ_t is the theoretical linear expression based on Rytov's theory. For conservatism in safety considerations, it may be better to scale this up by a factor of 1.28 so that its maximum is 1.6 instead of 1.25:

$$\sigma_m = \frac{1.28\sigma_t}{1+0.16\sigma_t^2} \quad . \tag{82}$$

Considering this maximum in the standard deviation of the log of the intensity (i.e., $\sigma_{\log I}=1.6$), and for further conservatism, taking a 3σ deviation from the average intensity, implies:

$$I_{max} = \log^{-1}\left(\log I_{AVE} + 3\sigma_{\log I}\right) = 4.8\ I_{AVE} \quad . \tag{83}$$

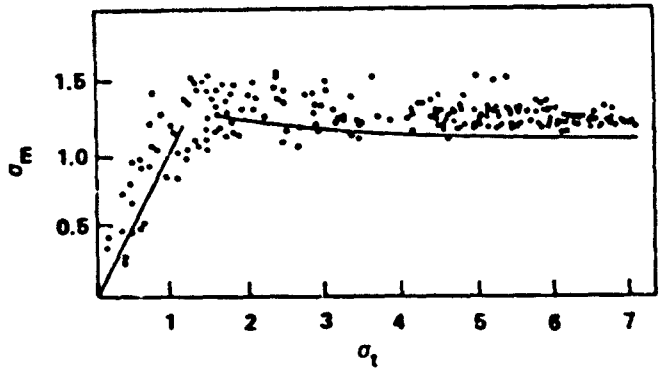

(a) TAKEN FROM REFERENCE 114.

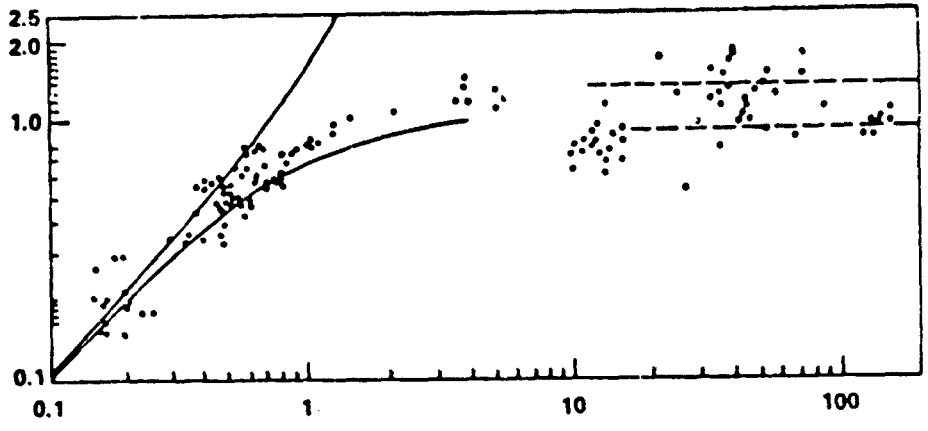

(b) TAKEN FROM REFERENCE 115.

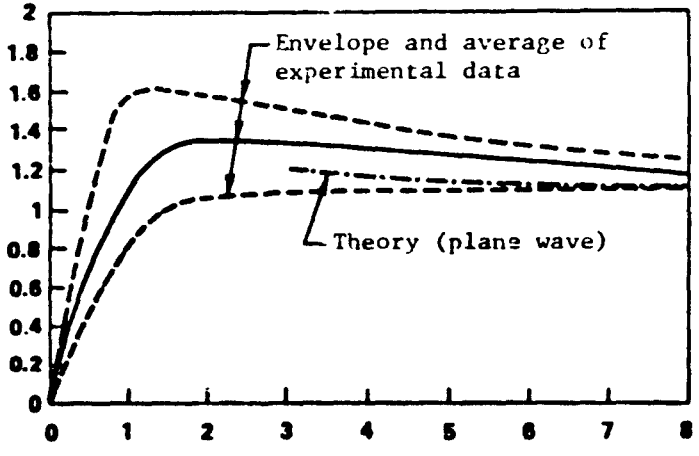

(c) TAKEN FROM REFERENCE 116.

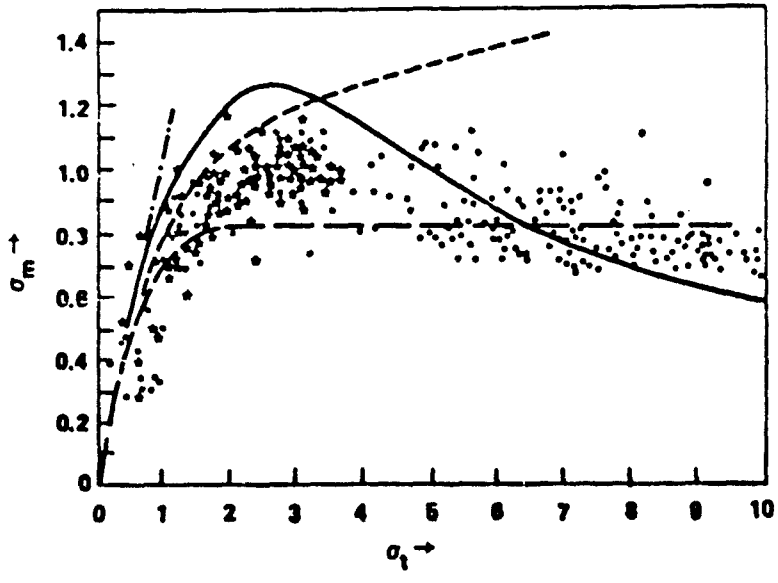

(d) TAKEN FROM REFERENCE 109. MEASUREMENTS BY GRACHEVA [113].

Figure 45. Measurements of log-intensity standard deviation σ_m versus theoretical (Rytov) σ_T. Curves indicate various theories (except in (c) and points indicate experimental data.

That is, the maximum effect that turbulence can have (on a 3σ basis) is to produce occasional irradiance values that are approximately five times the average value. This intensity would be reduced by molecular and aerosol extinction, as well as by beam divergence effects. The divergence due to turbulence appears to be much smaller than a microradian (for an example, see Reference 117), and thus can be neglected relative to the normal optical divergence (which is not an atmospheric effect and was not considered in this study).

CONCLUSIONS

The detailed conclusions of the evaluations of the various theories, experiments, and models discussed in the previous section will be presented in this section. The conclusions will be presented in the order in which the topics were discussed in the previous section in order to facilitate reference to the detailed discussion underlying each. Conclusions of major import to the objectives of the present program are indicated with an asterisk (*).

Atmospheric Molecular Concentration

(1)* Water vapor concentration is highly variable with time of day, time of year, altitude, and latitude, and can deviate strongly from nominal levels provided in the standard atmospheric models used in computer code LASER.

(2) Some measurements indicate a smaller water vapor concentration than standard atmospheric models at altitudes up to at least 3 km. Thus, the standard models would not be safety conservative.

Molecular Line Absorption

(1) Molecular line absorption of laser radiation is well represented, depending on the ambient pressure, by one of the simple Lorentz, Voigt, or Doppler theories, with the exception of the CO and HF laser radiation.

(2)* Large inaccuracies can be incurred when improper frequencies are used in the line-by-line calculation.

(3) In the CO and HF laser regions, the cutoff frequency should be 200 cm^{-1}, and the exponent on the $(\nu-\nu_0)$ term should be changed from 2 to 1.9.

Molecular Continuum Absorption

(1)* There is disagreement between various data on water vapor continuum absorption in the 2400-2800 cm^{-1} region.

(2) There is uncertainty in the form of the temperature dependence of the water continuum in the 400-1400 cm^{-1} region.

Molecular Scattering

Molecular scattering is well explained by the classical Rayleigh expression.

Aerosol Extinction Theory

The theory for aerosol extinction is well established and verified by experiment.

Aerosol Extinction Models

A number of models are available that use easily measured parameters such as visibility, relative humidity, and wind speed as inputs; however, none of these models have been verified to the extent that reliable predictions are possible.

Measurement Results

(1)* Extinction due to aerosols can change by more than three orders of magnitude during fog development and dispersal.

(2)* Extensive OPAQUE measurements (and others) indicate that extinction in the infrared cannot be reliably predicted from visible extinction information.

Turbulence Conditions

(1) Low-altitude turbulence conditions appear adequately predicted for present purposes by Hufnagel's 1978 model [85].

(2) High-altitude turbulence conditions are more difficult to treat, but Hufnagel's 1974 model [101] should be adequate.

Turbulence Effects

(1) The linear effects of turbulerce on the intensity variance is well represented by Rytov's theory [106].

(2)* The turbulence effects become saturated, so the maximum expected intensity (on a 3σ basis) is less than a factor of five larger than the average intensity.

RECOMMENDATIONS

Recommendations in this section are based on the evaluations and conclusions discussed in previous sections. Although the recommendations will be treated in the order in which specific topics were discussed earlier, they do not directly correspond, on a one-to-one basis, to the conclusions. Since the bases for these recommendations are discussed in detail in the "Evaluation" section, the following listing is intended to be concise.

Atmospheric Molecular Concentration

Whenever possible, the safety standards should be based on current local atmospheric concentrations (especially with regard to humidity) rather than relying on standard atmospheric models.

Molecular Line Absorption

(1) The AFGL LASER code (with inputs described below) should be used to evaluate the molecular line absorption at several parametric conditions of pressure, temperature, and humidity for the laser lines of

interest, to be used in semiempirical equations described in the next item. Inputs to the code should be:

- The AFGL Line Parameter Compilation updated with the latest experimental information.
- The best available information on laser frequencies.
- The best available information on the proper line shape and cutoff frequency (i.e., the maximum distance from laser line that absorption lines are considered) for the frequency range of interest (especially in the CO and HF laser regions).

(2) A simple algorithm based on the parametric LASER code results should be used to establish safety standards for the actual atmospheric path of concern.

Molecular Continuum Absorption

(1) The molecular continuum models incorporated in the AFGL LASER code (i.e., H_2O, N_2, CO_2) should be used in the evaluation recommended under Molecular Line Absorption.

(2) For conservatism in safety considerations, all other continua should be neglected.

(3) Efforts should be made to incorporate Kunde and Maguire's temperature functions [62] for the 400-1400-cm^{-1} water continuum into the AFGL model.

Molecular Scattering

The existing molecular scattering model incorporated in the AFGL LASER code should be used in the evaluation recommended under Molecular Line Absorption.

Aerosol Extinction

Because of large uncertainties in the results of current models, the safety-conservative Clear Model of LASER should be used, unless detailed aerosol size distributions and composition are available.

Turbulence Conditions

(1) Hufnagel's 1978 [85] low-altitude atmospheric turbulence model for maximum insolation should be used at altitudes below the first strong inversion.

(2) Hufnagel's 1974 [101] high-altitude atmospheric turbulence model, with a safety factor of 1.1, should be used at altitudes above the first strong inversion.

Turbulence Effects

The empirical model of Johnson, et al [109] (scaled up by a factor of 1.2, Eq. 82) should be used with Rytov's linear theory [107, and Eq. 79].

Additional Recommendations

The actual form of the model that should be used in setting safety standards will now be discussed briefly. It is assumed that this overall model should be highly user oriented so that people not familiar with the details of the effects can easily and rapidly obtain useful results. Due to the complex nature of the problem, a computer code is recommended. Ancillary charts and monographs should also be prepared to estimate some of the simpler parts of the problem (e.g., turbulence effects and molecular continuum absorption). On the other hand, the code should not be required to evaluate line-by-line absorpti ecause of the complexity and extensive computer time involved. These calculations would be parameterized and fit with a simple analytic function involving temperature, pressure, and humidity. The coefficients of this function, for the entire parameterized range of conditions required, should be stored in the code recommended here (i.e., simpler than line-by-line codes). To treat nonuniform, slant, or vertical paths in the atmosphere, a simple but physically correct interpolation scheme, which operates on the absorption coefficient, should be devised.

This function could also incorporate the molecular continuum absorption as well as molecular scattering and aerosol extinction, but

evaluating these separately would be more desirable since they involve such simple expressions and, in some cases, their individual contributions may be desired. Thus, the code would also contain simple analytic expressions for molecular continuum absorption and molecular scattering. Aerosol extinction requires a table of spectral coefficients in addition to a simple analytic expression, but the tables are not large. Finally, analytic expressions would be incorporated to estimate the effects of atmospheric turbulence. These should employ Hufnagel's low- or high-altitude model [85,101] (or both, depending on the path) to estimate the level of atmospheric turbulence, and use Rytov's linear expression [107] or Johnson's empirical expression [109] for saturated conditions. Non-uniform paths should be subdivided into a specified number of path elements that would then be considered uniform.

Several different options should be made available to the user so that information with as much detail as is available can be used in the calculations. For example, if actual measurements or other available information indicates atmospheric molecular concentrations different than nominal values, then these better values could be input. Similar alternate options should be available for measured aerosol size distributions, but such calculations should be limited to approximate expressions for the extinction efficiency factor rather than the complete Mie calculations. Some lasers emit at several different frequencies, and the power distribution between the various transitions should be specifiable. If such complete information is not available, nominal distributions should be stored within the code. The output of the code should also be straightforward and fully labeled so that it is easy to understand.

It is further recommended that this code have the capability of evaluating the probability that safe irradiance levels would not be exceeded, at specified ranges, as a function of time of year, by using statistics on meteorology, atmospheric constituents (molecular and aerosol), and turbulence. This feature should be available in operational and conceptual test planning.

REFERENCES

1. Tuer, T. W. Atmospheric effects on low power laser beam propagation: an annotated bibliography. Nichols Research Corporation, Ann Arbor, Mich., Feb 1979.

2. McClatchey, R. A., et al. Optical properties of the atmosphere (3rd ed.). AFCRL-TR-72-0497, 1972 (AD 753075).

3. McClatchey, R. A., et al. AFCRL atmospheric absorption line parameters compilation. ADCRL-TR-73-0096, 1973 (AD 762904).

4. Kelley, P. L., et al. Molecular absorption of infrared laser radiation in the natural atmosphere. Opt Quant Electron 8:117-144 (1976) (AD A027 C05/8ST).

5. Meredith, R. E., and T. W. Tuer. An assessment of aerosol and molecular extinction in the marine environment. Science Applications, Inc., Ann Arbor, Mich., May 1976.

6. Burch, D. E. Absorption of infrared radiant energy by CO_2 and H_2O-III, absorption by H_2O between 0.5 and 35 cm^{-1}. JOSA 58(10): 1383-1393 (1968).

7. Zhevakin, S. A., and A. P. Naumov. Absorption of centimeter and millimeter radiowaves by atmospheric water vapor. NASA-ST-AA-10209 (1964).

8. Woods, D. R., et al. High resolution spectral survey of molecular absorption in the DF laser region - measurements and calculations. Interim technical report from 1 August 1974 to 1 February 1975. RADC-TR-75-180, 1975 (AD A013 736/4ST).

9. Woods, D. R., et al. CO laser atmospheric absorption coefficient modeling. Science Applications, Inc., Ann Arbor, Mich., Mar 1978.

10. Watkins, W. R., et al. Water vapor absorption coefficient of HF laser wavelength (2.64-2.93 μm). Appl Opt 18(10):1582-1589 (1979).

11. Flaud, J. M., and C. Camy-Peyret. J Molec Spectrosc 55:278 (1975).

12. Leslie, D. H., and R. E. Meredith. Measurement of atmospheric transmission at HBr and Xe laser frequencies. Science Applications, Inc., Ann Arbor, Mich., May 1979.

13. McCoy, J. H., et al. Water vapor continuum absorption of carbon dioxide laser radiation near ten microns. Appl Opt 8(7):1471 (1969).

14. White, K. O., et al. Erbium laser propagation in simulation atmospheres. II. High resolution measurement method. Electronics Command (Army) ECOM-5398, 1971.

15. Rice, D. K. Absorption measurements of carbon monoxide laser radiation by water vapor. Northrop Report No. NLSD 72-11R, 1972 (AD 746170).

16. Spencer, D. J., et al. Atmospheric absorption at DF laser frequencies. Appl Opt 13:2855 (1974).

17. Long, R. K., et al. Experimental absorption coefficients for eleven CO laser lines. OSC Report No. 3271-5. RADC-TR-73-126 (1973).

18. Henry, L. Absorption of laser radiation in the atmosphere. Mitre Corp. Report No. M73-86, 1973.

19. Deaton, T. F., et al. Appl Phys Lett 26:300 (1975).

20. Mills, F. S. Absorption of deuterium fluoride laser radiation by the atmosphere. RADC-76-105, 1976.

21. Moskalenko, N. I., et al. Absorption of the emission of an He-CO_2 laser by CO_2, NH_3, and water vapor. Zh Prikl Spectrosk 17(5): 881 (1972).

22. Stephenson, J. C. et al. Appl Phys Lett 11:164 (1967).

23. Oppenheim, U. P., and A. D. Devir. Determination of CO_2 line parameters using a CO_2-N_2-HE laser. JOSA 58:585 (1968).

24. Gerry, E. T., and D. A. Leonard. Appl Phys Lett 8:227 (1966).

25. McCubbin, T. B., and T. R. Mooney. A study of the strengths and widths of lines in the 9.4 and 10.4 μ CO_2 band. J Quant Spectrosc Radiat Trans 8:1255-1264 (1968).

26. McCubbin, T. B., et al. Appl Phys Lett 8:118 (1966).

27. Long, R. K., and J. H. McCoy. Atmospheric absorption of 10.6 μ CO_2 laser radiation. JOSA 57(4):570 (1967).

28. Long, R. K. Laser absorption in the 5 micron band. OSU 3271-1. RADC-TR-71-314 (1971).

29. Ford, D. L. Laser absorption in the 5 micron band. OSU 3271-2. RADC-TR-72-140 (1972).

30. Ford, D. L., et al. Laser absorption in the 5 micron band. OSU-3271-3. RADC-TR-72-195 (1972).

31. Long, R. K., et al. Experimental studies of the partial and total pressure dependence of water vapor absorption coefficients for highly transmitting CO laser lines. OSU 3271-4. RADC-TR-73-125 (1973).

32. Long, R. K., et al. Measured water vapor absorption coefficients for two highly absorbed CO laser lines. RADC-TR-73-225 (1973).

33. Long, R. K. CO_2 and CO laser transmission measurments. Proc: Absorp of IR Laser Rad in the Atmos. Mitre Corp Report No. M73-86, Vol II:69-126 (1973).

34. Rice, D. K. Atmospheric attenuation measurements for several highly absorbed CO laser lines. Appl Opt 12(7):1401-1403 (1973).

35. Rice, D. K. Absorption measurements of carbon monoxide laser radiation by water vapor. Appl Opt 12(2):218-225 (1973).

36. Dowling, J. A., et al. Atmospheric extinction measurements at Nd-YAG and DF laser wavelengths performed in conjunction with the JAN propagation tests, June-September 1975. Naval Research Laboratory Report NRL-8058 (AD A053 271/3ST).

37. Cosden, T. H., et al. Data compendium for atmospheric laser propagation studies conducted at Cape Canaveral, Florida, February-May 1977. NRL Memo Report 3611, 1977 (AD A050 094).

38. Meyers, O. E. (General Dynamics, Convair Aerospace). Private communication with Dr. R. K. Long at Ohio State University.

39. Burch, D. E., et al. Investigation of the absorption of infrared radiation by atmospheric gases. Philco Ford Report No. U4784, 1970.

40. Borisov, V. A., Opt Mekh Prom-st' 7:11 (1970).

41. Adiks, T. G., et al. Influence of molecular absorption on propagation of CO_2 laser radiation in terrestrial atmosphere. Sov J Quant Electron 5(5):481 (1975).

42. McClatchey, R. A., and A. P. d'Agati. Atmospheric transmission of laser radiation computer code LASER. AFGL-TR-78-0029, 1978.

43. Woods, D. R., et al. DF laser propagation analysis, final report covering 5 Jan - 3 Dec 1976. Science Applications, Inc., Ann Arbor, Mich., 1977.

44. Burch, D. E., et al. Laboratory investigation of the continuum absorption of infrared radiation by atmospheric gases: water, nitrogen, nitrous oxide. Philco Ford Report No. U4897, 1971 (AD 882 876).

45. Damon, E. K., et al. Spectrophone measurement of the water vapor continuum at DF laser frequencies, interim report covering 1 Oct - 30 Dec 1974. OSU Report No. ESL-4045-1. RADC-TR-75-203, 1975 (AD A016 435/0ST).

46. White, K. O., et al. Water vapor continuum absorption in the 3.5-4.0 micrometers region. ERADCOM/ASL-TR-0004, 1978 (AD A005 580/5ST).

47. White, K. O., et al. Water vapor continuum absorption in the 3.5-4.0 μm region. Appl Opt 17(17):2711-2720 (1978).

48. McClatchey, R. A. General conclusions and summary of 2nd review conference on atmospheric transmission models. AFGL letter report, 13 June 1979.

49. McClatchey, R. A. (AFGL). Personal communication, 7 June 1979.

50. Kondrat'yev, K. Ya., et al. J Atmos Ocean Phys (Izv USSR) (4): 215-222 (1965).

51. Varanisi, P. Absorption coefficients for water vapor in the 600-1000 cm^{-1} region. J Quant Spectrosc Radiat Trans 8:1537-1541 (1968).

52. Benedict, W. S., and L. D. Kaplan. Atmospheric radiation. I. Theoretical basis by R. M. Goody. London: Oxford Univ Press, 1964.

53. Bignell, K. J. The water vapor infrared continuum. Q J Roy Meteorol Soc 96:390-403 (1970).

54. Moskalenko, N. I., et al. Absorption of the emission of an He-CO_2 laser by CO_2, NH_3, and water vapor. J Appl Spectrosc 17: 1477-1479 (1972).

55. Gryvnak, D. A., et al. Infrared absorption by CH_4, H_2O, and CO_2. AFGL-TR-76-0246, 1976.

56. Shumate, M. S., et al. Water vapor absorption of carbon dioxide laser radiation (optoacoustic detector measurement). Appl Opt 15(10):2480 (1976).

57. Coffey, M. T. Water vapor absorption in the 10-12 μm atmospheric window. Q J Roy Meteorol Soc 103:685-692 (1977).

58. Izatt, J. R. Self- and foreign-gas broadening in the pure rotation spectrum of water vapor. Ph.D. dissertation. John Hopkins Univ., 1960.

59. Montgomery, G. P., Jr. Temperature dependence of infrared absorption by the water vapor continuum near 1200 cm^{-1}. Appl Opt 17 (15):2299-2303 (1978).

60. Nordstrom, R. J., et al. Effects of oxygen addition on pressure broadened water vapor absorption in the 10 μm region. Appl Opt 17(17):2724 (1978).

61. Peterson, J. C., et al. Water vapor nitrogen absorption at CO_2 laser frequencies. Appl Opt 18(6):834-841 (1979).

62. Kunde, V. G., and W. C. Maguire. Direct integration transmittance model. NASA-X-622-73-258, 1973.

63. Tuer, T. W. Thermal imaging systems' relative performance. AFAL-TR-76-217, 1976.

64. Roberts, R. E., et al. Infrared continuum absorption by atmospheric water vapor in the 8-12 μm window. Final report covering Oct 1975 - Mar 1976. Inst Def Anal P-1184, 1976 (AD A025 337/3ST).

65. Burch, D. E., and D. A. Gryvnak. Laboratory measurements of the infrared absorption by H_2O and CO_2 in regions of weak absorption. Soc Photo-Opt Instrum Eng 142:16 (1978).

66. Ashcheulov, S. V., et al. Problems of atmospheric physics (5). Izd-vo Leningrad-skogo Gosudarstvennogo Universiteta, 1967.

67. Bolle, H. J. Memoires Roy Soc Sci Liege, Vol. 26, 1964.

68. Gates, D. M. Near infrared atmospheric transmission to solar radiation. JOSA 50(12):1299 (1960).

69. Penndorf, R. Luminous and spectral reflectance as well as colors of natural objects. AFCRL-TR-56-203, 1956.

70. McCartney, E. J. Optics of the atmosphere. New York: J. Wiley and Sons, 1976.

71. Deirmendjian, D. R. Electromagnetic scattering on spherical polydispersion. New York: American Elsevier, 1969.

72. Junge, C. E. Aerosols. Handbook of geophysics. New York: MacMillan, 1960.

73. Barnhardt, E. A., and J. L. Streete. A method for predicting atmospheric scattering coefficients in the infrared. Appl Opt 9(6):1337-1344 (1970).

74. Wells, W. C., et al. Aerosol distributions in maritime air and predicted scattering coefficients in the infrared. Appl Opt 16(3):654-659 (1977).

75. Hänel, G. Properties of atmospheric particles as functions of relative humidity at thermodynamic equilibrium with the surrounding air. Adv Geophys 19 (1976).

76. Fenn, R. W. OPAQUE - A measurement program on optical atmospheric quantities in Europe. AFGL-TR-78-0011, 1978.

77. Turner, R. E., et al. Model development for E-O SAEL: natural aerosol, contrast, laser transmission and turbulence. Science Applications, Inc., Ann Arbor, Mich., Dec 1978.

78. Chu, T. S., and D. G. Hogg. Effects of precipitation on propagation at 0.63, 3.5, and 10.6 micron. Bell Sys Tech J 47(5):723-759 (1968).

79. Neiburger, M., and C. W. Chien. Computation of the growth of cloud drops by condensation using an electronic digital computer. Proc Cloud Phys Conf Vol. 5, 1959.

80. Selby, J. E. A., et al. Atmospheric transmittance/radiance: computer code LOWTRAN IV. AFGL-TR-78-0053, 1978.

81. Roberts, R. E. Atmospheric transmission modeling: proposed aerosol methodology with application to the Grafenwohr atmospheric optics data base. Inst Def Anal P-1225, 1976.

82. Smith, F. G., et al. A study of current and future technology FLIR performance in the European environment. AFAL-TR-78-159, 1978.

83. Wyngaard, J. C., and Y. Izumi. Behavior of the refractive-index structure parameter near the ground. JOSA 61(12):1646-1650 (1971).

84. Tsvang, L. R. Microstructure of temperature fields in the free atmosphere. Radio Sci 4:1175 (1969).

85. Hufnagel, R. E. Propagation through atmospheric turbulence. Infrared Handbook. IRIA Center, Ann Arbor, Mich., 1978.

86. Fried, D. L., et al. Measurements of laser beam scintillation in the atmosphere. JOSA 57(6):787-797 (1967).

87. Subramanian, M. Atmospheric turbulence profile in troposphere. Proc Optical Society of America, Spring Meeting, 1971.

88. Wright, N. J., and R. J. Schultz. Measurement of the refractive index structure coefficient C_N. Ballistic Res Lab Memo 1885, 1967.

89. Lawrence, R. S., et al. Measurements of atmospheric turbulence relevant to optical propagation. JOSA 60(6):826-830 (1970).

90. Ochs, G. R., and R. S. Lawrence. Natl Oceanogr Atmos Adm TR ERL-251-WPL-22, 1972.

91. Tatarski, V. I. Wave propagaion in a turbulence medium. New York: McGraw-Hill, 1961.

92. Bufton, J. L., et al. Measurements of turbulence profiles in the troposphere. JOSA 62(9):1068-1070 (1972).

93. Morris, G. J. Airborne laser beam scintillation measurements in high altitudes. JOSA 63(3):263-270 (1973).

94. Barletti, R., et al. Mean vertical profile of atmospheric turbulence relevant for astronomical seeing. JOSA 66:1380-1383 (1976).

95. Hufnagel, R. E., and N. R. Stanley. Modulation transfer function associated with image transmission through turbulent media. JOSA 54(1):52 (1964).

96. Zwang, L. R. Bell Acad Sci USSR. Geophys Ser 8:1117 (1960).

97. Gossard, E. E. IRE Trans Antennas Prop 10:186 (1960).

98. Fried, D. L. Optical heterodyne detection of an atmospherically distorted signal wavefront. Proc IEEE 55:57-67 (1967).

99. Hufnagel, R. E. Restoration of atmospherically degraded images. Woods Hole Summer Study. Natl Acad Sci 2:14 (1966).

100. Brookner, E. Improved model for structure constant variations with altitude. Appl Opt 10(8):1960 (1971).

101. Hufnagel, R. E. Variations of atmospheric turbulence. Optical Soc of America topical mtg: Propagation through turbulence. Paper WA 1-1, 1974.

102. Chandrasekhar, S. A statistical basis for the theory of stellar scintillation. Monthly Notices. Roy Astron Soc 112:475-483 (1952).

103. Muchmore, R. B., and A. D. Wheelan. Line-of-sight propagation. Proc IEEE 43:1437-1449 (1955).

104. Wheelan, A. D. Near-field corrections to line-of-sight propagation. Proc IEEE 43:1459-1466 (1955).

105. Obukhov, A. M. On the influence of weak atmospheric inhomogeneities on the propagation of sound and light. Izv Akad Nauk SSSR, Ser Geofiz 2:155 (1953).

106. Rytov, S. M. Diffraction of light by ultrasonic waves. Izv Akad Nauk SSSR, Ser Fiz 2:223 (1937).

107. Chernov, L. A. Wave propagation in a random medium. New York: McGraw-Hill, 1960.

108. Fried, D. L., and J. B. Seidman. Laser beam scintillation in the atmosphere. JOSA 57(2):181-185 (1967).

109. Johnson, W. B., et al. Atmospheric effects upon laser eye safety, Pt 1. Stanford Res Inst, 1970.

110. Kerr, J. R. Experiments on turbulence characteristics and multi-wavelength scintillation phenomena. JOSA 62(9):1040-1051 (1972).

111. Gracheva, M. E., and A. S. Gurvich. Strong fluctuations in the intensity of light propagated through the atmosphere close to the earth. Radiophys Quant Electron 8:511 (1965).

112. Dietz, P. H., and N. J. Wright. Saturation of scintillation magnitude in near-earth optical propagation. Ballistics Research Laboratories BRL-MR-1941-Rev, 1968 (AD 68/352).

113. Gracheva, M. E., et al. Dispersion of strong atmospheric fluctuations in the intensity of laser radiation. Radiophys Quant Electron 13:40-42 (1970).

114. Prokhorov, A. M., et al. Laser irradiance propagation in turbulent media. Proc IEEE 63(5):790-811 (1975).

115. Khmelevtsov, S. S. Propagation of laser radiation in a turbulent atmosphere. Appl Opt 12(10):2421-2433 (1973).

116. Fante, R. L. Irradiance scintillations: comparison of theory with experiment. AFCRL-TR-74-0626, 1974 (AD A006 365/1ST).

117. Dowling, J. A., et al. Experimental studies of focused laser beams propagating through near-earth atmospheric turbulence, Proc Optical Society of America, Spring Meeting, 1971.

118. Reddy, S. P., and C. W. Cho. Induced infrared absorption of hydrogen and nitrogen foreign gas mixtures. Can J Phys 43: 2331-2343 (1965).

119. Shapiro, M. M., and H. P. Gush. The collision-induced fundamental and first overtone bands of oxygen and nitrogen. Can J Phys 44:949-963 (1966).

120. Burch, D. E., et al. Investigation of the absorption of infrared radiation by atmospheric gases. AFCRL-70-0373, 1970.

121. Elder, T., and J. J. Strong. Franklin Inst 225(3):189-208 (1953).

122. Streete, J. L. Infrared measurements of atmospheric transmission at sea level. Appl Opt 7(8):1545-1549 (1968).

123. Menzies, R. T., and M. S. Shumate. Appl Opt 15(9):2025 (1976).

124. Watkins, W. R., et al. Pressure dependence of the water vapor continuous absorption in the 3.5-4.0 μm region. Appl Opt 8(6): 1149 (1979).

APPENDIX A. MOLECULAR CONTINUUM ABSORPTION MEASUREMENTS

Experimenter	Date	Measured quantity	Range of data	Comments	Ref.
Reddy & Cho	1965	Nitrogen continuum (2100–2700 cm^{-1})	$107 < p_{N_2} < 1500$ amagats, T = 298 K	Good very high pressure data on the fundamental band.	118
Shapiro & Gush	1966	Nitrogen continuum (2200–2600 cm^{-1} & 4400–4800 cm^{-1})	$p_{N_2} = 20$ atm, T = 296 K	Good very high pressure, room temperature data on fundamental and first overtone pressure induced nitrogen absorption.	119
Burch et al.	1970	Nitrogen continuum (2400–2600 cm^{-1})	$p_{N_2} = 1$ atm, $T = 296$ K	Agrees with Shapiro and Gush.	120
Burch et al.	1971	Nitrogen continuum (2400–2650 cm^{-1})	T = 296, 380, and 457 K	Agrees well with earlier work at 296 K; extends data to higher temperatures.	44
Burch et al.	1970	Carbon dioxide continuum (1100–2000 cm^{-1})	T = 296 K	Absorption ascribed to intrinsic bands, pressure induced bands, and far wing absorption.	120
Burch et al.	1970	Carbon dioxide continuum (780–900 cm^{-1})	T = 296 and 240 K	Observed continuum near 890 cm^{-1} is 100 times less than that calculated from Lorentz line shapes.	39
Burch & Gryvnak	1978	Carbon dioxide continuum (6800–7100 cm^{-1})	$p_{CO_2} = 0.077$, 2, 14.6 atm	Both foreign- and self-broadened lines are very much sub-Lorentzian and show wing absorption that decreases with increasing temperature much faster than theory predicts.	65

APPENDIX A. MOLECULAR CONTINUUM ABSORPTION MEASUREMENTS (CONTINUED)

Experimenter	Date	Measured quantity	Range of data	Comments	Ref.
Elder & Strong	1953	Water vapor continuum (0.7–14 μm)		Summarizes, compares early low resolution data.	121
Streete	1968	Water vapor continuum (0.56–10.7 μm)	Field measurements, precipitable water vapor ranging from 21.5 to 43.3 cm.	Observed transmittance agrees with statistical model of band absorption.	122
Burch et al.	1971	Water vapor continuum (3.55–4.17 μm)	T = 338, 384, and 428 K	Temperature dependence of $C_s^\circ \sim e^{\text{const./temp.}}$ deduced: C_s° extrapolated to T = 296 K. Discusses anomalous absorption data due to absorbed water vapor on mirrors.	44
Damon et al.	1975	Water vapor continuum (3.64–3.93 μm)	P_{H_2O} = 14.3 torr P_{total} = 700 torr T = 297 K	Continuum absorption coefficients presented at 6 DF laser wavelengths (spectrophone data).	45
Menzies & Shumate	1976	Water vapor continuum (5.1–5.3 μm)	P_{H_2O} = 6, 10, 12 torr; T = 300 K	Spectrophone data at 23 CO laser lines; HDO extinction coefficients at several impartial pressures broadened by N_2 are presented along with H_2O extinction coefficients. Data in both cases are at 8 DF laser lines, taken in White cell.	123
Mills	1976	Water vapor continuum (3.73–3.93 μm)	T = 297 K		20

APPENDIX A. MOLECULAR CONTINUUM ABSORPTION MEASUREMENTS (CONTINUED)

Experimenter	Date	Measured quantity	Range of data	Comments	Ref.
White et al.	1978	Water vapor continuum (3.5–4.0 μm)	p_{H_2O} = 14.3, 65 torr T = 296, 338 K P_{total} = 760 torr	White cell at 338 K agrees with Burch's 338 K data [44]. White cell and spectrophone data at 296 K indicate continuum absorption twice as large as Burch extrapolation.	47
Watkins et al.	1979	Water vapor continuum (3.5–4.0 μm)	p_{H_2O} = 14.3 torr 6 buffer pressures T = 298 K	White cell data at 26 DF laser lines yield a ratio of foreign-to-self-broadening coefficient of 0.011 compared to Burch's determination of 0.12. Continuum absorption attributed to far wings and aggregate absorption.	124
Kondrat'yev et al.	1965	Water vapor continuum (8–12 μm)	Field data, conditions variable	Conclude absorption due to wings of bands centered at 6.3 μm.	50
Varanisi	1968	Water vapor continuum (10–16.7 μm)	p_{H_2O} = 2, 10 atm 400 < T < 500 K	Interpret data in terms of aggregate water molecule bound by H-bonding with binding energy on the order of 3–5 kcal/mole.	51
McCoy et al.	1969	Water vapor continuum (10.59, 9.55 μm)	296 < T < 299 K 0 < p_{H_2O} < 20 torr	Laboratory data compared with field data.	13
Burch et al.	1970	Water vapor continuum (8–12 μm)	T = 296, 358, 388 K	Self-broadened line absorptions much more than Lorentz lines in this region; absorption decreases with increasing temperature much more rapidly than constant line shape theory predicts.	39

APPENDIX A. MOLECULAR CONTINUUM ABSORPTION MEASUREMENTS (CONTINUED)

Experimenter	Date	Measured quantity	Range of data	Comments	Ref.
Bignell	1970	Water vapor continuum (8–12 μm)	333 < T < 388 K	Observes rapid decrease in absorption with increase in temperature.	53
Moskalenkc et al.	1972	Water vapor continuum (10.6 μm)	280 < T < 600 K	Observes increase in absorption with increase in temperature.	54
Adiks et al.	1975	Water vapor continuum (8–12 μm)	293 < T < 388 K	Observes decrease in absorption with increasing temperature.	41
Gryvnak et al.	1976	Water vapor continuum (8–12 μm)	T = 296, 392, 430 K	Conclude early (Burch [39]) values of C_s were 5–20 percent too high. Confirm rapid decrease in absorption with increase in temperature observed earlier.	55
Roberts et al.	1976	Water vapor continuum (8–12 μm)	$4 < p_{H_2O} < 14$ torr	Review of data to 1976 in 8–12 μm region. Conclude LOWTRAN must be modified to incorporate: (1) improved fit to H_2O continuum and (2) strong measured temperature dependence of continuum absorption coefficient.	64
Shumate et al.	1976	Water vapor continuum (9.2–10.7 μm)	p_{H_2O} = 5, 10, 15 torr T = 300 K	Spectrophone data on continuum absorption at 49 CO_2 laser lines in this wavelength region fall 5–10 percent lower than previous results (Burch [39]).	56

APPENDIX A. MOLECULAR CONTINUUM ABSORPTION MEASUREMENTS (CONCLUDED)

Experimenter	Date	Measured quantity	Range of data	Comments	Ref.
Coffey	1977	Water vapor continuum (10–12 μm)	Midlatitude, tropical field data	Concludes water-vapor dimers are responsible for continuum absorption.	57
Montgomery	1978	Water vapor continuum (8.3 μm)	333 < T < 473 K	Data for T < 398 K agree with earlier data [39] discuss role of H_2O vapor dimers in interpreting data.	59
Nordstrom et al.	1978	Water vapor continuum (~10.4 μm)	P_{H_2O} = 15 torr P_{total} = 760 torr T = 295.5 K	Data taken 5 CO_2 lines demonstrate O_2 is a less efficient broadening gas than N_2.	60
Peterson et al.	1979	Water vapor continuum (9.24–10.7 μm)	4 < P_{H_2O} < 15 torr P_{total} = 760 torr T = 298 K	White cell and spectrophone data show good internal consistency; results substantiate data of McCoy [13].	61